

E 870

JOURNAL ON

COMMUNICATIONS

VOLUME XLVI.

JANUARY 1995

PHOTONICS

Editorial I. Hábermajer 1

Lasing threshold calculations for mid- and far-infrared
intersubband semiconductor lasers W. M. Yee and K. A. Shore 2

The Y-laser as a multifunctional device for photonic switching D. Baums, K. Dütting,
O. Hildebrand, W. Idler, E. Lach, G. Laube, M. Schilling and K. Wünstel 12

Nonlinear optical phenomena in semiconductor lasers and amplifiers:
physics and applications W. Elsässer 20

Laser diode phase conjugate mirrors and optical repeater W. M. Yee and K. A. Shore 25

Products – Services

High optical power 1.22 micrometer InP/InGaAsP buried
heterostructure laser diode F. Koltai, S. Püski, V. Rakovics and M. Serényi 33

Business – Research – Education

Education of photonics at the Technical University of Budapest I. Hábermajer 36

JOURNAL ON COMMUNICATIONS

A PUBLICATION OF THE SCIENTIFIC SOCIETY FOR TELECOMMUNICATIONS, HUNGARY

Editor in chief
A. BARANYI

Senior editors
GY. BATTISTIG
T. KORMÁNY
G. PRÓNAY
I. SCHMIDEG
A. SOMOGYI

Editors
I. BARTOLITS
I. KÁSA
J. LADVÁNSZKY
J. OROSZ
M. ZÁKONYI
N. WILK


Editorial assistant
K. LESNYIK

Editorial board
GY. TÓFALVI
chairman


T. BERCELI
B. FRAJKA
I. FRIGYES
G. GORDOS
I. MOJZES
L. PAP
GY. SALLAI

Editorial office
Budapest XIV. Ungvár u. 64-66.
1525 Budapest, P.O.Box 15.
Hungary, H-1525
Phone: (361) 251-1163
(361) 201-7471
Fax: (361) 251-9878
(361) 201-7471


SPONSORED BY



**HUNGARIAN
TELECOMMUNICATIONS
COMPANY LIMITED**




**antenna
hungária**




ERICSSON

Ericsson Technika




SIEMENS


Siemens Telefongyár Kft



WESTEL
RÁDIÓTELEFON KFT



TKI



BHG
BUDAPEST

FOUNDATION FOR THE
"DEVELOPMENT
OF CONSTRUCTION"

HUNGARIAN
PRESS FOUNDATION

Subscription rates
Hungarian subscribers
1 year, 12 issues 6000 HUF, single copies 650 HUF
Hungarian individual subscribers
1 year, 12 issues 960 HUF, single copies 110 HUF
Foreign subscribers
12 issues 150 USD, 6 English issues 90 USD, single copies 24 USD
Transfer should be made to the Hungarian Foreign Trade Bank,
Budapest, H-1821, A/C No. MKKB 203-21411



The evidence of the great interest that the Hungarian engineering community takes in the field of optical communication is that this is the third special issue of the Journal on Communications dealing with this topic in the past three years. The bases of this attention are the rapidly increasing Hungarian telecommunication network, the scientific and some economical successes achieved in research and development institutions. These facts motivated the organization of the first Hungarian Workshop on Semiconductor Lasers (Budapest, 13-14 June 1994). The topic of the Workshop was concentrated around the physics and technology of new type semiconductor lasers and laser applications, but oral and poster presentations were given on the topics of femtosecond optics, integrated optics, optical transmissions and measurements moreover curricular questions of training in optoelectronics. The seminar has been organized by the Department of Semiconductor Optics of the Research Institute for Technical Physics and by the Department of Electron Devices of the Technical University of Budapest. The participants came from the following institutions: ALCATEL SEL AG Research Centre Stuttgart, Philipps-University Marburg (Germany), University of Bath, University of Lancaster (UK), University of Szeged, and from several departments of the Technical University of Budapest.

The papers of this issue are based on the lectures given at the Workshop, selected so that we could inform the

reader on the most up-to-date trends in semiconductor laser technology.

One of these trends aims the extension the range of the operating wavelength and/or the increase output power so that semiconductor lasers would be applicable in the infrared spectroscopy or as pump sources for fibre lasers and amplifiers. The paper presented by W.M. Yee and K.A. Shore deals with the realization problems of far-infrared lasers operating at 10–60 μm . F. Koltay and others reported about a high power (120 mW) laser at 1.22 μm .

The other very far-reaching branch of research aims to find laser structures that are well integrable to the optical telecommunications systems and may act as tuneable light sources, optical wavelength converters, optical switches, amplifiers, pulse regenerators. D. Baums and others introduce a very versatile laser structure for the purposes mentioned above. The inherent nonlinear effect of semiconductor lasers, the four-wave mixing, seems to be advantageously applicable for the ultrafast optical information technologies. W. Elsässer gives an overview of the physics and applications of nonlinear interactions in semiconductor lasers and amplifiers, while W.M. Yee and K.A. Shore theoretically investigate the exploitation of nearly degenerate four-wave mixing in laser diodes to implement phase conjugate mirrors and optical repeaters.

The guest editor hopes that these papers will be found interesting and useful by the readers.

I. HABERMAJER



István Habermajer graduated in electrical engineering from the Technical University of Budapest in 1959. He received the "dr.techn." degree in 1964, and the Candidate of Technical Sciences degree in 1989. From 1959 to 1963, he worked at the Hungarian Television Company. Since then he has been at the Technical University of Budapest, and became an Associate Professor at the

Department of Electron Devices. He is a technical advisor at the Research Institute for Technical Physics, and directed several R&D projects in the field of semiconductor device measurements. His current education activities are related to electron devices, semiconductor physics and optoelectronics. His main interests are analysis and design of semiconductor lasers and photodetectors. He is member of several technical committees.

LASING THRESHOLD CALCULATIONS FOR MID- AND FAR-INFRARED INTERSUBBAND SEMICONDUCTOR LASERS

W. M. YEE and K. A. SHORE

UNIVERSITY OF BATH
SCHOOL OF ELECTRONIC AND ELECTRICAL ENGINEERING
BATH BA2 7AY, UK

We study theoretically the conditions for achieving lasing action at mid-infrared and far-infrared wavelengths based on intersubband transitions in semiconductor quantum well structures. A carrier transport model related to the achievement of intersubband population inversion is presented, which takes into account resonant tunnelling and intersubband absorption-emission processes. The incorporation of optical loss analysis into the carrier transport model provides estimates of the lasing threshold current density consistent with the optical losses in the laser devices. It is shown that reasonably low threshold current density in the range of 1–5 kA/cm² is achievable for room temperature lasing at emission wavelength of 60 μ m. Significantly higher threshold current density of 40–50 kA/cm² is required for lasing at 10 μ m wavelength.

1. INTRODUCTION

The development of room-temperature semiconductor lasers operating in the mid- to far-infrared wavelength range has been pursued by various workers for over twenty years. The effort required to overcome the difficulties in achieving such laser action is expected to be repaid by the wide range of applications envisaged for the devices. Compact low-cost tuneable mid/far-infrared lasers would find ready uses in remote sensing, pollution monitoring, medicine, dentistry and free space telecommunications. In recent years, following spectacular advances in semiconductor material growth techniques, attention has been focussed on the use of quantum well (QW) semiconductor structures for enhancing the performance of a variety of semiconductor optoelectronic devices including semiconductor lasers. Although the thrust of that work has been in respect of near-infrared laser sources for optical fibre communications systems, some effort has also been given to the utilization of low-dimensional structures for the achievement of lasing at longer wavelengths. The primary target of those investigations has been the exploitation of intersubband transitions in semiconductor QW's. The principal attraction of QW structures is that the quantised bound-state energy levels in the wells are essentially determined by the thickness and depth of the QW's. Crucially, the well thickness and depth can be finely controlled during the semiconductor growth process. In principle, therefore, a semiconductor QW structure can be fabricated with prescribed energy levels. The task that remains is to arrange that population inversion and hence lasing action takes place between the chosen energy levels which correspond to a desired operating wavelength. Here is the essence of

the challenge to the device designer. It is found that for operating wavelengths of order 60 μ m and greater, structures may be relatively easily identified for the achievement of population inversion. However, at such wavelengths optical losses make it very difficult to sustain laser oscillation. On the other hand, at "shorter" wavelengths (between say 5 μ m to 10 μ m) optical losses become less daunting but it is relatively more difficult to achieve population inversion. In both cases the achievement of lasing action is more readily facilitated at lower temperatures.

The difficulties inherent in simultaneously meeting the challenges of achieving population inversion and overcoming optical losses have impeded the development of mid- and far-infrared semiconductor lasers. Consideration of the basic quantum mechanics of the transition process between quantum bound states by Henderson *et al.* [1] suggested that inter-bound-state laser action would not be possible. The core of that argument was that the ratio of the lifetimes of the upper and lower energy states was the opposite to that required for lasing. These findings prompted the authors to advance the case for the utilisation of above-well quasi-bound state transitions to achieve the required population inversion. On the other hand, a sustained effort by Capasso and co-workers has developed a detailed understanding of the requirements for achieving light emission and lasing action via intersubband transitions in coupled QW structures. Operation of electroluminescent diodes [2] was achieved at an emission wavelength of 5 μ m at operating temperatures up to room temperature. More spectacularly, lasing action at an operating wavelength of 4.3 μ m was demonstrated at temperatures up to about 125 °K [3].

The work of Capasso and co-workers has given new impetus to efforts directed at achieving long wavelength semiconductor lasers. From a fundamental viewpoint, it is seen that a new class of semiconductor lasers has been obtained which utilise only one kind of charge carrier. Such devices may be termed unipolar semiconductor lasers. In the present case electron intersubband transitions have been utilised but semiconductor lasers utilising transitions between hole intersubbands are also conceivable. The considerable efforts made by these workers to achieve this important milestone underlines the significance of their work. It is clear that careful design of the structure was complemented by extremely intricate and challenging semiconductor growth. The latter was required to obtain the

multiple coupled well structure which permits the operation of the 'quantum cascade' semiconductor laser.

The demonstration of the quantum cascade laser should, it is argued, be seen as providing an invaluable proof-of-concept demonstration of intersubband lasing. It is apparent, however, that much device development work is required to both raise the operating temperature of the intersubband lasers and to achieve lasing at longer wavelengths. The aim of the present paper is to quantify the challenges which need to be met to reach the goal of operating room-temperature mid- and far-infrared semiconductor lasers.

The report by West *et al.* [4] of the first observation of an extremely large dipole infrared transition between QW subbands has revived significant interest in the original proposal by Kazarinov and Suris [5] for the achievement of intersubband infrared emission in coupled QW structures and superlattices. Infrared photodetectors based on intersubband absorptions in QW structures have been extensively studied and successfully implemented recently for wavelengths in the 4–12 μm range [6]. Spontaneous intersubband radiative emission in GaAs-AlGaAs superlattices was first observed and reported by Helm *et al.* [7]. However, in order to obtain coherent infrared lasing from intersubband transitions, it is necessary to achieve a sufficiently high degree of intersubband population inversion at reasonably low pumping. This represents a major challenge because of the overwhelming contribution of nonradiative phonon emission which depopulates the upper lasing subband at a very fast rate. Many schemes have been proposed to achieve intersubband population inversion, most of which concentrate on current injection pumping [8]–[12], while a few approaches focus on optical pumping using a CO₂ laser source [13], [14].

In early studies on current injection pumped infrared semiconductor lasers based on intersubband transitions, sequential resonant tunnelling has been used to populate the excited state and depopulate the ground state of an electrically biased multiple QW structures. Although weak spontaneous emission has been observed using the sequential resonant tunnelling QW structure [7], intersubband population inversion has not been achieved. This is due to the fact that sequential resonant tunnelling from the ground state of one QW to the first excited state of the adjacent QW represents carrier transport in an essentially two-level system, and that population inversion cannot be achieved using just two states. On the other hand, while population inversion may be possible using sequential resonant tunnelling from the ground state to the second or higher excited state of an adjacent QW, the subsequent 'rain-down' of electrons to the first excited state and the ground state makes population inversion between these two states very difficult.

In order to facilitate the selective injection of electrons into the first excited state and the removal of electrons from the ground state of an emission QW, resonant tunnelling QW energy filters have been proposed and shown to lead to intersubband population inversion [9]–

[11]. These studies, however, assumed a simple relation between the intersubband population inversion and the injection current density, without taking into account the relevant physical mechanisms of resonant tunnelling and intersubband emission-absorption processes in the electron transport dynamics. The purpose of the present paper is to review a theoretical model which has been developed for the calculation of intersubband lasing conditions. The relevance of the model has been highlighted by the recent experimental activity on this topic and it is hoped that the present contribution will form a basis for future detailed device modelling of intersubband semiconductor lasers.

The main element of the model is a description of carrier transport in a generic coupled QW structure which has been outlined in an earlier publication [15]. That work was related to the achievement of intersubband population inversion in triple QW structures but the general formalism is applicable to, for example, the quantum cascade laser configuration. The second significant challenge in the design of long wavelength intersubband lasers is to meet the conditions necessary for achieving lasing action. The requirement here is to incorporate optical loss analysis which takes into account the semiconductor laser device configuration. Such a description was provided in a recent publication [16]. Here we show how the complete formulation provides estimates of lasing threshold current density consistent with the optical losses in the laser devices for emission wavelengths of 10 μm and 60 μm . In section 2, we present the transport model which describes the electron population dynamics in two prototype resonant tunnelling QW structures where account is taken of intersubband emission-absorption processes. The transparency current density is calculated in section 3 taking into account the dependence on electron transit time and intersubband relaxation time. In section 4, the issue of optical loss is addressed for different doping densities in the cladding layers. The solution of the four-level carrier rate equations from the transport model in conjunction with the balance of gain and optical loss yields the threshold current density. Finally, we summarize the results in section 5.

2. THEORETICAL MODEL

2.1. Resonant Tunnelling Quantum Well Structures

In this section, two prototype coupled QW structures are considered [15] for the achievement of intersubband population inversion. The two structures have intersubband energy separations of 124 meV (corresponding to an intersubband resonant wavelength $\lambda = 10 \mu\text{m}$) and 21 meV ($\lambda = 60 \mu\text{m}$), respectively. The schematic conduction band profiles of the two structures are shown in Figs. 1 (a) and 1(b), respectively. In order to facilitate the selective injection of electrons into the upper subband and the removal of electrons from the lower subband of the emission QW, resonant tunnelling QW energy filters are used [10], [11].

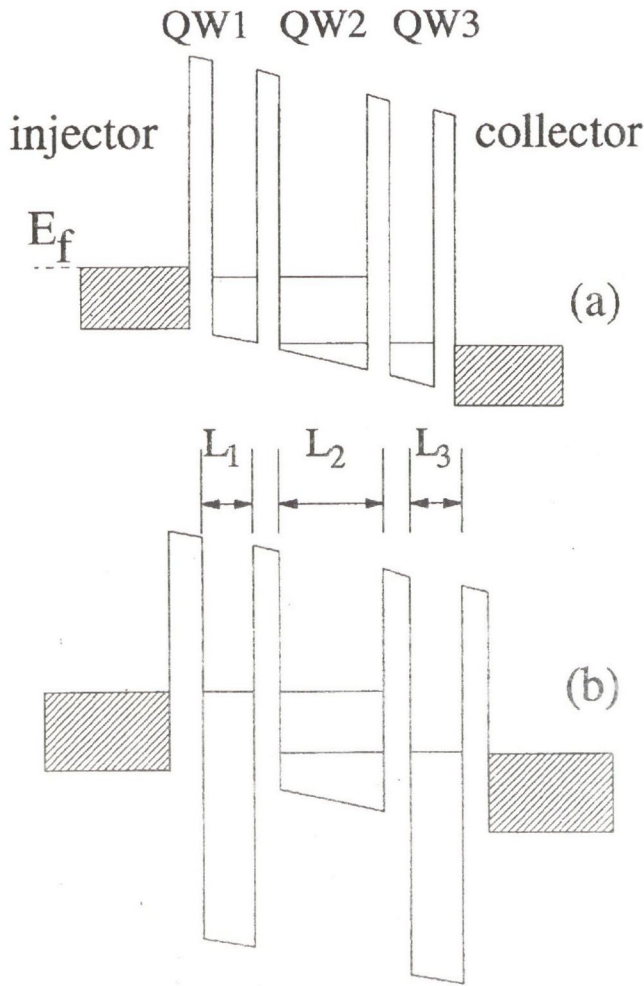


Fig. 1. Schematic conduction band profiles of the resonant tunnelling quantum well structures biased to the operating voltage (not drawn in proportion) for (a) mid-infrared lasing at $\lambda = 10 \mu\text{m}$ (structure I), and (b) far-infrared lasing at $\lambda = 60 \mu\text{m}$ (structure II). Hatched regions represent n-doped conducting layers. E_f is the Fermi energy level.

As shown in Figs. 1(a) and 1(b), QW2 is the emission well where intersubband transitions take place between the first excited state with energy $E_2^{(2)}$, and the ground state with energy $E_2^{(1)}$. The emission wavelength corresponding to the intersubband energy separation $E_2^{(2)} - E_2^{(1)}$ is determined mainly by the choice of the emission well thickness L_2 . QW1 and QW3 act as resonant tunnelling energy filters, which are designed to have only one quasi-bound state each (with energy E_1 and E_3 , respectively). Under zero bias, the well widths of the resonant tunnelling energy filters are engineered such that E_1 and E_3 are in the middle of $E_2^{(1)}$ and $E_2^{(2)}$ in the emission well. When the structures are biased to the operating voltage given by $V_b \approx (E_2^{(2)} - E_2^{(1)})/2$, the energy states are aligned as shown in Figs. 1(a) and 1(b). Electrons are efficiently injected into the first excited state of QW2 through filter well QW1, and are removed from the ground state of QW2 through QW3, via resonant tunnelling. The confined electrons in the emission well (QW2) undergo intersubband transitions such as intersubband relaxation, stimulated radiative emission and absorption. Because

QW3 has only one subband which is aligned with the ground state of QW2, it not only efficiently depopulates the ground state of QW2 via resonant tunnelling, but also enhances the confinement of electrons in the first excited state of QW2 by minimizing electron escape to the collector. As the whole device structure relies on energy filtering to selectively populate the respective subbands, the influence of any non-resonant energy bands would be small. In particular, the contribution of any other subbands which may exist in QW2 can be neglected since those states would not be resonant with the aligned states in QW1 and QW3.

The resonant tunnelling QW structures are sandwiched between n-doped regions of the cladding layers, which are called the injector and the collector. The injector and the collector serve not only to reduce space-charge effects but also to provide optical confinement to the active QW regions. This is because the refractive index drops significantly in the n-doped cladding regions owing to the higher electron density.

The $\text{GaAs}-\text{Al}_x\text{Ga}_{1-x}\text{As}$ ($x = 0.45$) material system is employed in structure I (Fig. 1(a)). On the other hand, because the intersubband energy separation of 21 meV corresponding to the far-infrared frequency of 5 THz in structure II is very small, rather wide emission well is required. As a result, the laser transition states in the emission well are situated very near to the bottom of the well. In order to ensure that the energy filter wells of structure II have only one quasi-bound state each and that the various energy states align properly under operating bias, very deep filter wells are required. These requirements are satisfied by using the $\text{In}_y\text{Ga}_{1-y}\text{As}-\text{Al}_x\text{Ga}_{1-x}\text{As}$ ($x = 0.45$, $y = 0.15$) material system in the filter wells and GaAs in the emission well for structure II (Fig. 1(b)).

2.2. Electron Transport Dynamics

Since the intersubband transition and resonant tunnelling processes occur at a much faster rate than the interband transitions, it is assumed that there is no carrier source or sink in the coupled QW structures. The temporal variations of electron density in the respective subbands are described by carrier rate equations of an essentially four-level system [15]:

$$\frac{dn_1}{dt} = \frac{J}{eL_1} + \frac{L_2}{L_1} \frac{n_2^{(2)}}{\tau_{12}} - \frac{n_1}{\tau_{12}}, \quad (1)$$

$$\frac{dn_2^{(2)}}{dt} = \frac{L_1}{L_2} \frac{n_1}{\tau_{12}} - \frac{n_2^{(2)}}{\tau_{12}} - (n_2^{(2)} - n_2^{(1)})X(P) - A_{sp}, \quad (2)$$

$$\frac{dn_2^{(1)}}{dt} = (n_2^{(2)} - n_2^{(1)})X(P) + A_{sp} + \frac{L_3}{L_2} \frac{n_3}{\tau_{23}} - \frac{n_2^{(1)}}{\tau_{23}}, \quad (3)$$

$$\frac{dn_3}{dt} = \frac{L_2}{L_3} \frac{n_2^{(1)}}{\tau_{23}} - \frac{n_3}{\tau_{23}} - \frac{J}{eL_3}, \quad (4)$$

where J is the external injection current density, $n_a^{(b)}$ denotes the electron density in quantum well a ($a = 1, 2, 3$) and subband b (since there is only one subband in QW1 and QW3, the superscript b is omitted), e is

the electronic charge, and X is the stimulated radiative emission coefficient (inverse time) which is a function of the photon density P .

The tunnelling times τ_{12} and τ_{23} between QW1 and QW2, and QW2 and QW3, respectively, are given by

$$\tau_{12} = \frac{\pi \hbar}{\Delta E}, \quad \tau_{23} = \frac{\pi \hbar}{\Delta E'}, \quad (5)$$

where \hbar is the Planck's constant divided by 2π , ΔE and $\Delta E'$ are the energy level broadening resulting from the coupling of QW1 and QW2, and QW2 and QW3, respectively. The total intersubband relaxation rate A_{sp} in QW2 (per-unit volume per-unit time), appropriate for a two-dimensional system, is given by [17]

$$A_{sp} = S(n_2^{(2)} - n_2^{(1)}) \frac{\exp(n_2^{(2)}/n_{c2}) - 1}{\exp(n_2^{(2)}/n_{c2}) - \exp(n_2^{(1)}/n_{c2})}, \quad (6)$$

where S is the intersubband relaxation coefficient (inverse time), $n_{c2} = (m_2^* k_B T) / (\pi \hbar^2 L_2)$ is the quasi-two-dimensional degeneracy concentration, $m_2^* = 0.067 m_0$ is the electron effective mass in GaAs, m_0 is the free electron mass, k_B is the Boltzmann constant and T is the electron temperature. The above expression incorporates energy dependence of the carriers using Fermi-Dirac statistics as appropriate to semiconductor laser operation [17].

Since the current injection is equal to the rate of total charge passing through the resonant tunnelling QW structure, J can be written as

$$J = \frac{e}{\tau_T} [n_1 L_1 + (n_2^{(1)} + n_2^{(2)}) L_2 + n_3 L_3], \quad (7)$$

where τ_T is the effective transit time of electrons through the whole structure, which includes not only the transmission times through the barriers and the intersubband transition times, but also time delays caused by intrasubband scattering and electron diffusion. The steady-state electron densities in the various subbands can be obtained as a function of the external injection current density by solving the electron rate equations subject to the constraint imposed by Eq. (7).

The coupled QW structures utilizing resonant tunnelling energy filters provide an efficient means of electron injection into the upper subband and electron removal from the lower subband of the emission well. It should be noted that without the energy filter QW's the structure becomes essentially a two-level system, and in that case intersubband population inversion cannot be obtained. To assess the possibility of intersubband population inversion in the proposed QW structures, the relevant physical mechanisms of intersubband emission-absorption processes have to be taken into account.

The principal intersubband transition processes include stimulated emission of radiation, absorption and intersubband relaxation. For current injection pumping and below lasing threshold operation of the coupled QW infrared laser structures, the stimulated emission and absorption rates are negligibly small compared to the intersubband relaxation rate. As a result, the term proportional to $X(P)$ in the electron rate equations can be neglected.

The intersubband relaxation coefficient S is given by the inverse of the intersubband relaxation time τ_R . For intersubband energy separation greater than the optical phonon energy (≈ 36 meV in GaAs), optical phonon scattering is the main intersubband relaxation process. The reported intersubband relaxation times arising from optical phonon scattering vary over more than one order of magnitude. Relaxation times of the order of 10 ps at 300 °K for an intersubband energy separation of 120 meV in GaAs QW were reported by Seilmeier and co-workers [18]. However, recent experimental measurements [19] and theoretical calculations [20] reported subpicosecond to 1 ps relaxation times arising from optical phonon scattering. In general, the optical phonon scattering time of InGaAs-InAlAs QW's is slightly longer than that of GaAs-AlGaAs QW's. This is attributed to the lower effective mass of InGaAs as compared to GaAs.

Acoustic phonon scattering is expected to be the dominant mechanism for intersubband relaxation if the intersubband energy separation is less than the optical phonon energy. Oberli *et al.* [21] reported intersubband relaxation times of the order of several hundred picoseconds arising from acoustic phonon scattering in wide GaAs-AlGaAs MQW at low temperatures. Recent measurement [22] reported intersubband relaxation times of (300 ± 100) ps, corresponding to the emission of acoustic phonons. Table 1 shows the parameter values used in the calculation.

Table 1. Parameter values used in the calculation

	Structure I	Structure II	
λ	10	60	μm
L_1	40	70	\AA
L_2	82	285	\AA
L_3	40	70	\AA
ΔE	7	0.2	meV
$\Delta E'$	5	0.1	meV
S	10^{12}	$(3 \times 10^{-10})^{-1}$	s^{-1}

2.3. Intersubband Population Inversion

The carrier densities in all subbands increase as the external injection current density is increased. The dependence of carrier density in the upper and the lower subbands of QW2 on injection current density for structure II is illustrated in Fig. 2. It is observed that the intersubband population inversion, $\Delta n = n_2^{(2)} - n_2^{(1)}$, becomes positive when the external injection current density exceeds the level J_0 , which is termed the transparency current density.

Figs. 3(a) and 3(b) show the calculated intersubband population inversion as a function of J at different temperatures for structures I and II, respectively. It is noted that significantly higher injection current density is needed to achieve intersubband population inversion in structure I as compared to structure II. This is because the upper lasing state of structure I is depopulated at a very fast rate by intersubband relaxation with the emission of optical phonons, whereas a much slower acoustic phonon scattering limits the downward transition in structure II. It therefore appears that lasing action based on intersubband transition may, at reasonable level of injection current, be feasible only in the far-infrared

wavelength range. However, the absorptive loss is greater for longer wavelengths, and thus there is a trade-off to be considered when designing such a laser.

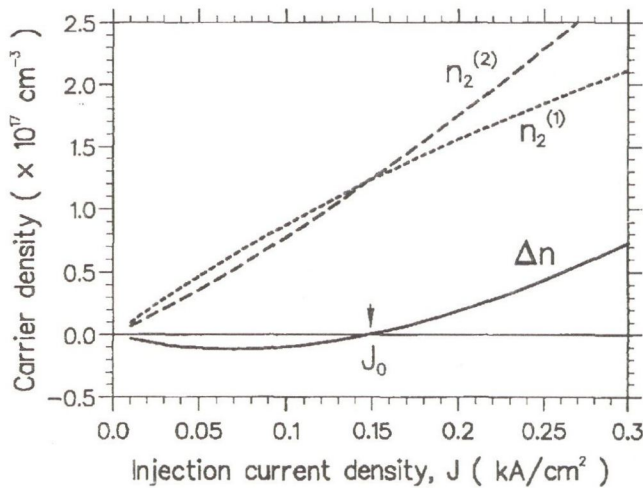


Fig. 2. Dependence of electron density on injection current density for QW structure II. Intersubband population inversion becomes positive when J exceeds the transparency value, J_0 .

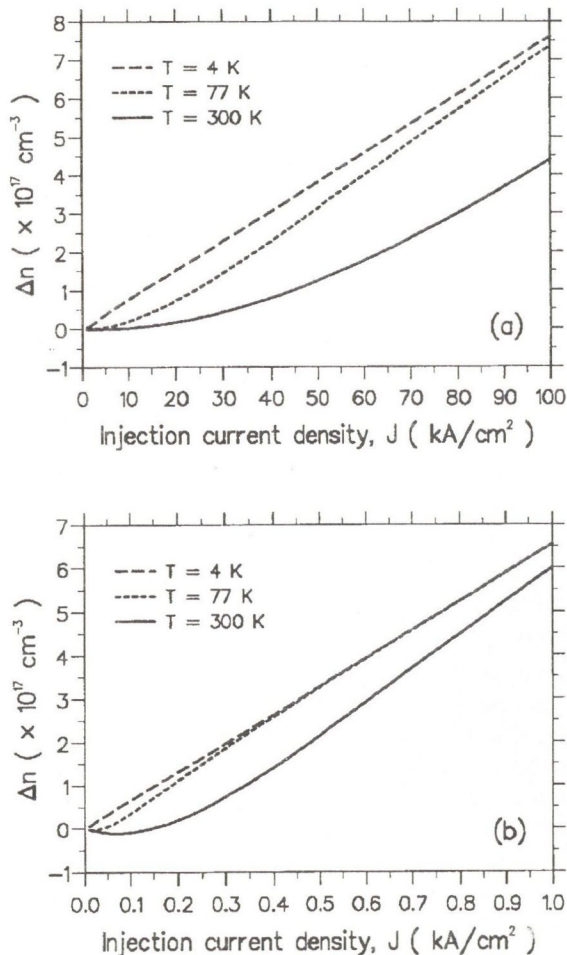


Fig. 3. Intersubband population inversion versus injection current density at different temperatures for (a) structure I, $\tau_T = 4.0$ ps, and (b) structure II, $\tau_T = 1.5$ ns.

It is also observed that higher injection current densities are needed to obtain a given level of population inversion as the temperature is increased. It has been assumed that non-resonant tunnelling and thermionic induced carrier leakage from the upper subband of QW2 to the collector are negligibly small. In view of the uncertainties in the reported experimental values of the intersubband relaxation time, it is difficult to incorporate the temperature dependence of the intersubband relaxation time in the analysis. The temperature dependence of Δn arises mainly because of the quasi-two-dimensional degeneracy density n_{c2} being a function of temperature. In practice, the intersubband relaxation rates increase with temperature and this may affect the temperature dependence of Δn .

3. CALCULATION OF TRANSPARENCY CURRENT DENSITY

In this section, the dependence of transparency current density J_0 on effective electron transit time τ_T , and intersubband relaxation time τ_R is calculated for the two prototype resonant tunnelling QW structures.

3.1. Dependence of Transparency Current Density on Electron Transit Time

Figs. 4(a) and 4(b) show the transparency current density as a function of the effective electron transit time τ_T for QW structure I ($\lambda = 10 \mu\text{m}$) and structure II ($\lambda = 60 \mu\text{m}$), respectively. The effective transit time includes not only the tunnelling times τ_{12} and τ_{23} , and the intersubband relaxation time τ_R , but also tunnelling times through the outer barriers, electron dephasing times in the various subbands, and electron diffusion time. The electron dephasing time is governed by intrasubband scattering processes which are believed to be dominated by electron-electron scatterings. Any extra time delays caused by these intrasubband processes will lead to higher electron accumulation in the various quantum subbands and further increase J_0 .

It is noted from Figs. 4(a) and 4(b) that transparency current densities of a few tens of kA/cm^2 are required to obtain room-temperature intersubband population inversion at $\lambda = 10 \mu\text{m}$ (structure I). On the other hand, significantly lower transparency current densities in the range of 0.1 – 0.3 kA/cm^2 are achievable at $\lambda = 60 \mu\text{m}$ (structure II) for room-temperature operation. In both cases, the achievement of intersubband population inversion is more readily facilitated at lower temperatures. Furthermore, the minimum transit times for the two coupled QW structures can be obtained from Figs. 4(a) and 4(b), respectively. The minimum transit time for structure I is approximately 3.8 ps. The transit time dependence of J_0 for structure II is less sensitive; a large change in τ_T (of the order of nanoseconds) produces only a relatively small change in J_0 . This is possibly because the transit time of structure II is much larger than the electron dephasing time (of the order of subpicosecond). From Fig. 4(b), the minimum τ_T is approximately 1.2 ns for structure II.

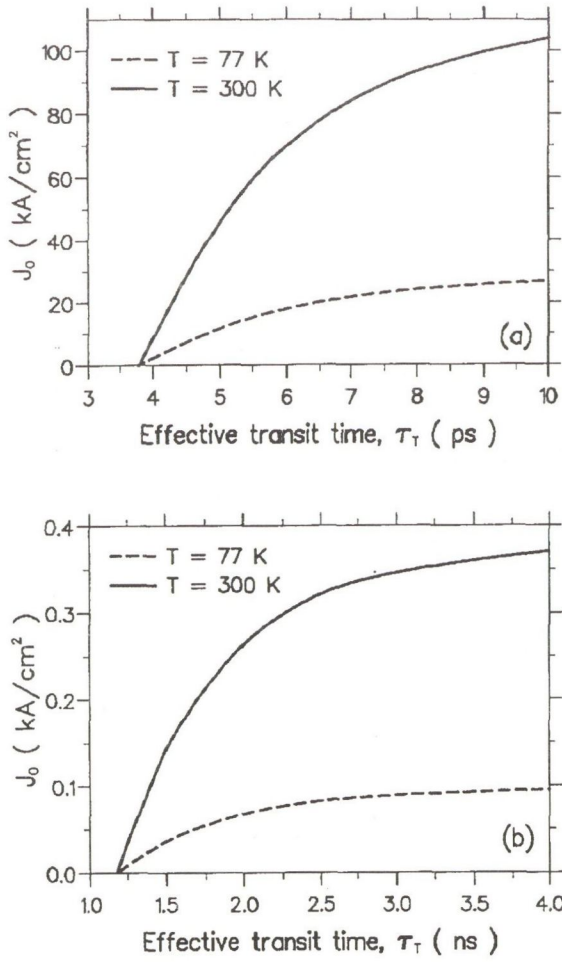


Fig. 4. Dependence of transparency current density on effective electron transit time for (a) structure I and (b) structure II.

3.2. Dependence of Transparency Current Density on Intersubband Relaxation Time

As has been noted earlier, the reported experimental values of intersubband relaxation time τ_R arising from optical phonon scattering for GaAs-AlGaAs quantum wells differ by more than one order of magnitude. For intersubband energy separation less than the optical phonon energy, the intersubband relaxation rate is reduced by about two orders of magnitude [22], being limited by the slower acoustic phonon emission. In view of such uncertainties in the values of the intersubband relaxation time, it is instructive to investigate the sensitivity of the dependence of transparency current density on intersubband relaxation time.

Figs. 5(a) and 5(b) show the transparency current density as a function of the intersubband relaxation time τ_R for structure I and structure II, respectively. J_0 increases by more than two orders of magnitude if τ_R is reduced from 1.0 ps to 0.1 ps for structure I. Similarly, J_0 increases by approximately one hundred times when τ_R is reduced from 0.35 ns to 0.035 ns for structure II. The results suggest that intersubband population inversion is highly dependent on τ_R , and that in order to reduce the transparency current density, it is crucial to reduce the intersubband relaxation rate. Several ways may be used to reduce the intersubband relaxation rate:

1) Phonon emission rate can be reduced considerably by lowering the temperature of operation of the device, thus enhancing the electron lifetime in the upper subband of the emission well.

2) It is found that material with a lower effective mass has a longer intersubband relaxation time. Hence material such as InGaAs, with a lower effective mass and a longer intersubband relaxation time than GaAs [19], may be used to fabricate the emission QW.

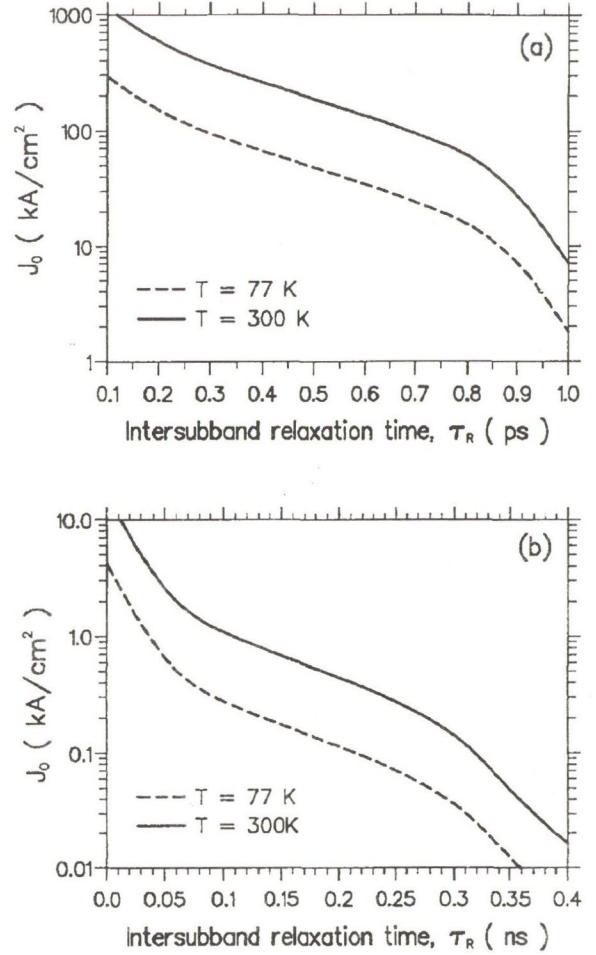


Fig. 5. Dependence of transparency current density on intersubband relaxation time for (a) structure I and (b) structure II.

3) For intersubband energy separation larger than the optical phonon energy, the intersubband relaxation rate can be reduced by reducing the quantum well width [18], [20]. This is because a larger intersubband energy separation (corresponding to a smaller well width) requires a larger wavevector for the intersubband transition, whilst the density of final states decreases with increasing wavevector. Therefore, intersubband population inversion may be achieved at lower injection current densities for emission wavelength $\lambda < 10 \mu\text{m}$. This, together with the fact that optical absorptive loss decreases for shorter wavelengths, indicates that lasing action based on intersubband transitions may be easier to achieve for $\lambda < 10 \mu\text{m}$ compared to $\lambda = 10 \mu\text{m}$. The above discussion suggests that experimental investigation into intersubband population inversion and lasing for wavelengths shorter than $10 \mu\text{m}$ could be of considerable interest with a view to de-

signing mid-infrared lasers operating at the $\lambda = 3 - 5 \mu\text{m}$ atmospheric window [3].

4. CALCULATION OF THRESHOLD CURRENT DENSITY

Having shown that intersubband population inversion can indeed be achieved at reasonable injection current densities in the proposed resonant-tunnelling QW structures, this section is devoted to quantifying the lasing threshold conditions which need to be met for the achievement of room-temperature mid- and far-infrared lasing. In this respect, optical loss analysis is carried out [16] taking into account the infrared QW laser geometry in a way similar to Borenstain [10]. Threshold current density is explicitly calculated as a function of free electron density in the n-doped regions of the cladding layers of the two proposed QW laser structures.

4.1. Calculation of Optical Absorption

The optical properties of III-V semiconductor materials at energies smaller than the fundamental bandgap energy are determined by two major physical processes, namely lattice vibrations (photon-phonon interactions) and collective oscillation of free carriers (photon-plasmon interactions). The refractive index \bar{n} and the extinction coefficient k can be calculated through the complex dielectric constant [10], [23] as given by

$$\epsilon(\omega) = (\bar{n} - ik)^2 = \epsilon_\infty \left[1 + \frac{\omega_L^2 - \omega_T^2}{\omega_T^2 - \omega^2 + i\omega\gamma_{ph}} - \frac{\omega_p^2}{\omega(\omega - i\gamma_{pl})} \right], \quad (8)$$

where ϵ_∞ is the high frequency dielectric constant, ω_L , ω_T and ω_p are the angular frequencies of the longitudinal optical (LO) phonons, the transverse optical (TO) phonons and the plasmons, respectively, γ_{ph} and γ_{pl} are the damping constants of the phonons and the plasmons, respectively, $\gamma_{pl} = e/2\pi\mu_e m^*$, μ_e is the electron mobility, $\omega_p^2 = N_c e^2 / m^* \epsilon_\infty \epsilon_0$, ϵ_0 is the permittivity of free space, and N_c is the free electron density in the n-doped cladding layers (the injector and the collector). The absorption coefficient in the n-doped cladding layers is calculated from the extinction coefficient in Eq. (8) using

$$\alpha_c = \frac{4\pi k}{\lambda}. \quad (9)$$

The parameter values used in the calculation are: $\epsilon_\infty = 11.1$, $\omega_L = 291.5 \text{ cm}^{-1}$, $\omega_T = 268.2 \text{ cm}^{-1}$, $\gamma_{ph} = 2.3 \text{ cm}^{-1}$, and $\mu_e = 5000 \text{ cm}^2 \text{V}^{-1} \text{s}^{-1}$.

Figs. 6(a) and 6(b) show the effects of varying the free electron density on optical absorption and refractive index for wavelengths of $10 \mu\text{m}$ and $60 \mu\text{m}$, respectively. The effects of increasing the free electron density in the n-doped region of the cladding layers are to increase the optical absorptive loss, and to decrease the refractive index in the cladding layers. These effects are particularly pronounced at the longer wavelength. It is noted that, for $N_c = 1 - 5 \times 10^{17} \text{ cm}^{-3}$, optical absorption of $10 - 40 \text{ cm}^{-1}$ is obtained at $\lambda = 10 \mu\text{m}$. However, at $\lambda = 60 \mu\text{m}$, significantly higher absorption of $500 - 6000 \text{ cm}^{-1}$ results

over the same range of N_c . Therefore, despite the lower transparency current densities achievable at an operating wavelength of $60 \mu\text{m}$ (as revealed in the previous section), high optical losses may lead to high threshold current densities for laser operation in this emission wavelength. However, at $\lambda = 10 \mu\text{m}$, optical losses become less daunting, but it is relatively more difficult to achieve population inversion. Hence, it is concluded that the critical issue in designing mid-infrared ($1 - 30 \mu\text{m}$) semiconductor lasers is to reduce the intersubband relaxation rates so as to lower the transparency current density. On the other hand, the challenge to designing far-infrared ($> 30 \mu\text{m}$) semiconductor lasers is to overcome optical absorptive losses so as to lower the lasing threshold current density.

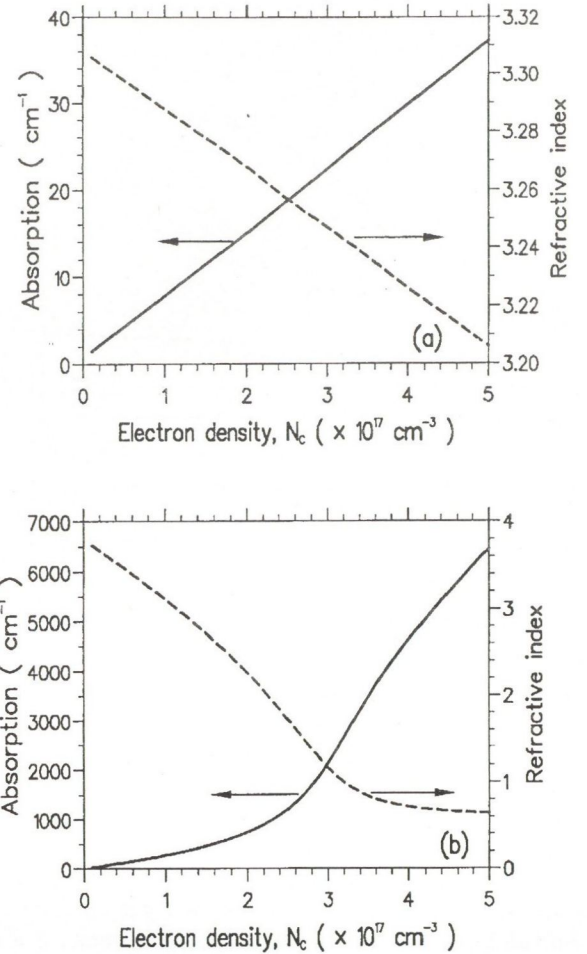


Fig. 6. Effects of variation of free electron density on optical absorption and refractive index at (a) $\lambda = 10 \mu\text{m}$ and (b) $\lambda = 60 \mu\text{m}$.

From Figs. 6(a) and 6(b), it appears that lower threshold current density may be achieved by reducing the free electron density in the n-doped region of the cladding layers. However, it is also noted that reducing the electron density leads to an increase in the refractive index of the cladding layers. This gives rise to an anti-guiding effect on the generated photons and thus reduces the optical confinement. As a result, higher threshold current density may be required to achieve laser action if the doping density in the cladding region is low. There is, therefore, a trade-off to be considered when designing an

infrared semiconductor laser. The effect of varying N_c on refractive index is particularly pronounced at $\lambda = 60 \mu\text{m}$; a significant drop of refractive index from 3 to 0.6 is obtained when N_c is increased from $1.0 \times 10^{17} \text{ cm}^{-3}$ to $5.0 \times 10^{17} \text{ cm}^{-3}$. This optical property of the material is useful when consideration is given to designing a waveguiding structure to improve the optical confinement in a far-infrared semiconductor laser.

4.2. Lasing Threshold Condition

The optical gain, g (per unit length) in the emission quantum well can be written as

$$g(\lambda) = \frac{\lambda^2}{4\pi\epsilon_r\tau_e} \frac{T_2}{1 + (\omega - \omega_0)^2 T_2^2} \Delta n, \quad (10)$$

where $\Delta n = n_2^{(2)} - n_2^{(1)}$, ϵ_r is the relative permittivity of GaAs, T_2 is the electron dephasing time in the quantum subbands, ω_0 is the angular frequency at resonance and τ_e is the spontaneous radiative time given by

$$\tau_e^{-1} = (2\pi\epsilon_r^{1/2}e^2/m^*\epsilon_0\lambda^2c)f_{ij}, \quad (11)$$

where c is the velocity of light in vacuum and f_{ij} is the oscillator strength of the transition from the i level to the j level, which can be approximated by $f_{ij} = 64(ij)^2/\pi^2(i^2 - j^2)^3$.

To establish the lasing threshold condition, the device structures as shown in Figs. 1(a) and 1(b) are considered. It is assumed that free electrons are confined to just two n-doped conducting layers (the injector and the collector) with total thickness t_c . The generated photons are confined to an effective mode thickness of $t_m = \lambda/2\pi$. Lasing action in the structures occurs when the optical gain equals the total losses, i.e.,

$$\frac{L_2}{t_m} g_{th} = \frac{L_2}{t_m} \alpha_a + \eta_c \alpha_c + \eta_i \alpha_i + \frac{1}{L_c} \ln \left(\frac{1}{R} \right), \quad (12)$$

where α_a , α_c and α_i are the loss coefficients (per unit length) in the active QW layer, the conducting layers and the intrinsic region of the cladding layers, respectively, η_c and η_i are the mode filling factors in the conducting and the intrinsic cladding layers, respectively. The last term accounts for mirror loss of the laser structures with cavity length L_c and facet reflectivity R .

The loss coefficient in the conducting layers α_c is calculated using Eqs. (8) and (9). The loss coefficient in the intrinsic regions α_i is similarly calculated by putting $N_c = 0$. Absorption by plasmon interaction in the emission quantum well (active region) is negligible because radiation emitted from intersubband transitions is polarized perpendicular to the QW layers, whereas plasmon oscillations can interact only with radiation polarized parallel to the QW layers. Furthermore, because of the small active layer thickness, absorption from photon-phonon interaction in the emission well is negligibly small for wavelengths well above or below the reststrahlen region (at wavelengths between ≈ 34 and $37 \mu\text{m}$). Hence it can be assumed that $\alpha_a \approx 0$.

It is assumed that $t_c = 2 \mu\text{m}$ in both structures. Since $t_c > t_m \approx 1.43 \mu\text{m}$ in structure I, the mode filling factors are given by $\eta_c = (t_m - L_2)/t_m$ and $\eta_i = 0$. In structure II, however, $t_c < t_m$ and

in this case $\eta_c = t_c/t_m$ and $\eta_i = (t_m - t_c)/t_m$. The intersubband population inversion at lasing threshold $(\Delta n)_{th}$ is obtained by equating Eqs. (10) and (12) for $\omega = \omega_0$. The electron rate equations from the transport model are then solved in steady-state for J_{th} consistent with the obtained threshold population inversion. The parameter values used in the calculation are: $\epsilon_r = 12.25$, $T_2 = 0.21 \text{ ps}$, $R = 0.3$, and $L_c = 1.0 \text{ mm}$.

Figs. 7(a) and 7(b) show the calculated threshold current density as a function of free electron density in the conducting layers for the two infrared laser structures respectively. As N_c is increased through doping, the absorption arising from plasmon interaction increases, thus increasing the threshold gain and J_{th} . It is observed from Fig. 7(b) that J_{th} remains relatively low at low N_c but increases sharply when N_c exceeds $\approx 2.3 \times 10^{17} \text{ cm}^{-3}$ for structure II. This is because for electron density above this value, the plasma frequency ω_p in the conducting layers becomes higher than the emission frequency ($\approx 5 \text{ THz}$) of structure II. Since the generated laser wave cannot propagate through the free carrier plasmas at frequencies below the plasma frequency, optical absorption through photon-plasmon interaction increases rapidly. No such rapid increase in J_{th} is observed in Fig. 7(a) because the plasma frequency is lower than the emission frequency ($\approx 30 \text{ THz}$) of structure I over the range of N_c considered here.

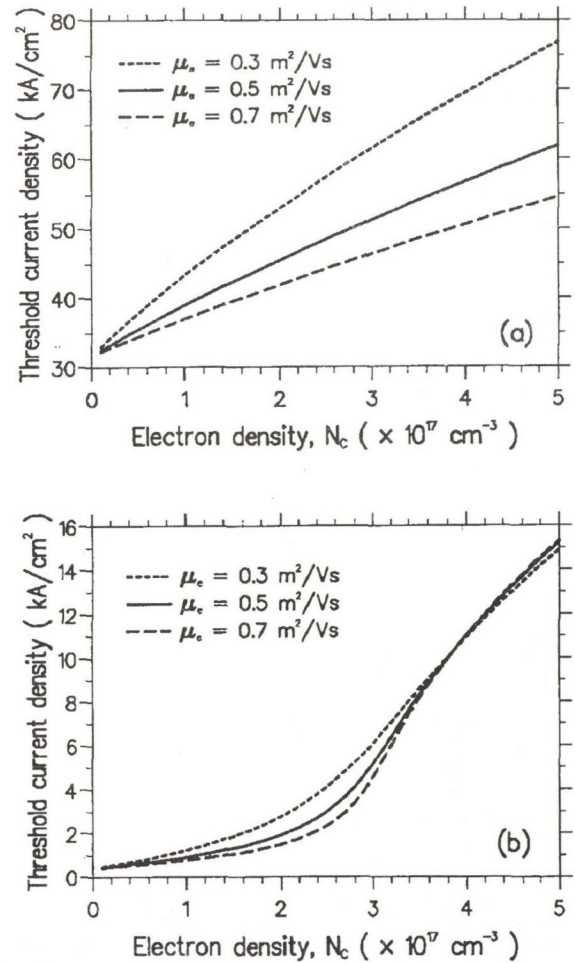


Fig. 7. Dependence of threshold current density on electron density in the n-doped cladding layers for (a) structure I and (b) structure II.

It is also observed that increasing the electron mobility reduces the threshold current density at a given N_c . This is because higher electron mobility means longer scattering time (or lower scattering rate) of free electrons in the n-doped cladding layers, which leads to lower plasmon damping and thus lower optical absorption. The dependence of threshold current density on electron mobility is less sensitive in the case of structure II. This is possibly due to the very high absorption at the far-infrared wavelength of $60\text{ }\mu\text{m}$, and hence a change in electron mobility will not affect the optical absorption significantly. It is also noted that electron mobility is inversely related to temperature. Thus, at high temperature electron mobility decreases and higher threshold current density is required for lasing. This is consistent with results shown in Figs. 7(a) and 7(b). Assuming $\mu_e = 0.5\text{ m}^2\text{V}^{-1}\text{s}^{-1}$ at $T = 300\text{ }^\circ\text{K}$, it is found that reasonable threshold current densities of order $1\text{--}5\text{ kA/cm}^2$ is achievable in structure II for room-temperature far-infrared ($\lambda = 60\text{ }\mu\text{m}$) lasing with N_c in the range of $1\text{--}3 \times 10^{17}\text{ cm}^{-3}$. To achieve room-temperature mid-infrared ($\lambda = 10\text{ }\mu\text{m}$) lasing using structure I, J_{th} around $40\text{--}50\text{ kA/cm}^2$ is required over the same range of N_c .

The analysis of carrier transport and lasing threshold operation presented here is based on the triple-coupled resonant tunnelling QW structures. Further optimization of these device structures may be required to lower the threshold current density for practical device operation. In this respect, the triple-coupled resonant tunnelling QW structures may be periodically repeated to form a superstructure. Such a superstructure, with graded-gap spacer [3] between each unit block of triple-coupled QW's to ensure efficient electron injection and charge screening, will effect a much higher multiplicative optical gain as well as provide better optical confinement. In addition, resonant optical waveguide structures may be considered for enhancing the waveguiding properties of the infrared laser devices. Optimization of the triple-coupled resonant tunnelling QW structures based on the

above design proposals would be expected to yield lower threshold current density for room-temperature operation of mid- and far-infrared semiconductor lasers.

5. CONCLUSION

We have presented a theoretical model of electron transport in resonant tunnelling QW structures, incorporating the relevant physical mechanisms of resonant tunnelling and intersubband emission-absorption processes. The transparency current density at $\lambda = 10\text{ }\mu\text{m}$ and $\lambda = 60\text{ }\mu\text{m}$ has been calculated and shown to be extremely sensitive to variation of the intersubband relaxation time. Optical loss analysis has also been carried out taking into account the laser device structures. Solution of the four-level electron rate equations from the transport model, consistent with the balance of optical gain and loss in the laser devices, enables the threshold current density to be calculated explicitly as a function of electron doping density in the cladding layers. The results show that a reasonably low threshold current density in the range of $1\text{--}5\text{ kA/cm}^2$ is achievable for room-temperature lasing at $\lambda = 60\text{ }\mu\text{m}$. A significantly higher threshold current density of $40\text{--}50\text{ kA/cm}^2$ is required or lasing at $\lambda = 10\text{ }\mu\text{m}$. The present analysis of carrier transport and optical loss in the mid- and far-infrared wavelengths demonstrates the feasibility of using current injection resonant tunnelling QW structures to realize semiconductor lasers based on intersubband transitions.

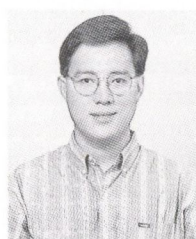
It is considered that the present model gives a useful prescription of the microscopic processes which determine the conditions for population inversion in intersubband semiconductor lasers. Incorporation of optical losses into the theoretical model underlines the challenge which remains to be faced in order to attain low-threshold devices. Attention now needs to be given to device design aspects which may serve to mitigate optical losses and thence assist in the implementation of practical room-temperature mid- and far-infrared semiconductor lasers.

REFERENCES

- [1] G.N. Henderson, T.K. Gaylord, E.N. Glytsis, E. Anemogianis, L.C. West, C.W. Roberts, and M.T. Asom: "Nanostructure optical emitters based on quasibound electron energy levels", *Microelectronics Journal*, 24, 805-816 (1993).
- [2] J. Faist, F. Capasso, C. Sirtori, D.L. Sivco, A.L. Hutchinson, S.N.G. Chu, and A.Y. Cho: "Quantum-well intersubband electroluminescent diode at $\lambda = 5\text{ }\mu\text{m}$ ", *Electron. Lett.*, 29, 2230-2231 (1993).
- [3] J. Faist, F. Capasso, C. Sirtori, D.L. Sivco, A.L. Hutchinson, and A.Y. Cho: "Quantum cascade laser: an intersubband semiconductor laser operating above liquid nitrogen temperature", *Electron. Lett.*, 30, 865-866 (1994).
- [4] L.C. West and S.J. Eglash: "First observation of an extremely large-dipole infrared transition within the conduction band of a GaAs quantum well", *Appl. Phys. Lett.*, 46, 1156-1158 (1985).
- [5] R.F. Kazarinov and R.A. Suris: "Possibility of the amplification of electromagnetic waves in a semiconductor with a superlattice", *Sov. Phys. Semicond.*, 5, 707-709 (1971).
- [6] B.F. Levine: "Device physics of quantum well infrared photodetectors", *Semicond. Sci. Technol.*, 8, S400-S405 (1993).
- [7] M. Helm, P. England, E. Colas, F. Derosa, and S. J. Jr. Allen: "Intersubband emission from semiconductor superlattices excited by sequential resonant tunnelling", *Phys. Rev. Lett.*, 63, 74-77 (1989).
- [8] H.C. Liu: "A novel superlattice infrared source", *J. Appl. Phys.*, 63, 2856-2858 (1988).
- [9] K.L. Wang and P.F. Yuh: "Theory and applications of band-aligned superlattices", *IEEE J. Quantum Electron.*, 25, 12-19 (1989).
- [10] S.I. Borenstain and J. Katz: "Evaluation of the feasibility of a far-infrared laser based on intersubband transitions in GaAs quantum wells", *Appl. Phys. Lett.*, 55, 654-656 (1989).
- [11] Q. Hu and S. Feng: "Feasibility of far-infrared lasers using multiple semiconductor quantum wells", *Appl. Phys. Lett.*, 59, 2923-2925 (1991).
- [12] A. Kastalsky, V.J. Goldman, and J.H. Abeles: "Possibility of infrared laser in a resonant tunnelling structure", *Appl. Phys. Lett.*, 59, 2636-2638 (1991).
- [13] K.M. Lau and W. Xu W: "Optically pumped submillimeter wave semiconductor lasers", *IEEE J. Quantum Electron.*, 28, 1773-1777 (1992).
- [14] G. Sun and J.B. Khurgin: "Optically pumped four-level infrared laser based on intersubband transitions in multiple quantum wells: feasibility study", *IEEE J. Quantum Electron.*,

29, 1104-1111 (1993).

- [15] W.M. Yee, K.A. Shore, and E. Schöll: "Carrier transport and intersubband population inversion in coupled quantum wells", *Appl. Phys. Lett.*, 63, 1089-1091 (1993).
- [16] W.M. Yee and K.A. Shore: "Threshold current density calculations for far-infrared semiconductor lasers", *Semicond. Sci. Technol.*, 9, 1190-1197 (1994).
- [17] R.E. Kunz and E. Schöll: "Bistability and negative photoconductivity in optically induced real-space transfer", *Phys. Rev. B*, 47, 4337-4347 (1993).
- [18] A. Seilmeier, H.J. Hübner, M. Wörner, G. Abstreiter, G. Weimann, and W. Schlapp: "Direct observation of intersubband relaxation in narrow multiple quantum well structures", *Solid-State Electron.*, 31, 767-770 (1988).
- [19] J. Faist, F. Capasso, G. Sirtori, D.L. Sivco, A.L. Hutchinson, S.N.G. Chu, and A.Y. Cho: "Measurement of the intersubband scattering rate in semiconductor quantum wells by excited state differential absorption spectroscopy", *Appl. Phys. Lett.*, 63, 1354-1356 (1993).
- [20] R. Ferreira and G. Bastard: "Evaluation of some scattering times for electrons in unbiased and biased single and multiple quantum well structures", *Phys. Rev. B*, 40, 1074-1086 (1989).
- [21] D.Y. Oberli, D.R. Wake, M.V. Klein, T. Henderson, and H. Morkoc: "Intersubband relaxation of photoexcited hot carriers in quantum wells", *Solid State Electron.*, 31, 413-418 (1988).
- [22] J. Faist, C. Sirtori, F. Capasso, L. Pfeiffer, and K.W. West: "Phonon limited intersubband lifetimes and linewidths in a two-dimensional electron gas", *Appl. Phys. Lett.*, 64, 872-784 (1994).
- [23] E.D. Palik (editor): *Handbook of Optical Constants of Solid*, Orlando: Academic Press (1985).



Wai Mun Yee received the B.Eng. degree in electronic and communication engineering in 1990 from the University of Bath, UK, where he has just completed his PhD degree. He spent a year working as a communication engineer in Intel Technology, Malaysia before continuing his postgraduate studies. His thesis work has involved the theory of FM semiconductor lasers, multiwave mixing and wavelength tuning in

semiconductor lasers, and analysis of the conditions for population inversion and lasing in intersubband semiconductor lasers. He is the principal author of 16 international journal and conference papers.



K. Alan Shore graduated in mathematics from the University of Oxford, England and obtained a PhD at University College, Cardiff, Wales, UK. His thesis work was concerned with the electrical and optical properties of double-heterostructure semiconductor lasers. He was a lecturer at the University of Liverpool (1979-1983) and then at the University of Bath where he became a Senior Lecturer in 1986 and

Reader in 1990. His work has been in the area of optoelectronic device modelling and design with particular emphasis on nonlinearities in laser diodes and semiconductor optical waveguides. He has authored or co-authored about 190 contributions to professional journals, books and conferences. He co-founded and acts as Organizer and Programme Committee Chair for the international conference on Semiconductor and Integrated Optoelectronics (SIOE) held annually in Cardiff, Wales, UK. He is member of the Quantum Electronics Committee of the Institute of Physics, UK. He was a visiting researcher in the USA, in Japan, in the Netherlands, in Denmark and in Spain respectively. His current research interests include multiwave mixing and harmonic generation in semiconductor lasers, intersubband semiconductor lasers, vertical cavity semiconductor lasers and dynamical properties of semiconductor nonlinear optical waveguides.

THE Y-LASER AS A MULTIFUNCTIONAL DEVICE FOR PHOTONIC SWITCHING

D. BAUMS, K. DÜTTING, O. HILDEBRAND, W. IDLER
E. LACH, G. LAUBE, M. SCHILLING, and K. WÜNSTEL

ALCATEL SEL AG RESEARCH CENTRE
OPTOELECTRONIC COMPONENTS DIVISION ZFZ/WO
LORENZ STR. 10, D-70435 STUTTGART, GERMANY

The Y-laser was originally invented for use as a tunable light source. Since that time it has demonstrated its capabilities not only with respect to wide and fast wavelength tuning. Additionally it has been shown that this type of interferometric laser is well suited for multiple photonic switching operations. These are wavelength translation from one fibre optic transmission window to another, wavelength conversion from one wavelength channel to another inside one transmission window and space switching. Those switching operations are likely to be used in future high capacity all-optical fibre trans-switching systems. In this paper recent results obtained with the technologically simple Y-laser structures are reviewed. We address the topics of interest such as the achievable tuning range of over 50 nm, the resulting conversion span and the conversion speed up to 5 Gb/s with signal regeneration capabilities. The transparency for 10 Gb/s signal and the packet switching capability is presented. Further functions of the device demonstrated include bistable wavelength and intensity operation for memory applications and short pulse generation. The Y-laser is thus a multifunctional device that can serve different photonic switching purposes with a basic technologically simple structure.

1. INTRODUCTION

In future, fibre-optic communication systems will have more complex system architectures than just point-to-point links. The aim is an optically transparent network which implies switching of data streams without conversion between optical and electrical carrier [1].

Optoelectronic InP based components do follow this trend and evolve from optoelectronic converters (laser-diodes, light emitting diodes, PIN detectors, APD detectors) to photonic switching and processing devices (amplifiers, gates, filters, switches, splitters, combiners, multiplexers, demultiplexers). The processing capabilities of the future optoelectronic components will have to include time, space, and wavelength dimensions [2]. For the time domain delay lines are being used because of a lack of optical memories which are far from being practical in spite of many optically bistable effects investigated. The realization of a true optical memory is still an intense research object.

Much progress has been made in the area of space switches based on LiNbO₃ and InP [3] and first products are already available. The light experiences relatively high losses in passive devices. Integration of amplifiers or use of active devices helps to overcome this problem. The Y-laser is inherently suited for lossless space switching because of its Y-branch structure.

The extra dimension available for optical transmission and processing is the wavelength domain. It adds more bandwidth for the transmission when wavelength division multiplexing (WDM) is used and reduces the need for optical memory in switching systems [4]. The basic component is a wavelength tunable light source. Monolithic and fast tunable devices are preferred.

There have been different approaches to monolithic wavelength tuning like interferometric lasers, multisegment DBR lasers [5] and transversal coupling devices like TTG [6] and VCF [7] lasers. Interferometric lasers have been investigated for a long time [8]. Two examples of this type of lasers are the C3 laser [9] and the Y-laser [10]. Derived from the basic component, the tunable Y-laser, is the monolithic wavelength converter Y-laser which changes the wavelength of an incoming light data stream to another one for the outgoing data stream. Simultaneous regeneration of pulses is desired for maintaining the signal quality (without an electronic regenerator which makes optoelectronic conversion necessary). Tunable multisegment DBR [11] and Y-lasers [4] have been successfully employed for wavelength conversion.

This article will give a comprehensive review of the work performed in exploiting the Y-laser. Special emphasis will be given on the tuning and wavelength conversion characteristics. The Y-laser can advantageously be used for the tuning and conversion as well as the space switching task with only minor modifications (for space switching e.g. an antireflection coating is appropriate). Furthermore the Y-laser has shown capabilities of short pulse generation and bistable operation giving the possibility of a wide use of the same basic simple structure.

2. THE STRUCTURE OF THE Y-LASER

The Y-laser consists of two Fabry-Perot lasers coupled together by a common part. The splitting of the light into the two sub-resonators is done with a Y-shaped branch. A schematic drawing is shown in Fig. 1. The device thus has three ports and needs no gratings. The typical length of the finished Y-laser devices is 1.5 mm. The structure is divided into four electrically separated segments. Wavelength selection is accomplished by the interferometric effect introduced by the optical path length difference in the two parallel arms. This can be made by a geometrical difference or by different driving conditions changing the effective index of refraction via the bandfilling effect.

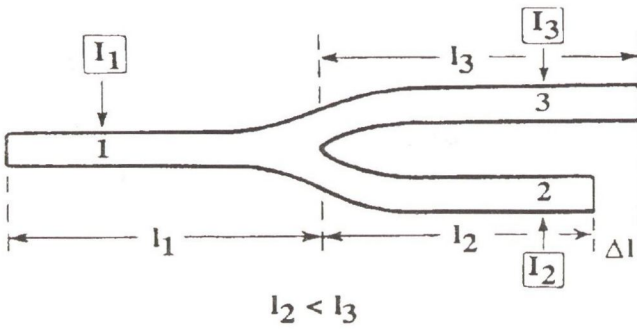


Fig. 1. Schematic drawing of the Y-laser with three arms as treated in the theoretical part (part 3)

3. THEORETICAL TREATMENT

The oscillation wavelength of the interferometric laser must obey a self consistency condition. The amplitude and phase of the wave must match after one roundtrip. In the case of the Y-laser this reads

$$P_1^2 R_1 (1/2(P_2^2 R_2) + 1/2(P_3^2 R_3)) = 1. \quad (1)$$

R_i are the facet reflection coefficients for the three ports and P_i are the propagation factors

$$P_i = \exp(\Gamma g_i l_i) * \exp(2\pi j n_i l_i / \lambda) \quad (2)$$

in the laser arms between the branching point and the corresponding facet according to Fig. 1. The extra electrical segment for the branching point is contained in the effect of the common segment P_1 . The l_i are the arm lengths, g_i are gain coefficients and n_i the indices of refraction, $L_i = n_i l_i$ are the optical path lengths and $G_i = \exp(\Gamma g_i l_i)$ the gain factors. Separation of the real and imaginary part gives two equations which have to be solved simultaneously [12]. This implies either the spacing of the allowed modes of the combined Fabry-Perot (FP) cavities

$$\Delta \lambda_{FP} = \lambda^2 / (2L_1 + L_2 + L_3) \quad (3)$$

and an interferometric modulation of the Mach-Zehnder type

$$4A^2(\lambda) = 1 / [G_1^4 * G_2^4 * \cos^2((2\pi/\lambda) * (L_2 - L_3))] \quad (4)$$

which has minima with a spacing of

$$\Delta \lambda_{MZ} = \lambda^2 / (2(L_2 - L_3)). \quad (5)$$

The combined filter curve is the superposition of the Fabry-Perot resonance filter and the Mach-Zehnder (MZ) filter together with the gain curve.

The emission wavelength will be the one in the minimum of the combined filter loss curve (Fig. 2). The tuning behaviour is determined by the dependencies of the gains g_i and indices of refraction n_i on the currents I_i . Additionally, the gain peak wavelength shifts with the current. The dependencies have been modelled in [12] and yield step tuning behaviour with small steps $\Delta \lambda_{FP}$ in the order of 0.2 nm induced by variation of the currents into the parallel arms I_2 and I_3 and with larger steps $\Delta \lambda_{MZ}$ (e.g. 10 nm) caused by a change in the current into the common segment I_1 .

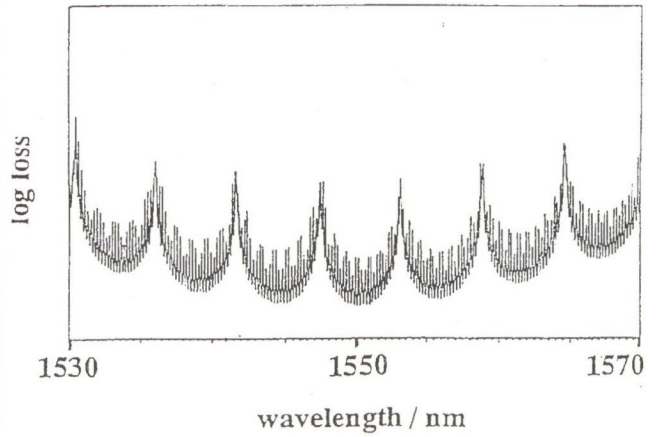


Fig. 2. Typical filter characteristic of the Y-laser. The curve shows the combined loss of the MZ interferometer (broad structure) multiplied with the FP filter characteristic (closely spaced lines) and the gain curve of the material (parabolic curvature)

4. TECHNOLOGY OF THE Y-LASER STRUCTURE

The active layers of the Y-lasers consist of five quaternary quantum wells grown by LP MOVPE. The branched waveguide mesa is defined by a combined dry and wet etch step. Selective regrowth is done with iron-doped semiinsulating InP in a second LP MOVPE step forming a semiinsulating buried heterostructure (SIBH). The segments are defined by separating the metallization. The facets are finally introduced by cleaving or dry etching [13]. The final structure is depicted in Fig. 3. Only standard technological steps are needed to build up this interferometric laser structure. Threshold currents are 4 * 20 mA typically for 1.5 mm long devices. If three segments are prebiased appropriately a small additional current of 5 mA into the remaining one is sufficient to reach threshold.

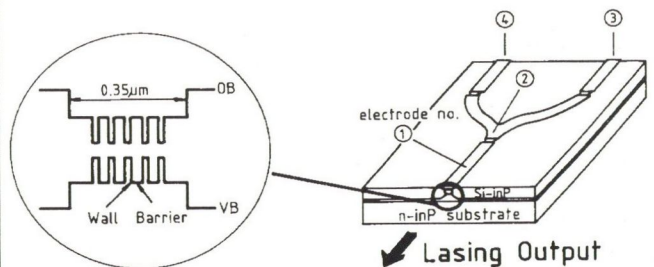


Fig. 3. Y-laser with SIBH (semiinsulating buried hetero-) structure and four electrically separated segments

5. TUNING CHARACTERISTICS

As outlined in section 3, there are two different ways of tuning with a single current. The first one shifts the MZ resonances with respect to the FP resonances and the second one shifts the gain maximum with respect to the MZ resonances. Both methods give step tuning behaviour with different step sizes.

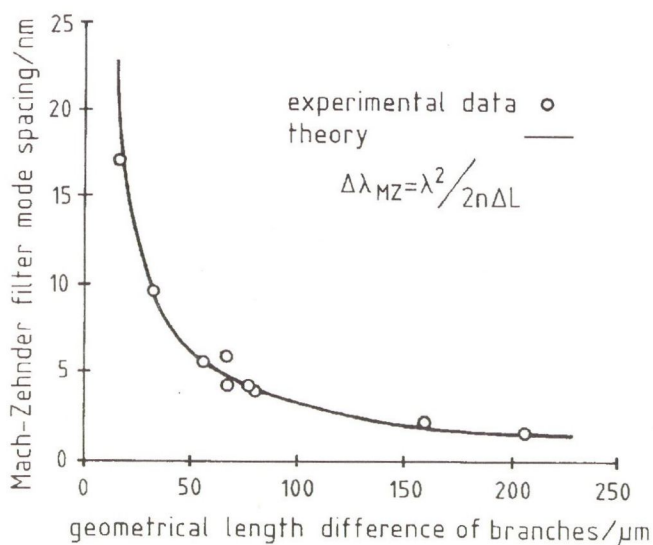


Fig. 4. Relationship between the MZ mode spacing and arm length difference. The symbols refer to measurements and the hyperbola represents the formula (5)

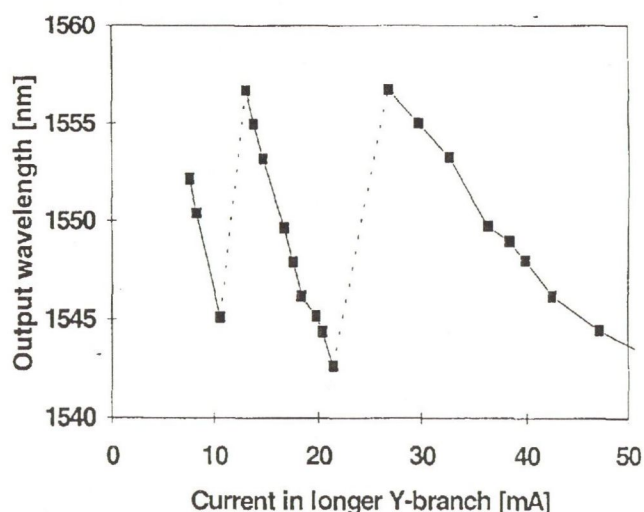
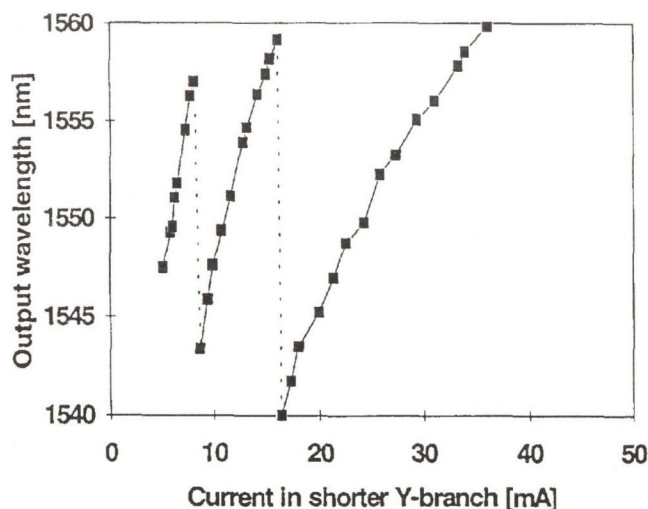


Fig. 5a. Tuning of a Y-laser by variation of the current injected into one of the parallel arms. Points are experimental data with SMSR > 20 dB

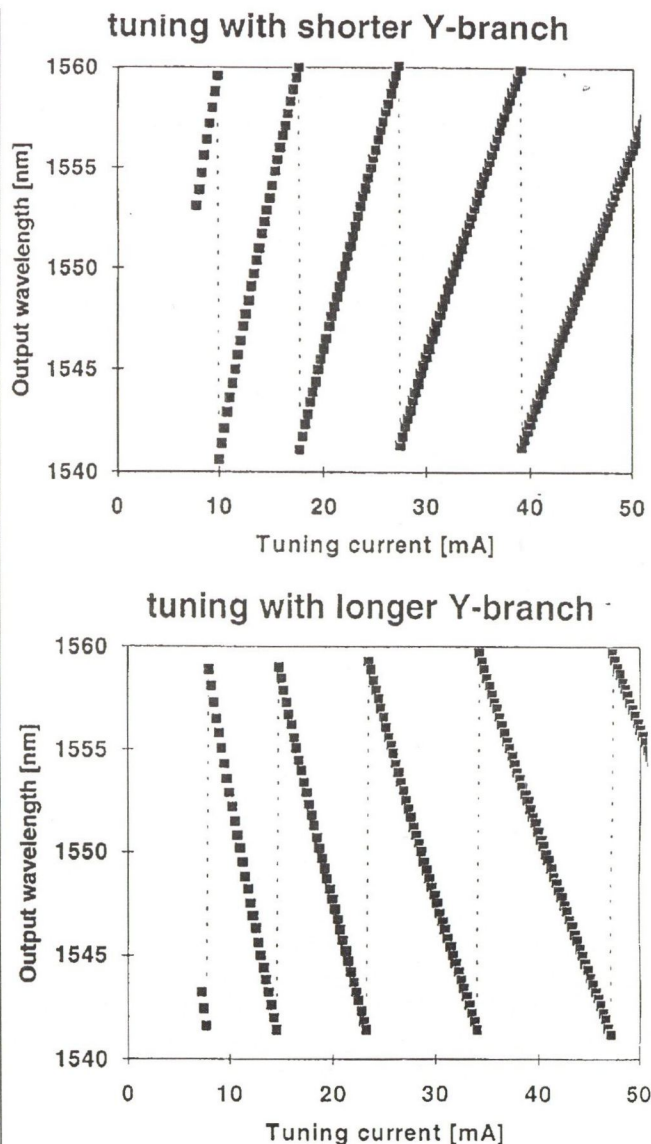


Fig. 5b. Theoretical prediction of tuning with a single current into one of the parallel arms of the Y-laser

In the first case the tuning range is limited by the MZ spacing $\Delta\lambda_{MZ}$ given by (5). By adjusting the optical geometrical arm lengths this range can be changed in a wide range (Fig. 4). When the MZ resonance closest to the gain maximum shifts out of the maximum the neighbouring MZ resonance shifts in and takes over the minimum loss condition at a certain current. The same tuning interval is then covered once again with higher currents. This behaviour has been observed multiple times (Fig. 5a) and compares well with the theory (Fig. 5b). Especially the reversal in tuning direction is seen for a change in arm used for tuning. 20 nm single current tuning has been achieved for $\Delta l = l_2 - l_3 = 16 \mu\text{m}$ recently [14].

Tuning by MZ spacings with the current into the common segment (second method) is limited by the possible shift in gain curve. A combined tuning (MZ and gain) can address every FP mode inside the gain tuning interval [12].

The MZ spacing is determined by the optical path length difference $\Delta L = L_2 - L_3$. Geometrical arm length

differences Δl from 0 μm (symmetrical Y) up to 200 μm have been realized and give the theoretically predicted hyperbolic dependence (5) of $\Delta\lambda_{MZ}$ versus Δl [15]. In the special case of the symmetric Y-laser (0 μm) a tuning range of 51 nm has been demonstrated (Fig. 6). Usually all four currents have to be adjusted in this case.

For system applications the switching speed is of great importance. Changing from one wavelength to another by the first tuning method needs 2 to 0.5 ns (rise and fall times) depending on the distance of the two switched wavelengths [16]. An intermediate mode is suppressed by at least an order of magnitude and is only visible in the time during switching.

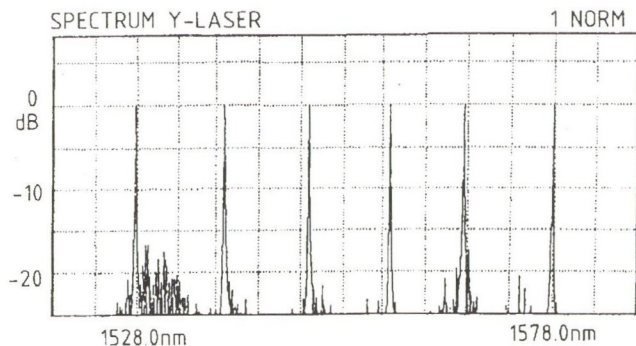


Fig. 6. 51 nm tuning span of a symmetrical Y-laser

6. WAVELENGTH TRANSLATION AND CONVERSION WITH Y-LASERS

With a Y-laser tuned to a specific wavelength optical signals can be transformed to this wavelength. In the case of wavelength translation the Y-laser is biased below threshold. An external short wavelength signal optically pumps the Y-laser to reach threshold. In the on-state the Y-laser emits the tuned wavelength. The absorption is not polarisation or wavelength sensitive so that transformation from e.g. 1310 nm multimode signal to 1561 nm single mode (Fig. 7a) is possible and has been demonstrated up to 155 Mb/s (Fig. 7b) [17]. A possible application is the connection of a LAN to a long distance transmission system.

In the case of wavelength conversion input and output wavelengths both lie in the 1.5 μm fibre window. Then the Y-laser emits at the tuned wavelength λ_{out} as long as the optical input signal is off. When the input signal at λ_{in} is exceeding a power limit of approximately $P_{in} = 200 \mu\text{W}$ the Y-laser is forced to lock on the injected wavelength λ_{in} [18]. There is a strong thresholding behaviour accompanying this effect (Fig. 8) which can be used for pulse reshaping. The conversion range is only limited by the tuning range and red and blue shift are possible within these limits. Conversion over 45 nm has been demonstrated [19] at 2.5 Gb/s. Since the device is optically triggered, device parasitics do not limit the operation speed. Operation at 5 Gb/s has been shown with BER down to 10^{-10} [20]. The extinction ratio is improved for small input extinction ratios. In Fig. 9 an example is shown for improvement from 4 : 1 to 10 : 1 during wavelength conversion over 8 nm.

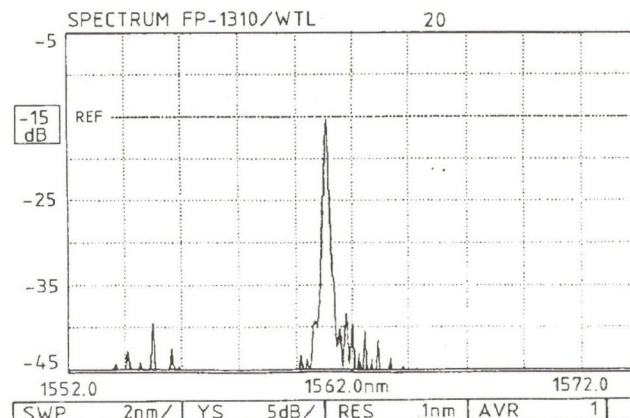
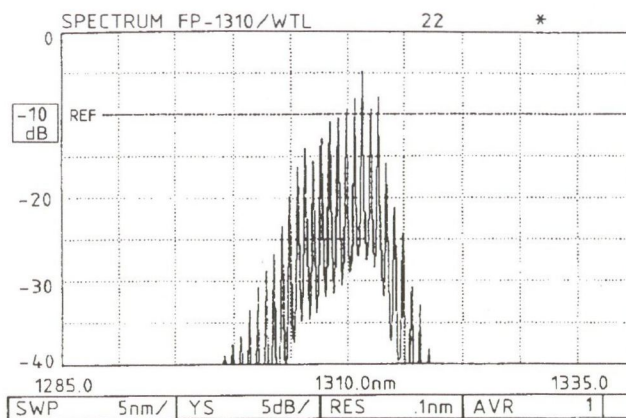


Fig. 7a. Wavelength transformation: 1310 nm Fabry-Perot spectrum of the injecting laser (top), and single mode emission spectrum of the Y-laser at 1561 nm (bottom). (Wavelengths/nm)

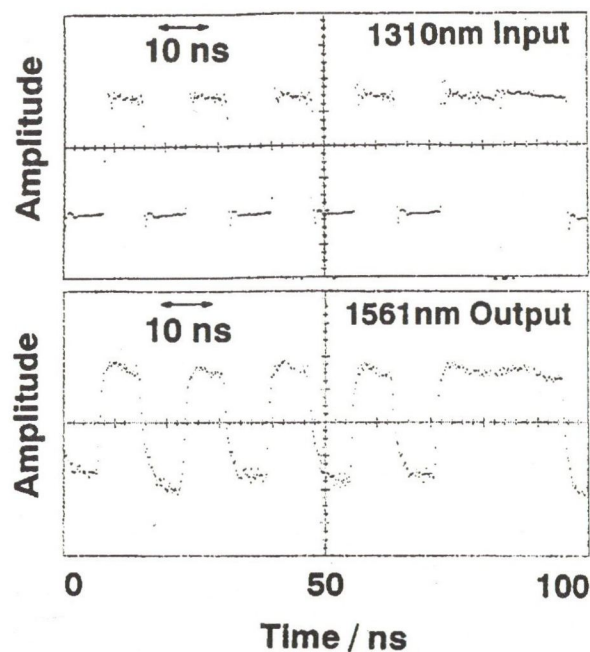


Fig. 7b. Dynamic wavelength transformation from $\lambda_{in} = 1310 \text{ nm}$ to $\lambda_{out} = 1561 \text{ nm}$. Upper trace is a 155 Mb/s data stream injected into the Y-laser, lower trace is the transformed data stream emitted by the Y-laser

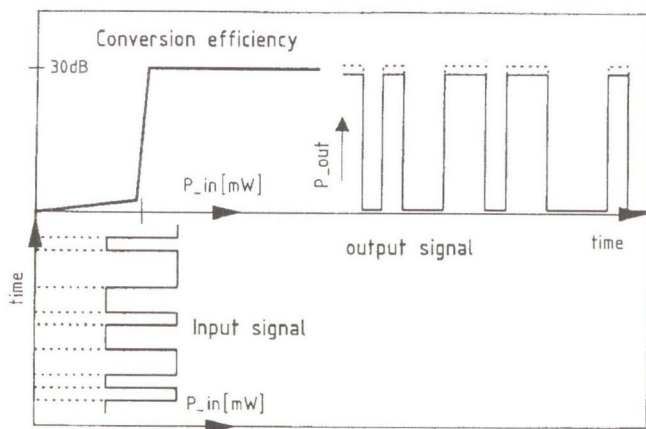


Fig. 8. Wavelength conversion: Power P_{out} of output wavelength of the Y-laser in dependence of the injected input power P_{in}

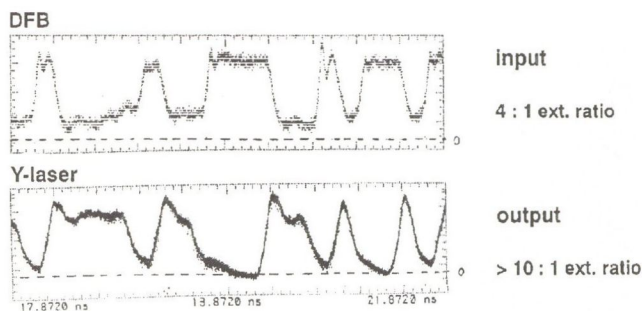


Fig. 9. Extinction ratio generation from 4:1 (top) to 10:1 (bottom) during wavelength conversion from 1566.8 nm (top) to 1558.8 nm (bottom)

7. MODULE

For easier handling tunable Y-lasers have been built into butterfly-type modules incorporating a thermoelectric cooler and a thermistor. The coupling of the facet of segment number 1 to a lensed fibre is done by laser welding technique. The layout of the module is presented in Fig. 10a together with the tuning ability. Six equidistant channels with 4 nm separation are tuned (Fig. 10b). The power in the fibre reaches up to -3 dBm [4].

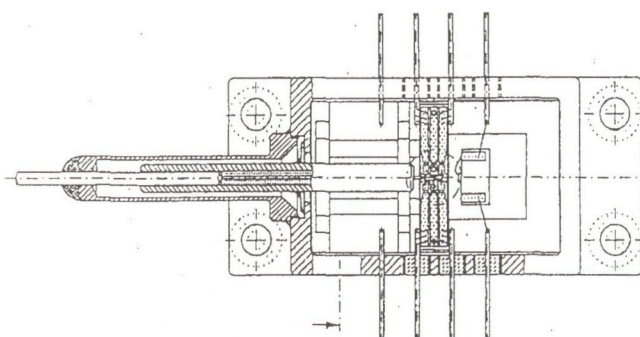


Fig. 10a. Layout of a single side coupled Y-laser module

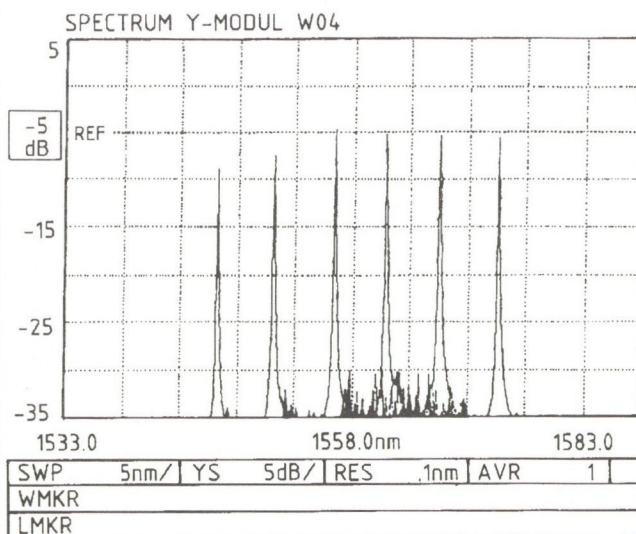


Fig. 10b. Tuning ability of a single side coupled Y-laser module

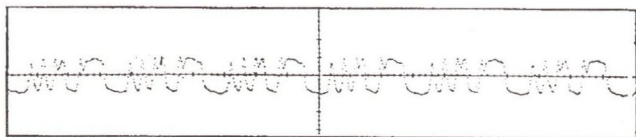
Even wavelength conversion can be performed with such a single side coupled Y-laser module. Input and output are coupled through a fibre splitter in a contradirectional way and are extracted by filters. In all four channels BER values below 4×10^{-10} have been measured [21]. This type of module is employed for the wavelength conversion in the multidimensional switching system [22]. Recently double side coupled modules have been realized [14].

8. SPACE SWITCHING

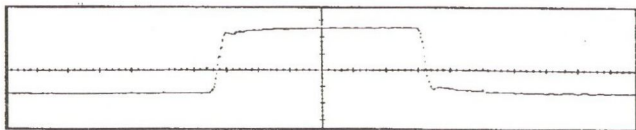
The branch incorporated in the Y-laser can favourably be used for space switching from one input port to two output ports or as a combiner in the reverse direction. The "laser" must then be driven below threshold like a semiconductor amplifier. The segments in the parallel arms of the Y serve as the gates when switched between absorption and transparency or gain. The gain of the common segments like the linear and the branching one serve for compensating part of the losses originating from coupling, reflection, absorption and splitting. The whole device has a gain large enough to over-compensate for the sum of the losses which is measured by the insertion loss. We have thus achieved net gain while switching signals through Y-structures. The switching contrast exceeds 30 to 40 dB with switching (gateing) currents of 30 mA [17]. Dynamic Operation is possible up to a speed of 1 Gb/s.

The light sent through the Y-laser can be a data stream up to a bitrate of 10 Gb/s. The Y-structure switch is transparent up to those bitrates. Gateing a data stream, e.g. 5 Gb/s, with a slower current signal, e.g. 155 Mb/s, performs the operation of packet switching which is shown in Fig. 11. Switching times are 0.5 ns which requires 2 bits as a guardband [23]. Integration of several Y-structures has been done by cascading. Two cascades yield a 1x4 splitter which has been presented in [24].

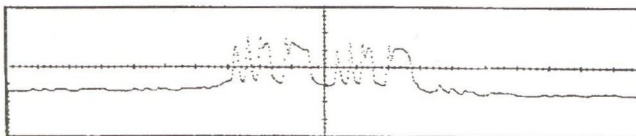
5 Gb/s OPTICAL INPUT PATTERN



155 Mb/s ELECTRICAL GATE SIGNAL



GATED 5 Gb/s OPTICAL OUTPUT PATTERN



0 10 20
Time / ns

Fig. 11. Packet switching of a 5 Gb/s data stream with a rate of 155 Mb/s selecting one packet

9. BISTABLE OPERATION

For optical memory applications bistability is a prerequisite. The Y-laser shows two different kinds of bistability. The first one is the intensity bistability induced by a saturable absorber segment. This absorber segment has been added to the common segment on the Y-laser and is voltage (reverse bias) controlled. The output intensity of the Y-laser switches discontinuously either by internally raising the photon density via the currents into the other segments (Fig. 12) or by injecting external light. Up to now there is only the possibility of electrical resetting.

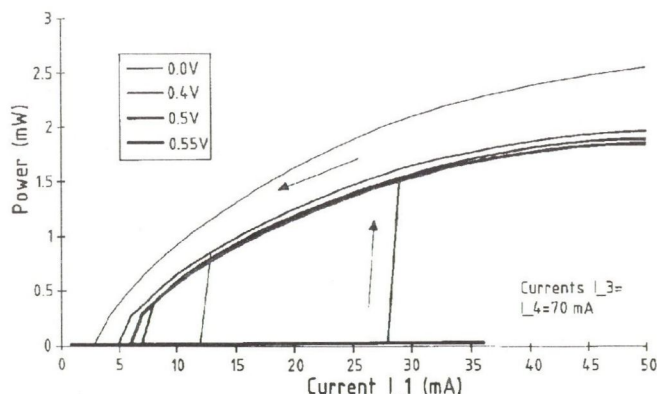
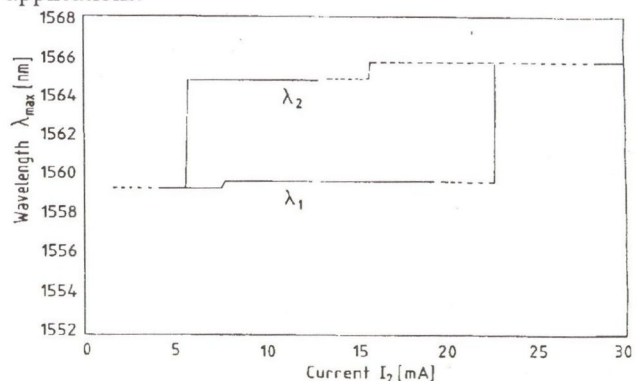


Fig. 12. Bistable intensity switching by current injection into segment number 1 of a Y-laser with an additional saturable absorber segment. Opening of the hysteresis loop is controlled by the reverse voltage on the saturable absorber segment

The other type of bistability is the wavelength bistability reported in [25]. A bistable loop with a width of 5.5 nm and 17 mA has been observed while changing the current into the branching segment (Fig. 13). The effect turns out to be of refractive origin. It is that fast that it can follow a modulation of up to 565 Mb/s. This is a new type of bistability offering the possibility of new types of switching

applications.



— Single Mode, SMSR ≥ 15dB --- Multimode, SMSR < 15dB

Fig. 13. Hysteresis loop of the emitted wavelength versus current into segment number 2. The other currents are held constant at $I_1 = 59$ mA, $I_3 = 28$ mA, $I_4 = 44$ mA

10. SHORT PULSE GENERATION WITH Y-LASERS

Y-lasers have additionally been employed for short pulse generation by mode-locking. In an external resonator configuration the devices were antireflection coated on the facet of the common segment. The residual reflectivity was estimated to be 10^{-4} , the length of the external resonator was 0.5 m corresponding to an inverse roundtrip time of 300 MHz. One segment of the laser was driven electrically with a signal from a comb generator or a sinusoid at this frequency. The shortest pulses observed were 18 ps for 1.3 μm devices and 23 ps for 1.5 μm devices (Fig. 14). The shortest time-bandwidth-product achieved 0.97 at 27 ps pulsewidth [26]. This result leaves a factor of three for improvement. There is a large variety of configurations which could be very interesting to investigate and might lead to the reductions in pulsewidth or bandwidth necessary to reach the physical limit of the time-bandwidth-limitation.

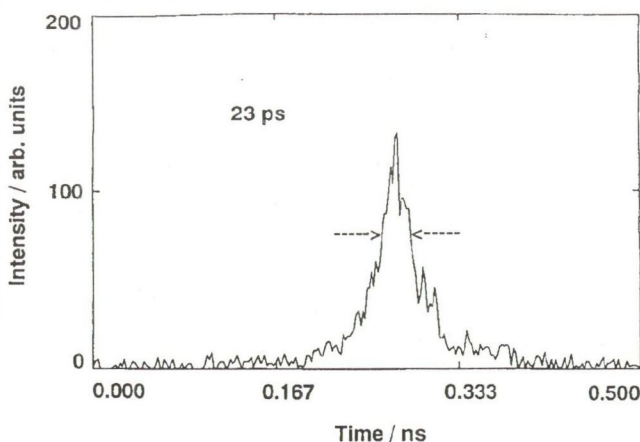


Fig. 14. Short pulses generated by the Y-laser by mode-locking in an external resonator at 1550 nm. The pulsedwidth is 23 ps

11. CONCLUSION

We have been reviewing the status of the capabilities of the multifunctional Y-laser device. We have shown the abilities of the Y-laser concerning wide and fast wavelength tuning and all-optical wavelength conversion. Further functions of the Y structure being presented

are wavelength translation, space and packet switching, bistable operation and short pulse generation. All features have been obtained with the same basic SIBH interferometric waveguide structure. Only minor modifications are needed for modifications towards one of the presented applications. We are thus able to cover different required functions of future all-optical trans-switching fibre systems with the same basic technologically simple device. A widespread use of such a multifunctional device will lead to cost reductions during implementation of future fibre networks.

12. ACKNOWLEDGEMENTS

We would like to thank all our colleagues at ALCATEL-

REFERENCES

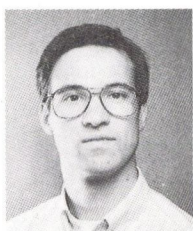
- [1] H.S. Hinton: "Architectural considerations for photonic switching networks", *IEEE J. Select. Ar. Comm.*, Vol. 6, pp. 1209-1226, 1988.
- [2] E.-J. Bachus: "Photonic switching — a keystone of multiplexed broadband communication systems", Proc. 16th ECOC'90, Amsterdam, pp. 739-747, 1990.
- [3] M. Erman: "InP Optoelectronic devices and photonic integrated circuits for high speed packet switching", invited paper, Topical Meeting on Photonic Switching '92, Minsk, 1992 and Proc. SPIE, Vol. 1807, pp. 295-306, 1993.
- [4] K. Wüstel, M. Schilling, W. Idler, G. Eilenberger, S. Bunse, W. Rehm: "Multidimensional optical switching with advanced key components", Proc. 19th ECOC'93, Montreux, CH, paper TuP3.4, pp. 89-92, 1993.
- [5] K. Kobayashi, I. Mito: "Single frequency and tunable laser diodes", *IEEE J. Lightwave Technol.*, Vol. LT-6, pp. 1623-1633, 1988.
- [5a] S. Murata, I. Mito, K. Kobayashi: "Tuning ranges for 1.5 μ m wavelength tunable DBR lasers", *Electron. Lett.*, Vol. 24, pp. 577-579, 1988.
- [6] M.-C. Amann, S. Illek, C. Schanen, W. Thulke, H. Lang: "Continuously tunable single-frequency laser diode utilising transverse tuning scheme", *Electron. Lett.*, Vol. 25, pp. 837-839, 1989.
- [7] R.C. Alferness, U. Koren, L.L. Buhl, B.I. Miller, M.G. Young, T.L. Koch, G. Raybon, C.A. Burrus: "Broadly tunable InGaAsP/InP laser based on a vertical coupler filter with 57 nm tuning range", Topical Meeting on Integrated Photonics Research '92, New Orleans, LA, USA, 1992.
- [8] S. Wang, H.K. Choi, I.H.A. Fattah: "Studies of semiconductor lasers of the interferometric and ring types", *IEEE J. Quantum Electron.*, Vol. QE-18, pp. 610-617, 1982.
- [8a] I.H.A. Fattah, S. Wang: "Semiconductor interferometric laser", *Appl. Phys. Lett.*, Vol. 41, pp. 112-114, 1982.
- [9] S.W. Corzine, L.A. Coldren, C.A. Burrus, T.L. Koch: "Continuous tunability in three-terminal coupled-cavity lasers", *Appl. Phys. Lett.*, Vol. 48, pp. 1190-1192, 1986.
- [10] M. Schilling, H. Schweizer, K. Dütting, W. Idler, E. Kühn, A. Nowitzki, K. Wüstel: "Widely tunable Y-coupled cavity integrated interferometric injection laser", *Electron. Lett.*, Vol. 26, pp. 243-244, 1990.
- [11] P. Ottolenghi, A. Jourdan, J. Jacquet: "All-optical wavelength conversion with extinction ratio enhancement using a tunable DBR laser", Proc. 19th ECOC'93, Montreux, CH, paper TuC5.5, pp. 141-144, 1993.
- [12] K. Dütting, O. Hildebrand, D. Baums, W. Idler, M. Schilling, K. Wüstel: "Analysis and simple tuning scheme of asymmetrical Y-lasers", *IEEE J. Quantum Electron.*, Vol. 30, pp. 654-659, 1994.
- SEL Research Center who contributed to the work, especially K. Daub, T. Feeser, G. Luz and A. Nowitzki. State-of-the-art antireflection coatings have been provided by J. Sacher Lasertechnik, Marburg. We thank the group for Solid State Electronics, particularly E. O. Göbel, W. Elsässer and M. Hofmann, of the University of Marburg for the possibility to do mode-locking experiments at their facility. The work was financially supported in part by the German Minister for Research and Technology within two projects: TK0440 (tunable light source), as a part of an R&D project of the Heinrich-Hertz-Institute fuer Nachrichtentechnik GmbH, Berlin, and 01 BS211/1, as a part of the German Joint Research Program on Optical Signal Processing. Further financial support in part is by the RACE 2039 ATMOS project of the European Community.
- [13] M. Schilling, K. Daub, E. Lach, G. Laube: "Tunable Y laser with reactive ion etched mirror facets suitable for integration", 6th Int. Conf. on InP and Rel. Mat., Santa Barbara, CA, USA, paper MC3, March 1994.
- [14] E. Lach, D. Baums, K. Daub, K. Dütting, T. Feeser, W. Idler, G. Laube, G. Luz, M. Schilling, K. Wüstel, O. Hildebrand: "20 nm single current tuning of asymmetrical Y-lasers", Proc. 20th ECOC'94, Florence, I, paper We. P8, 1994.
- [15] M. Schilling, K. Dütting, W. Idler, D. Baums, G. Laube, K. Wüstel, O. Hildebrand: "Asymmetrical Y-laser with simple single current tuning response", *Electron. Lett.*, Vol. 28, pp. 1698-1699, 1992.
- [16] W. Idler, D. Baums, E. Lach, G. Laube, M. Schilling, K. Wüstel: "Ultra-fast wavelength tuning and wavelength conversion with strained MQW Y lasers", Proc. Topical Meeting on Photonics in Switching, Palm Springs, CA, USA, paper PWC3, March 1993.
- [17] K. Wüstel, W. Idler, M. Schilling, G. Laube, D. Baums, O. Hildebrand: "Y-shaped semiconductor device as a basis for various photonic switching applications", Proc. Optical Fiber Conference '92, San José, CA, USA, p. 125, 1992.
- [18] M. Schilling, W. Idler, D. Baums, G. Laube, K. Wüstel, O. Hildebrand: "Multifunctional photonic switching operation of 1500 nm Y-coupled cavity laser (YCCL) with 28 nm tuning capability", *IEEE Photon. Technol. Lett.*, Vol. 3, pp. 1054-1057, 1991.
- [19] M. Schilling, W. Idler, D. Baums, K. Dütting, G. Laube, K. Wüstel, O. Hildebrand: "6 THz tunable 2.5 Gb/s frequency conversion by a multiquantumwell Y laser", *IEEE J. Quantum Electron.*, Vol. 29, pp. 1835-1843, 1993.
- [20] E. Lach, D. Baums, K. Daub, T. Feeser, W. Idler, G. Laube, G. Luz, M. Schilling, K. Wüstel: "5 Gb/s wavelength conversion with simultaneous regeneration of extinction ratio using Y-lasers", Proc. 19th ECOC'93, Montreux, CH, paper TuC5.4, pp. 137-140, 1993.
- [21] E. Lach, D. Baums, K. Daub, W. Idler, G. Laube, M. Schilling, K. Wüstel: "High performance features of all-optical lambda-conversion with Y-lasers", Topical Meeting on Integrated Photonics Research, San Francisco, CA, USA, paper FC3, 1994.
- [22] D. Böttle, G. Eilenberger, K. Lösch, W. Rehm, K. Wüstel, M. Schilling: "System approach for a photonic multidimensional switching technique", *IEEE Int. Conf. on Communications (ICC'93)*, Geneva, CH, May 1993.
- [23] W. Idler, M. Schilling, G. Laube, D. Baums, K. Wüstel, O. Hildebrand: "High speed wavelength and spatial switching with a YCCL", Topical Meeting on Photonic Switching '91, Salt Lake City, UT, USA, paper FC1, 1991.
- [24] M. Schilling, D. Baums, K. Daub, W. Idler, E. Lach, G. Laube, K. Wüstel: "Progress in Y laser technology:

Towards application specific designs", 5th Int. Conf. on InP and Rel. Mat., Paris, F, invited paper WD1, pp. 509-512, 1993.

- [25] D. Baums, M. Schilling, W. Idler, G. Laube, K. Wünnstel: "Observation of wavelength-bistability in the interferometric Y-laser", Topical Meeting on Photonic Switching '92, Minsk,

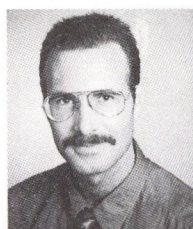
1992 and Proc. SPIE Vol. 1807, pp. 494-499, 1993.

- [26] M. Hofmann, D. Baums, J. Sacher, W. Elsässer, M. Schilling, W. Idler, K. Wünnstel, E. Zielinski, O. Hildebrand: "Mod-
elocking of interferometric Y-lasers in an external cavity",
IEEE Photon. Technol. Lett. Vol. 7, pp. 1135-1137, 1993.



Dieter Baums received the Diploma degree in physics in 1986 at the Technical University in Munich and the Justus-Liebig-University in Giessen. His work dealt with noise properties of superconducting microbridges. During his Ph.D. thesis he was working on nonlinear dynamics and mode-locking of semiconductor lasers. He received the Ph.D. from Philipps-University of Marburg, in 1990.

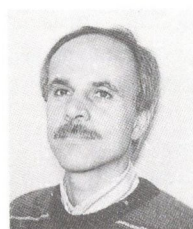
Since then he is in the Optoelectronic Components Division of the SEL Research Center, Stuttgart, working on standard lasers, tunable lasers and photonic integrated devices.



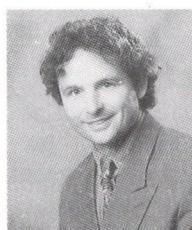
Kaspar Dütting received the Diploma degree in physics at the University of Tübingen in 1986. In 1986 he joined the SEL Research Center, Stuttgart, where he is engaged in the design and realization of high-performance laser structures.



Olaf Hildebrand received Dipl.-Phys. degree in 1973 and a Ph.D. in 1977, both from University of Stuttgart, denoted with 'summa cum laude'. His thesis was dealing with basic research on GaAs and InP based lasers. In 1978 he changed to PIN and avalanche photodetectors based on GaSb and InP. In 1983 he joined the SEL Research Center in Stuttgart where, since 1985, he has been head of the Optoelectronic Components Division.



Wilfried Idler received the Diploma degree in physics in 1987 at the University of Stuttgart. In 1987 he joined the SEL Research Center, Stuttgart, where he was primarily engaged in noise investigations of DFB lasers. Currently his main activities are modelling and characterization of photonic integrated devices.



Eugen Lach received the Diploma degree in physics in 1986 at the University of Stuttgart. In 1991 he received the Ph.D. degree from the University of Stuttgart. In 1992 he joined the SEL Research Center in Stuttgart, where he was primarily engaged in the investigation of Y-lasers and electro-absorption modulators. Currently he is mainly involved in modelling of DFB lasers and the design and characterization

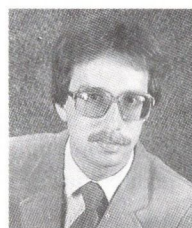
of photonic integrated devices for optical communication and switching.



Gert Laube received the Diploma degree in chemistry in 1983 from the University of Ulm and, in 1988, the Ph.D. degree from the University of Stuttgart. In 1988, he joined the SEL Research Center, Stuttgart, where he is working on MOVPE of discrete and integrated laser structures.



Michael Schilling received the Diploma degree in physics from the University of Erlangen-Nürnberg, in 1982. In 1983, he joined the SEL Research Center, Stuttgart, where he has been involved in III-V epitaxy and development of various optoelectronic components based on InP. Currently, he is engaged in design and processing technologies of photonic integrated devices for optical communications and switching.



Klaus Wünnstel received the physics Diploma in 1979 from the University of Karlsruhe. From 1979 to 1983 he was engaged in electrical and optical analysis of Si- and II-VI semiconductors at the Max-Planck-Institute for Solid State Research in Stuttgart. In 1982, he received the Ph.D. at the University of Stuttgart. He joined the Research Center of SEL in 1983, where he has been involved in research and development of InP-based optoelectronic devices. His main research areas are high-speed, dynamic single mode lasers, wavelength tunable lasers, and laser integration. In 1986, he became responsible for laser device technology. Since 1989 he is manager of the laser processing group of the Optoelectronic Components Division.

development of InP-based optoelectronic devices. His main research areas are high-speed, dynamic single mode lasers, wavelength tunable lasers, and laser integration. In 1986, he became responsible for laser device technology. Since 1989 he is manager of the laser processing group of the Optoelectronic Components Division.

NONLINEAR OPTICAL PHENOMENA IN SEMICONDUCTOR LASERS AND AMPLIFIERS: PHYSICS AND APPLICATIONS

W. ELSÄSSER

PHILIPPS-UNIVERSITÄT MARBURG
FACHBEREICH PHYSIK UND WISSENSCHAFTLICHES ZENTRUM FÜR MATERIALWISSENSCHAFTEN
RENTHOF 5, D-35032 MARBURG, GERMANY

Within the framework of nonlinear optics we present and discuss data of intracavity four-wave mixing within the active volume of semiconductor lasers and amplifiers and demonstrate both, their importance for an understanding of the fundamental nonlinear and ultrafast processes in semiconductor waveguide devices and their potential for photonic applications.

1. INTRODUCTION

More than 30 years after the first realization of semiconductor laser operation in 1962 the semiconductor laser has developed to a high technological and sophisticated optoelectronic device. The application oriented development of laser technology has been accompanied by the investigation of many basic principles and physical problems.

The present article will discuss some selected problems within the area of nonlinear optical phenomena in semiconductor lasers and amplifiers with particular emphasis on photonic applications. We would like to review some of the recent progress of Four-Wave Mixing (FWM) in active and passive semiconductor waveguides, i.e. in semiconductor lasers and amplifiers. First we discuss three topics of FWM in lasers, both with the aspects of applications as well as fundamental physics. The first being the highly efficient nonlinear optical process of the generation of new frequencies for photonic applications which is considered with respect to efficiency and microscopic origin including the study of polarization dependence and the third order susceptibility of low dimensional carrier systems. The second topic will be the optical bistability and the nearly degenerate four-wave mixing in a GaAlAs laser under intermodal injection. And third, noncollinear interaction in broad area devices is illustrated and discussed with the potential of beam steering and spatial switching, again with the aspects of photonic potential.

Finally, highly degenerate FWM in amplifiers with frequency detuning of the interacting fields in the THz regime, are discussed to understand from the view point of ultrafast intraband dynamics of semiconductors, both, the physical processes involved in the modulation response and FWM properties of semiconductor lasers and the cross talk between multiplexed signals in semiconductor amplifiers.

2. NONLINEAR OPTICAL FOUR-WAVE MIXING IN SEMICONDUCTOR LASERS AND AMPLIFIERS

2.1. Nearly degenerate cascade FWM mixing in lasers

Investigations in the field of nonlinear optics ran parallel to the developments and progress in lasers. In particular intracavity process represent a very elegant and effective technique due to the combination of nonlinear and amplifying medium at once. The basic description of nonlinear optics relies on an expansion of the polarization P according to powers of the electric field E

$$P = \epsilon_0 \chi^{(1)} E + \epsilon_0 \chi^{(2)} E^2 + \epsilon_0 \chi^{(3)} E^3. \quad (1)$$

The relevant coefficients are the nonlinear susceptibilities $\chi^{(n)}$ of the order n .

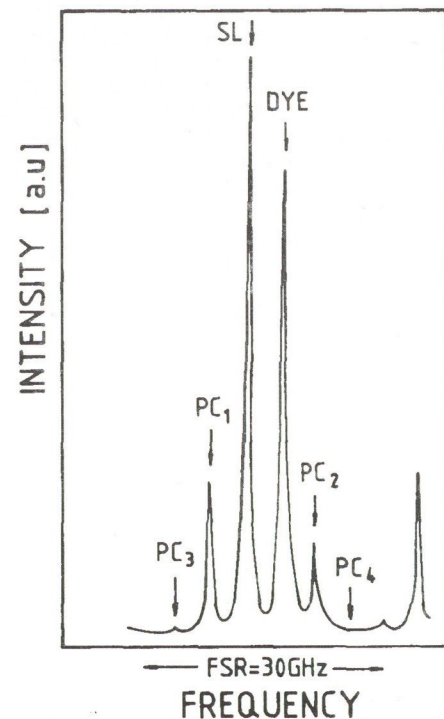


Fig. 1. Optical spectrum of a four-wave mixing process in a semiconductor laser in a Fabry-Perot interferometer depiction

A very efficient intracavity nonlinear optical process is four-wave mixing within the semiconductor laser cavity [1], [2], [3]. Light from a second laser source (e.g. a dye laser or another semiconductor laser) at frequency ω_2 is coupled into the active region of the semiconductor laser which operates at frequency ω_1 . These frequencies interact and generate new frequency $\omega_1 \pm (\omega_2 - \omega_1)$ which can be spectroscopically detected. An experimental result obtained by Fabry-Perot spectroscopy is shown in Fig. 1.

Obviously, not only the primarily generated signals at $\omega_1 \pm (\omega_1 - \omega_2)$ and $\omega_2 \pm (\omega_2 - \omega_1)$ are resolved but also new generated frequencies at multiple detunings, signals denoted by PC_3 and PC_4 which can be understood as result of a so-called cascade FWM process by which the new generated fields themselves interact with the fundamental ones [4].

Systematic studies have been performed in order to clarify the basic underlying mechanism of this high efficient intracavity FWM process [5]. First, the dependence of the third order susceptibility, derived from the experimental data and applying Eq. (1), on the intensity of the injected light $I_2 (= I_{Dye})$ has been investigated. This result is shown in Fig. 2. Obviously, $\chi^{(3)}$ decreases with increasing intensity (I_{Dye}). This observed behaviour reflects the decreasing carrier concentration N depopulated by the increased stimulated emission and has been modelled by the rate equations. Consequently, $\chi^{(3)}$ is a function of N (and $h\omega$).

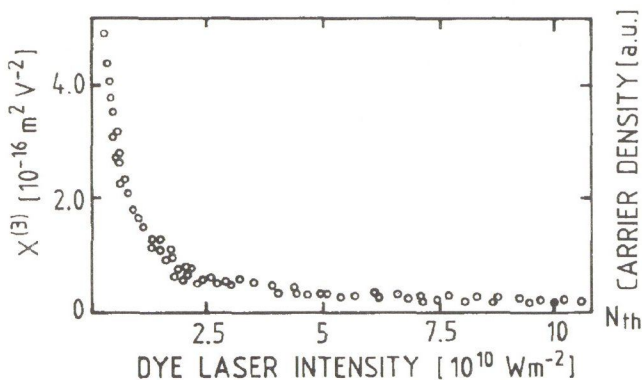


Fig. 2. Measured dependence of the third order susceptibility $\chi^{(3)}$ on the injected laser intensity

Second, the detuning frequency dependence has been studied (Fig. 3). The observed spectra can be classified as follows:

- For detunings above 1 GHz, the FWM process occurs, with generated sidebands determined by the detuning frequency.
- For detunings below 1 GHz, sidebands at a constant separation, corresponding to the relaxation resonance frequency appear, independent of the detuning.

These observations demonstrate that in both cases the excitation is related to the inverted carrier system. The system responds with its characteristic eigen frequency, the relaxation resonance frequency for small detuning (c.f. case b)) whereas the response occurs as externally driven oscillations if the detuning is higher (case a)). These oscillations of the population (inversion) of a laser are well known, in particular in multimode laser theory [6], but have not yet been discussed in the connection with nonlinear optical interaction in a laser active medium. Semiconductor laser allow a very elegant access to these population pulzation due to the fact that fluctuations in the inverted carrier system can be probed by analyzing the injection current. By simultaneous performance of an optical four-wave mixing process and the frequency analysis of the injection current we have been able to demonstrate directly that population pulzations excited with the detun-

ing frequency are the basic origin of FWM in a semiconductor laser [7]. Directly related to this interpretation is the question of the maximum possible detuning. If the population pulzations in a semiconductor laser, in the context as discussed above are due to an interband excitation of the inverted bandstructure the maximum excitation frequency is the relaxation resonance frequency and for frequencies above, the response drops [8]. However, if intra-band processes with their characteristic scattering time in the fs regime contribute, a much more extended frequency response should be possible [9] and thus efficient FWM processes with detunings exceeding 10 GHz should be performed. By simple increased detuning frequencies FWM signals up to 21 GHz have successfully generated [5]. In principle by even higher detuning more information on the microscopic origin should be obtained. However, for lasers efficient light coupling has not been able for higher detunings due to the tiny function transmission characteristics of the semiconductor laser-cavity. Therefore, to overcome this problem, highly degenerate FWM (HDFWM) in an orthogonal geometry in a BA laser over a frequency separation of one longitudinal mode spacing has been proposed and performed (paragraph 2.2), whereas results for intramodal FWM exceeding one-longitudinal mode spacing will be discussed in paragraph 2.4. Finally, HDFWM in amplifiers without any Fabry-Perot resonator restrictions will be described in paragraph 3.

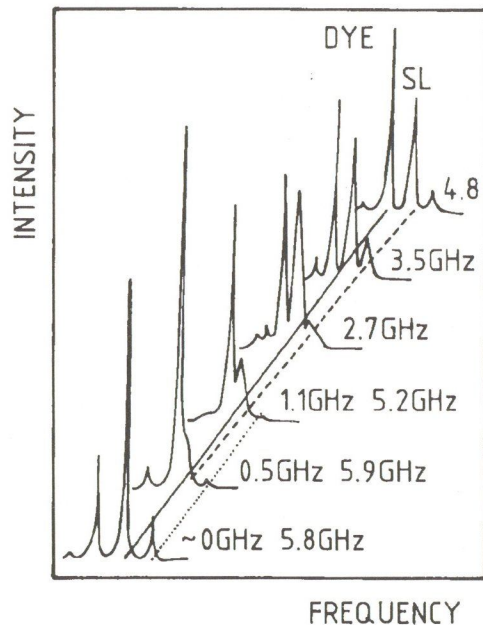


Fig. 3. FWM spectra for different detunings $\Delta\omega$ between semiconductor laser field and injected laser field

2.2. FWM at high detuning (HDFWM)

As discussed in the previous chapter one of the important questions related to nonlinear optical processes, besides their importance for frequency generation, concerns the microscopic origin. Two mechanisms have been proposed and demonstrated to be responsible for NDFWM in semiconductors. One is carrier density modulation caused by interband photomixing of pump and probe fields. This interband process generates gain and index gratings in the active layer, leading to significant NDFWM signals at fre-

quencies below a few GHz, corresponding to the spontaneous carrier lifetime. Additional ultrafast gain saturation, referred to as the gain nonlinearity effect, is the other mechanism. In this case the occupation probability of carriers in each energy band, rather than the actual carrier population, is modulated by the pump and probe fields. This intraband relaxation process is much weaker than the interband process at low frequencies, but, owing to its ultrafast dynamics, can dominate the HDFWM process at frequencies well beyond the corner frequency of the carrier density modulation. These frequency domain NDFWM experiments are equivalent to time-domain pump-probe experiments.

The basic idea of our experiment [10] was the direct demonstration of the appreciably cavity-enhanced modulation response of the semiconductor laser at the longitudinal mode spacing frequency Ω which is more than an order of magnitude higher than the relaxation frequency Ω_{RO} as discussed by Lau [12]. We considered the broad area (BA) laser as the medium in which the nonlinear interaction takes place. The nonlinear interaction of the longitudinal modes generates a population pulzation with the characteristic beating frequency $\Delta\nu_{BA} = 170$ GHz. As a probe for the modulation we injected in an orthogonal geometry (i.e. perpendicular to the laser resonator) a single mode DFB laser. The light of a DFB laser which interacts with these population pulzations consequently experiencing sidebands at $\nu_{DFB} \pm m\Delta\nu_{BA}$, which have been detected and indeed they look very similar to the cascade FWM spectra of paragraph 2.1. Finally we have analyzed the process quantitatively. From the absolute signal strength of the new generated FWM signals the response as a function of frequency has been determined. The result is shown in Fig. 4 including FWM response values at 13 and 21 GHz. We find a 170 times enhancement (45 dB above the 40 dB/decade roll-off) proving that FWM with detunings much higher than the relaxation oscillation frequency is possible and at quite considerable signal strength, which can be attributed to the resonator-enhanced response in semiconductor lasers at the longitudinal mode difference frequency Ω , in accordance with theoretical predictions [11].

The next important question is how the cavity enhanced peak height at 170 GHz in our case depends on frequency. So if we are able to perform a FWM experiment at multiples of the longitudinal mode frequency from their frequency dependence it might be possible to deduce the microscopic origin of HDFWM, carrier heating or spectral hole burning, an answer equivalent to the question discussed in the context of NDFWM [8], [9].

Finally our conclusions and interpretation concerning the carrier density system responsible for FWM have been supported by studies in QW lasers. For comparable experimental conditions we find that $\chi^{(3)}$ mediating the nonlinear optical process is enhanced by a factor of 3–5 as compared to bulk lasers. This can be understood if we consider the different phase-space filling in the low-dimensional carrier system of QW semiconductor lasers.

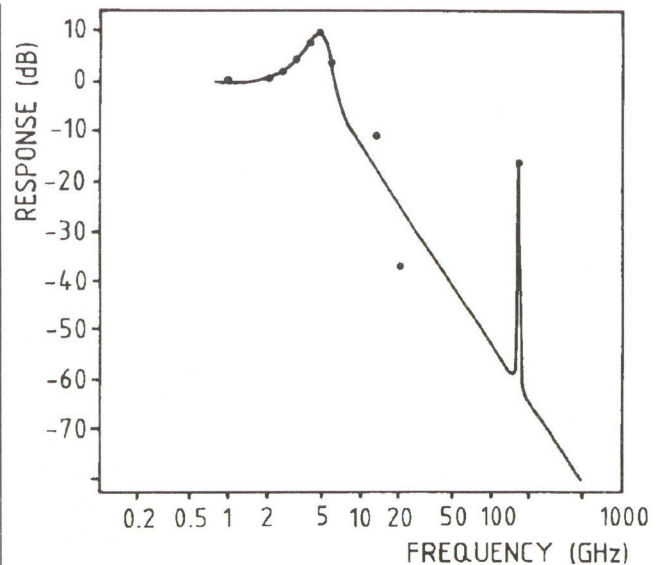


Fig. 4. Summary of the experimental results for the response of a semiconductor laser as deduced from the various FWM experiments

2.3. Polarization dependence of FWM

Next we addressed the polarization dependence of FWM for detunings $\Delta\omega \simeq \omega_{rel}$ where population pulzations are responsible for FWM supporting further evidence for the carrier system as origin of FWM. So far, FWM has mainly been studied in TE-configuration with the master and slave laser having the same polarization. Orthogonal polarization experiments have been only performed in a travelling-wave amplifier by Grosskopf [12], with the results of very small FWM-signals. We compared the FWM behaviour for TE- and TM-light injection in a bulk and a MQW-laser as a slave laser. We find that in a bulk laser a FWM-signal is observed for TM-injection, opposite to a quantum well laser. This is attributed to the interaction of the injected light with the residual TM-light in the cavity of the slave laser [13]. In QW-lasers, the FWM signal does not show up because the residual TM-light is strongly suppressed, due to the larger gain difference between TE- and TM-mode.

2.4. Optical bistability and NDFWM under intramodal injection

Finally we studied optical bistability and NDFWM under intramodal injection [14]. Under intermodal injection, where the injection occurs in the vicinity of a nonlasing longitudinal side mode, the nonlinear optical behaviour of the slave laser is dramatically different as compared to intramodal FWM, where the master laser frequency is close to the slave laser frequency and the slave laser oscillates either in the injection locked regime or in the NDFWM regime. We have observed that a single mode GaAlAs laser could then oscillate in three regimes, depending on the injected power P_{inj} and on the detuning $\delta\omega = \omega_1 - \omega_{inj}$, where ω_1 and ω_{inj} are, respectively the sidemode (denoted E_1) and the injected field (E_{inj}) frequencies. The different regimes are qualitatively depicted in Fig. 5.

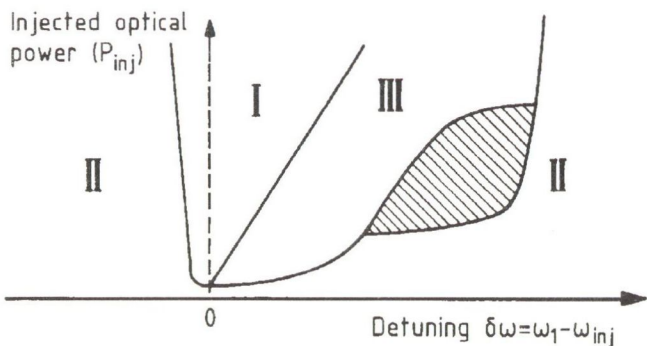


Fig. 5. Schematic representation of the different operation regimes of a laser under intermodal injection

Domain I is the injection-locking domain, which has been theoretically studied by Frey and Provost [15]. In domain II, the free-running mode (E_0) remains the dominant lasing mode. A surprising feature is the existence of domain III, where the sidemode E_1 becomes the dominant lasing mode and, instead of the occurrence of injection locking, the coexisting fields E_{inj} give rise to strong NDFWM processes at the beat frequency $\delta\Omega$. Unlike the intramodal injection, NDFWM only appears for $\delta\omega$ positive and below a critical value, which sometimes exhibits a strong hysteresis with respect to increasing or decreasing $\delta\omega$: for certain values of P_{inj} the jump from regime III to regime II occurs for a detuning higher than the detuning initiating the reverse jump. This bistable domain borderline is obvious from Fig. 5. The bistable domain borderline of the slave laser. The experimental borderline of the bistable domain, denoted $\delta\Omega_{111-11}$ are (P_{inj}) and $\delta\Omega_{11-111}(P_{inj})$ are depicted in Fig. 6 (left part). Simulation results obtained by a two-mode rate equation model are shown in Fig. 6 (right part) reproducing very clearly the bistable behaviour [14]. These findings may be promising for optical switching and optical multiplexing applications, since, in the bistable domain, a small (a few GHz) and only temporarily change of the injected light frequency induces a large (up to 5 THz), rapid and persistent change of the slave laser frequency.

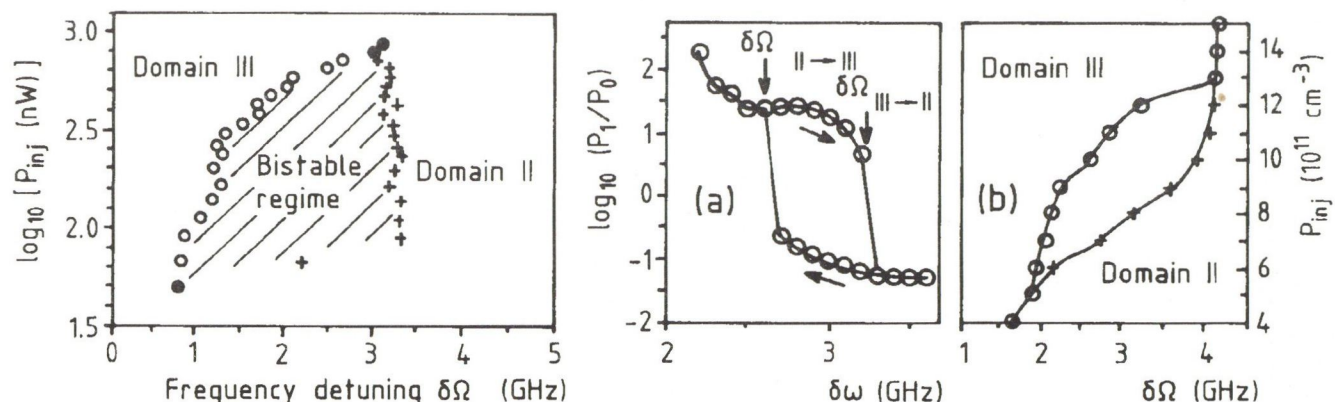


Fig. 6. Measured (left) and calculated values (right) for the bistable transition domain

2.5. Noncollinear FWM in lasers

Instead of using the collinear FWM geometry as depicted in Fig. 1, the two external fields can be injected into the device using a phase conjugation geometry [16], as shown in Fig. 7.

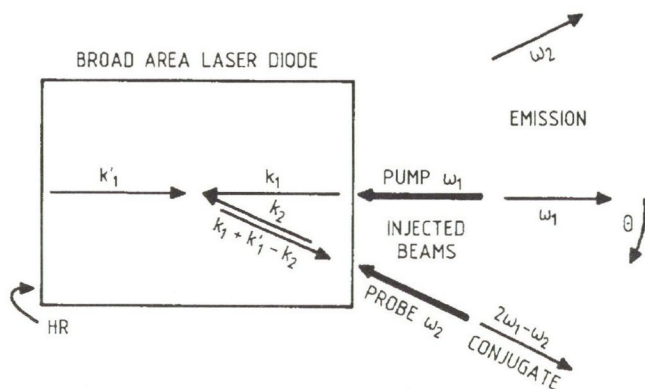


Fig. 7. Schematic depiction of the noncollinear FWM geometry in a BA laser

Using a broad-area device permits the excitation of distinct cavity modes. The nonlinear mixing behaviour is then studied in spectrally resolved far-field measurements. From the results and the analysis of the spatial and

frequency dependence of the FWM process, spatially dependent carrier effects, including ambipolar diffusion coefficients under highly excited resonator conditions can be deduced, in addition to the effects as discussed for collinear interaction geometry [17]. From the applications point of view, all-optical modulation schemes, spatially addressable device as well as the restoring properties of phase conjugation seems very promising.

3. NONLINEAR HDFWM IN AMPLIFIERS

Finally, we review some of the recent work on amplifiers, with particular emphasis on the key points we discussed in connection with nonlinear optics in semiconductor lasers. Highly degenerate FWM in semiconductor travelling wave amplifiers (TWAs) have been used as a frequency domain technique to study ultrafast dynamics in semiconductors. Until now even contradictory results and interpretation of the relevance of the microscopic origin have been given. Two leading candidate mechanisms have been discussed that can cause a significant NDFWM effect. They are carrier heating and spectral hole burning [18]-[24]. An early theoretical treatment of NDFWM in semiconductors by Agrawal considered spectral hole burning [8], [9]. Recent measurements by Kikuchi [17] sup-

port this mechanism. However, femtosecond pump-probe measurements by Hall *et al.* [29] concluded that dynamic carrier heating was the major source of nonlinear gain. This was supported by an experiment by Tiemeijer [23].

By applying detunings up to the THz regime it should be possible to separate the various contributions, as e.g., spectral hole burning and dynamic carrier heating. Very recent results [18], [20], [24] ended up with the conclusion that it seems that both mechanisms contribute, however with a variation of the strength of these two mechanisms, depending on laser structure, wavelength and structure.

4. SUMMARY AND CONCLUSION

We discussed FWM in semiconductor lasers and amplifiers including very recent results with respect to a qualitative and quantitative description incorporating the basic underlying mechanisms. The relevant contributions of the carrier system to the nonlinear optical process, both in lasers and amplifiers were attributed to carrier density or occupation probability modulation, i.e. interband or intra-

band processes depending on the detuning frequency of the interacting fields. Besides the fundamental frequency domain spectroscopy technique to study ultrafast nonlinear optical processes in semiconductor the potential of this nonlinear optical process was always adequately and simultaneously emphasized. Typical applications as frequency generators, spatial switches or elements and bistable devices have been demonstrated and discussed within the context of FWM.

5. ACKNOWLEDGEMENT

I am indebted to Prof. E. O. Göbel for supporting this work and for many stimulating discussions. H.-J. Heinrich, R. Nietzke, P. Panknin, J. Sacher, they all contributed with ideas, results and discussions. Basis has been the semiconductor laser, which we appreciated from Hitachi and SEL-Alcatel. Finally, the work was supported by the Deutsche Forschungsgemeinschaft and the Bundesministerium für Forschung und Technologie.

REFERENCES

- [1] W. Elsässer: Festkörperprobleme. *Advances in Solid State Physics*, Vol. 30, 321 (1990).
- [2] H. Nakajima and R. Frey, *Appl. Phys. Lett.* 769 (1985).
- [3] H. Nakajima, R. Frey, *IEEE J. Quant. Electron.* QE-22, 1349 (1986).
- [4] R. Nietzke, P. Fenz, W. Elsässer, E. O. Göbel, *Appl. Phys. Lett.* 51, 1298 (1987).
- [5] R. Nietzke, P. Panknin, W. Elsässer, E. O. Göbel, *IEEE J. Quant. Electron.* QE-25, 1399 (1989).
- [6] W. E. Lamb, *Phys. Rev.* A134, 1429 (1964)
H. Haken, "Laser Theory", (Springer, 1984).
- [7] W. Elsässer, R. Nietzke, P. Panknin, E. O. Göbel, *Opt. Lett.* 14, 617 (1989).
- [8] G. P. Agrawal, *J. Opt. Soc. Am.* B5, 147 (1988).
- [9] G. P. Agrawal, *Appl. Phys. Lett.* 51, 302 (1987).
- [10] R. Nietzke, W. Elsässer, A. N. Baranov, K. Wünstel, *Appl. Phys. Lett.* 58, 554 (1991).
- [11] K. Lau, *Appl. Phys. Lett.* 52, 2214 (1988).
- [12] G. Grosskopf, *Electron. Lett.* 24, 31 (1988).
- [13] H.-J. Heinrich, W. Elsässer, E. O. Göbel, submitted
- [14] P. Schanne, H.-J. Heinrich, W. Elsässer, E. O. Göbel, *Appl. Phys. Lett.* 61, 2135 (1992).
- [15] R. Frey, G. Provost, *IEEE J. Quant. Electron.* QE-26, 1705 (1990).
- [16] M. Lucente, G. M. Carter, J. G. Fujimoto, *Appl. Phys. Lett.* 53, 467 (1988).
- [17] M. Lucente, J. G. Fujimoto, G. M. Carter, *Appl. Phys. Lett.* 53, 1897 (1988).
- [18] R. Frankenberger, R. Schimpe, *Appl. Phys. Lett.* 60, 2720 (1992).
- [19] K. Kikuchi, M. Kakui, C. E. Zah, T. P. Lee, *IEEE J. Quant. Electron.* QE-28, 151 (1992).
- [20] J. Zhou, N. Park, J. W. Dawson, K. J. Vahala, M. A. Newkirk, U. Koren, I. Miller, *Appl. Phys. Lett.* 62, 2301 (1993).
- [21] J. Zhou, N. Park, J. W. Dawson, K. J. Vahala, M. A. Newkirk, I. Miller, *Appl. Phys. Lett.* 63, 1179 (1993).
- [22] K. L. Hall, J. Mark, E. P. Ippen, G. Eisenstein, *Appl. Phys. Lett.* 56, 1740 (1992).
- [23] L. F. Tiejmeier, *Appl. Phys. Lett.* 59, 499 (1991).
- [24] J. Mark, J. Mork, *Appl. Phys. Lett.* 61, 2281 (1992).

Wolfgang Elsässer received a Diploma degree in physics from the University of Karlsruhe in 1980. In 1981 he moved to the Max-Planck Institute for Solid State Research, Stuttgart. In 1984 he got a Ph.D. degree in physics ("summa cum laude") from the University of Stuttgart. In 1985 he moved to the Philipps University Marburg. In 1991 he completed a Habilitation degree in Physics and became Assistant Professor at Marburg. His research interests are picosecond phenomena in semiconductor lasers, including the generation of picosecond pulses by mode locking, Nonlinear Optics in semiconductor lasers and Nonlinear Dynamics of semiconductor lasers, respectively. In 1985, he was honored with the Otto-Hahn Medal of the Max-Planck Society, in 1986 with the Werner-von-Siemens Medal and in 1991 with the Rudolf-Kaiser Award, respectively. In 1990 he spent a research stay at the Trinity College, Dublin, Ireland and in 1992 a sabbatical at the ENST, Paris, France.

LASER DIODE PHASE CONJUGATE MIRRORS AND OPTICAL REPEATERS

W. M. YEE and K. A. SHORE

UNIVERSITY OF BATH
SCHOOL OF ELECTRONIC AND ELECTRICAL ENGINEERING
BATH BA2 7AY, UK

The exploitation of nearly degenerate four-wave mixing in above-threshold laser diodes to implement phase conjugate mirrors and optical repeaters is investigated theoretically. It is shown that conjugate reflectivity and four-wave mixing bandwidth are enhanced in symmetric laser diodes with low reflectivity facets. It is shown in particular that a 7 – 8 dB enhancement of conjugate reflectivity can be obtained in an asymmetric laser diode, compared to a symmetric laser, by reducing the input facet reflectivity. Longitudinal variations of both the nonlinear wave-mixing interaction and the gain distribution in the laser cavity are taken into account in the model. Such variations are shown to be essential in describing four-wave mixing in laser diodes with low or strongly asymmetric facet reflectivities. The phase conjugate properties of twin-section laser diodes have also been investigated. It is shown that, under appropriate biasing conditions, such devices exhibit a uniform phase conjugate reflectivity over a frequency detuning range of more than 10 GHz.

1. INTRODUCTION

The aim of this paper is to identify novel semiconductor laser structures capable of acting as versatile phase conjugate optical repeaters and amplifiers (PCORA). The proposed structures — due to their resonant cavity configuration — generate a phase conjugate signal in both transmission and reflection modes. The phase conjugate transmission can be utilised to remove cross-talk arising due to four-wave mixing in multichannel wavelength division multiplexed (WDM) optical fibre communication systems. Reduction in co-channel interference by the use of the PCORA will facilitate an increase of the transmission capacity of WDM optical communication systems. Phase conjugate reflection can, on the other hand, be utilised to implement efficient phase conjugate mirrors (PCM) which, used in conjunction with a laser diode, offer the opportunity for achieving ultra-narrow linewidth single-mode laser diodes.

Four wave mixing (FWM) has been identified for effecting a number of functions in ultra-high-speed optical transmission and signal processing systems (see e.g., [1]). Such processes as high-speed demultiplexing, chromatic dispersion compensation via spectral inversion and clock recovery have already been demonstrated at speeds up to 100 Gbit/s. Laser diode amplifiers, due to their size and ease of utilisation, are perceived as having advantages for performing such high-speed functions. Complementary to those efforts, considerable attention has also been given to the development of stable narrow-linewidth semiconductor lasers for a variety of applications in optical communications and optical signal processing. One approach to this objective is the utilisation of external optical feedback to

control the phase fluctuations which give rise to the finite laser linewidth in laser diodes. A particularly attractive approach is to utilise feedback from phase conjugate mirrors. Such mirrors have the property of reversing the phase of incident light and, in consequence, would be expected to reduce phase fluctuations in the target laser. Although linewidth narrowing in semiconductor lasers has been successfully demonstrated using barium titanate phase conjugate mirrors, the complexity of the arrangement effectively precludes their utilisation in a general engineering context. On the other hand, the generation of phase conjugate signals via multiwave mixing in semiconductor optoelectronic devices does offer a practical means for laser linewidth control.

The physics of multiwave mixing in laser diodes [2], [3] and semiconductor optical amplifiers [4], [5] has also attracted considerable attention in recent years. Optical phase conjugation through nearly-degenerate four-wave mixing (NDFWM) in semiconductor lasers is of particular interest because very high conjugate reflectivities in the order of 30-40 dB can be achieved owing to the amplifying effect of the semiconductor gain medium and the cavity enhancement of the mixing process [6]. Wave mixing also represents one of the fundamental nonlinear optical processes and has an important effect on the dynamical and spectral behaviour of laser diodes. In multi-longitudinal mode InGaAsP laser diodes, intrinsic multiwave mixing occurring in the presence of nonlinear gain has been shown to effect self-locked FM operation [7]-[9]. FWM may also be used to extract basic information on gain saturation [10]-[13] and to characterize many fundamental parameters of semiconductor lasers [14], [15]. Furthermore, all-optical frequency conversion using FWM has been proposed and demonstrated [16] in optical coherent multicarrier systems.

In a seminar paper [17], Agrawal presented a theory of nondegenerate FWM in semiconductor lasers and amplifiers with particular emphasis on the physical processes that lead to population pulsations. Although the FWM theory presented by Agrawal is based on a travelling-wave formulation, most of the attention is devoted to the discussion of FWM in semiconductor laser amplifiers, and Fabry-Perot (FP) cavity effects were not included. Recently, Mecozzi *et al.* [18] presented a detail theoretical analysis of NDFWM in a distributed feedback (DFB) laser using the travelling-wave formulation. By using the mean-field approximation, they derived analytical expressions for the probe and the conjugate wave outputs, and demonstrated good agreement between theoretical and experimental re-

sults. On the other hand, several theoretical treatments of NDFWM in FP laser diodes biased above threshold have emphasized the temporal field-matter interactions in the FWM process [19], [20], without taking into account longitudinal variations of the wave-mixing interactions along the laser cavity. Although the time-domain rate-equation approach is adequate for the analysis of NDFWM in FP laser diodes with symmetric and high facet reflectivities, the coupled-mode travelling-wave formulation has to be used in the description of NDFWM in laser diodes with low and/or unequal (asymmetric) facet reflectivities and in laser diodes with longitudinal structural variations. In these latter cases, the longitudinal carrier and photon density distributions are highly nonuniform, and hence, the mean-field approximation is no longer valid. Another important feature of the spatially-dependent coupled-mode analysis of FWM is that it allows the comparison of optical probe injection into either facet of a asymmetric FP laser diode (or into either section of a twin-section laser diode), whereas in a model which uses the mean-field approximation, this would not be possible.

In the present paper, a summary is given of our recent theoretical work on cavity-enhanced NDFWM in above threshold laser diodes with low and/or asymmetric facet reflectivities. The work [21] represents a generalisation of the theory of Agrawal [17] to take into account Fabry-Perot cavity effects and, at the same time, incorporate the longitudinal variations of both the nonlinear interactions and the gain distribution in a theoretical description of NDFWM in laser diodes. In this way it has been possible to obtain a model that is widely applicable and that is, in particular, capable of describing FWM properties in laser diodes where the longitudinal field and gain distributions are significantly nonuniform. The model has also been applied to tailoring the phase conjugate response of two-section asymmetric laser diodes [22]. Here the main outcome has been the prescription of operating conditions to obtain an enhanced phase conjugate response without relying upon narrow resonances associated with either the cavity structure or the relaxation resonances in the device.

2. THEORETICAL MODEL

In this section, we present a theoretical model of cavity-enhanced NDFWM in above-threshold laser diodes based on a theory proposed by Agrawal [17], generalized to take into account resonant-cavity effects and longitudinal variations of the nonlinear wave-mixing interaction and internal gain distribution. The laser is assumed to oscillate in a single transverse and longitudinal mode providing the pump wave at frequency ω_0 . A collinear probe wave at frequency ω_1 is injected into the pumped laser through the front facet with power reflectivity R_1 at $z = 0$, where z is the distance along the longitudinal direction of the laser. The nonlinear coupling of the intracavity waves modulates the carrier density at the beat frequency $\Omega = \omega_1 - \omega_0$, and generates a conjugate wave at frequency $\omega_2 = \omega_0 - \Omega$ through NDFWM.

We assume that the laser structure supports only the fundamental wave-guide TE mode, and that the field E is normalized such that the optical intensity I (in units

of watts per square meter) is given by $I = |E|^2$. Using the plane-wave expansion, we write the field E and the induced polarization P as the sum of the Fourier components:

$$E(x, y, z, t) = U(x, y) \sum_j E_j(z) \exp(-i\omega_j t), \quad (1)$$

$$P(x, y, z, t) = U(x, y) \sum_j P_j(z) \exp(-i\omega_j t), \quad (2)$$

where $U(x, y)$ is the transverse distribution of the fundamental waveguide TE mode, and $j = 0, 1, 2$ correspond to the pump, the probe and the conjugate waves, respectively. The one-dimensional wave equation for the various field components is written as

$$\frac{d^2 E_j}{dz^2} + k_j^2 E_j = -\frac{\Gamma \omega_j^2}{\epsilon_0 c^2} P_j, \quad (3)$$

where ϵ_0 is the vacuum permittivity, c is the velocity of light in vacuum, Γ is the mode confinement factor, $k_j = \bar{n}\omega_j/c = \omega_j/v_g$ are the wavenumbers, \bar{n} is the group refractive index pertaining to the waveguide mode, and v_g is the group velocity.

The dominant physical mechanism of NDFWM in semiconductor lasers was explained by Agrawal to be the modulation of the carrier density at the beat frequency Ω of the pump and the probe waves. The carrier density modulation results in temporal refractive-index and gain modulation which act as index and gain gratings to the pump and probe waves. Diffraction of the pump and the probe waves from these dynamic gratings generates the conjugate wave. The static carrier density \bar{N} at an injection current density J , and the carrier density modulation ΔN_Ω can be obtained by solving the carrier rate equation [17]. Because the pump-probe frequency detuning in the nearly degenerate case is much smaller than the gain-spectrum bandwidth, it can be assumed that all waves experience the same gain given by

$$g(N) = a(N - N_0)(1 - \epsilon|E|^2), \quad (4)$$

where N is the carrier density, N_0 is the carrier density at transparency, a is the differential gain, and ϵ is the nonlinear gain compression factor.

The field-carrier interaction is governed by the relation

$$P = \epsilon_0 \chi E, \quad (5)$$

where the susceptibility is defined as $\chi(N) = -nc(\beta + i)g(N)/\omega_0$ and β is the linewidth enhancement factor which accounts for the carrier-induced index change. The induced polarization components P_j are found [21] in the form:

$$P_0(z) = \epsilon_0 Ag(\bar{N})E_0, \quad (6)$$

$$P_1(z) = \epsilon_0 Ag(\bar{N})[E_1 - \Delta n_\Omega E_0 - \delta_{NL} E_0], \quad (7)$$

$$P_2(z) = \epsilon_0 Ag(\bar{N})[E_2 - \Delta n_\Omega^* E_0 - \delta_{NL}^* E_0], \quad (8)$$

where

$$A = -(nc/\omega_0)(\beta + i), \quad (9)$$

$$\Delta n_\Omega = \frac{-\Delta N_\Omega}{(\bar{N} - N_0)} = \frac{(E_0^* E_1 + E_0 E_2^*)/P_s}{(1 + |E_0|^2/P_s - i\Omega\tau_s)}, \quad (10)$$

$$\delta_{NL} = \frac{\epsilon(E_0^* E_1 + E_0 E_2^*)}{1 - \epsilon|E_0|^2}, \quad (11)$$

$$g(\bar{N}) = a(\bar{N} - N_0)(1 - \epsilon|E_0|^2) = \frac{(a\tau_s/ed)J - aN_0}{1 + |E_0|^2/P_s}(1 - \epsilon|E_0|^2), \quad (12)$$

where $P_s = \hbar\omega_0/(\Gamma a\tau_s)$ is the saturation intensity, \hbar is Planck's constant divided by 2π , τ_s is the spontaneous carrier lifetime, e is the electronic charge and d is the active layer thickness. The term δ_{NL} is included to account for the nonlinear gain saturation effects.

2.1. Fabry-Perot Cavity Effects

To incorporate the effect of resonant cavity into the analysis, it is necessary to treat both the forward and the reverse propagating waves. In this case, therefore, the z -dependence of the fields is assumed to be

$$E_j(z) = \sqrt{P_s}[A_j^+(z)\exp(ik_0z) + A_j^-(z)\exp(-ik_0z)], \quad (13)$$

where $A_j^+(z)$ and $A_j^-(z)$ are the normalized complex slowly-varying fields of the forward and the reverse propagating waves, respectively. Similarly, the induced polarization at the corresponding frequency is expressed as the sum of the forward and the reverse propagating components:

$$P_j(z) = P_j^+(z)\exp(ik_0z) + P_j^-(z)\exp(-ik_0z). \quad (14)$$

We substitute equations (13) and (14) into (3) and apply the slowly varying envelope and the rotating wave approximations to obtain

$$\frac{dA_0^\pm}{dz} \pm \frac{\alpha_{int}}{2}A_0^\pm = \pm \frac{i\omega_0\Gamma}{2nc\epsilon_0\sqrt{P_s}}P_0^\pm, \quad (15)$$

$$\frac{dA_1^\pm}{dz} \mp \frac{i\bar{n}\Omega}{c}A_1^\pm \pm \frac{\alpha_{int}}{2}A_1^\pm = \pm \frac{i\omega_1\Gamma}{2nc\epsilon_0\sqrt{P_s}}P_1^\pm, \quad (16)$$

$$\frac{dA_2^\pm}{dz} \mp \frac{i\bar{n}\Omega}{c}A_2^\pm \pm \frac{\alpha_{int}}{2}A_2^\pm = \pm \frac{i\omega_2\Gamma}{2nc\epsilon_0\sqrt{P_s}}P_2^\pm, \quad (17)$$

where α_{int} is the internal loss coefficient introduced to take into account all losses (diffusion, free-carrier absorption, scattering, etc.) other than mirror loss.

Substituting the induced polarization components from equations (6)-(8) as the source terms into (15)-(17), we obtain the coupled-wave equations which describe the evolution of three sets of forward and reverse propagating fields along the z direction:

$$\frac{dA_0^\pm}{dz} = \pm\alpha_0A_0^\pm \mp \frac{\alpha_{int}}{2}A_0^\pm, \quad (18)$$

$$\frac{dA_1^\pm}{dz} = \pm \frac{i\bar{n}\Omega}{c}A_1^\pm \pm \alpha_0[A_1^\pm - (X+Y)Q]A_0^\pm \mp \frac{\alpha_{int}}{2}A_1^\pm, \quad (19)$$

$$\frac{dA_2^\pm}{dz} = \mp \frac{i\bar{n}\Omega}{c}A_2^\pm \pm \alpha_0[A_2^\pm - (X^*+Y)Q^*]A_0^\pm \mp \frac{\alpha_{int}}{2}A_2^\pm, \quad (20)$$

where

$$\alpha_0(z) = \frac{1}{2} \frac{g_0}{1 + P_T}(1 - \epsilon P_s P_T)(1 - i\beta), \quad (21)$$

$$P_T(z) = |A_0^+(z)|^2 + |A_0^-(z)|^2, \quad (22)$$

$$Q(z) = A_0^+(A_2^+)^* + A_0^-(A_2^-)^* + (A_0^+)^*A_1^+ + (A_0^-)^*A_1^-, \quad (23)$$

$$X(z) = 1/(1 + P_T - i\Omega\tau_s), \quad (24)$$

$$Y(z) = \epsilon P_s/(1 - \epsilon P_s P_T), \quad (25)$$

and where $\Delta n_\Omega = XQ$, $g_0 = \Gamma aN_0(J/J_0 - 1)$ is the small signal gain and $J_0 = edN_0/\tau_s$ is the transparency current density. The effect of nonlinear gain saturation has been reported [18] to damp the FWM response around the relaxation oscillation frequency of the pumped laser. The cavity standing waves generated by counterpropagating wave coupling gives rise to additional damping of the relaxation resonance peak of the FWM response through the mechanism of spatial hole-burning. However, experimental results showed that the effect on FWM spectra of spatial hole-burning is negligibly small compared to that arising from nonlinear gain saturation [18]. Consequently, longitudinal cavity standing wave effects are neglected and only copropagating wave coupling is taken into account in the model. The z dependence of the normalized intracavity pump intensity P_T is retained in the model. This is of importance when consideration is given to lasers with very low or unequal facet reflectivities where significant nonuniformity in the field distribution is anticipated. We consider the case where the probe signal injection is very small so that the effect of probe-induced carrier depletion in the pumped laser is negligible. The intracavity pump signal can thus be assumed free-running. This assumption is consistent with reported experimental investigations of nearly degenerate FWM in laser diodes in which very small probe signal injection power of about 0.02 μ W was used [18], [19].

The coupled-wave equations must satisfy the boundary conditions at the two laser facets with power reflectivities R_1 and R_2 , respectively:

$$A_j^+(z=0) = \sqrt{1-R_1}A_{in} + \sqrt{R_1}A_j^-(z=0), \quad (26)$$

$$A_{R,j} = \sqrt{1-R_1}A_j^-(z=0) + \sqrt{R_1}A_{in}, \quad (27)$$

$$A_j^-(z=L)\exp(-ik_0L) = \sqrt{R_2}A_j^+(z=L)\exp(ik_0L), \quad (28)$$

$$A_{T,j} = \sqrt{1-R_2}A_j^+(z=L)\exp(ik_0L), \quad (29)$$

where A_{in} is the normalized incident probe signal amplitude which is zero for $j = 0, 2$, L is the laser cavity length, $A_{R,j}$ and $A_{T,j}$ are the output fields from the front ($z = 0$) and the rear ($z = L$) facet, respectively, at the corresponding frequency.

We define the probe (conjugate) reflectivity R_p (R_c) as the ratio of the probe (conjugate) output power from the front facet ($z = 0$) to the incident probe power at the same facet. Similarly, we define the probe (conjugate) transmittivity T_p (T_c) as the ratio of the probe (conjugate) output from the rear facet ($z = L$) to the incident probe power at the front facet, ie.,

$$R_p = \left| \frac{A_{R,1}}{A_{in}} \right|^2, \quad T_p = \left| \frac{A_{T,1}}{A_{in}} \right|^2, \quad (30)$$

$$R_c = \left| \frac{A_{R,2}}{A_{in}} \right|^2, \quad T_c = \left| \frac{A_{T,2}}{A_{in}} \right|^2. \quad (31)$$

Details of the numerical technique used to solve this system of equations are given in reference [21].

3. RESULTS AND DISCUSSIONS

A small probe injection power of $P_{in} = 0.02 \mu\text{W}$ [18], [19] is assumed to be incident at the laser front facet at $z = 0$. The following parameter values appropriate to GaAs/AlGaAs laser diodes are used in the analysis (unless stated otherwise): laser volume $V = (300 \mu\text{m} \times 2.0 \mu\text{m} \times 0.2 \mu\text{m})$, reference wavelength $\lambda_0 = 0.83 \mu\text{m}$, $\Gamma = 0.4$, $a = 3 \times 10^{-16} \text{ cm}^2$, $N_0 = 1.1 \times 10^{18} \text{ cm}^{-3}$, $\beta = 3$, $\tau_s = 1 \text{ ns}$, $\alpha_{int} = 20 \text{ cm}^{-1}$, and $\epsilon = 2.8 \times 10^{-13} \text{ m}^2/\text{W}$ (which corresponds to $5.0 \times 10^{-18} \text{ cm}^3$).

3.1. Symmetric Laser Diodes

To illustrate the longitudinal variations of the NDFWM interactions, the amplitudes of the normalized carrier density deviation Δn_Ω along the z axis are plotted in Fig. 1. Significant longitudinal nonuniformity is observed in the carrier density deviation distribution, especially for lasers with highly asymmetric facet reflectivities. In as much as it is the carrier density fluctuations which drive the FWM process, it is to be expected that such carrier variations will influence achievable phase conjugate reflectivities in these devices. Furthermore, it is observed that the carrier density deviation is the largest in the device with low-reflective front facet and high-reflective rear facet. It is therefore to be expected that the efficiency of optical phase conjugation is enhanced in devices with $R_1 < R_2$, with the probe injection incident at the facet with reflectivity R_1 .

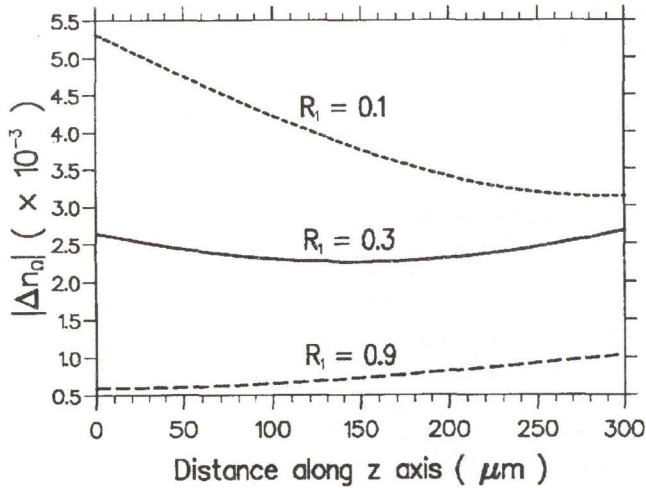


Fig. 1. Amplitudes of normalized carrier density deviation along the longitudinal axis of the laser cavity for three laser devices with different facet reflectivities. $R_1 \times R_2 = 0.09$ in all three cases.

The evolution of the conjugate signal intensity along the z direction of the laser is illustrated in Fig. 2, where the laser facet reflectivities are $R_1 = R_2 = 0.1$. The solid curves are obtained with the piecewise constant inversion population (PCIP) model [21]. The dashed curves are

obtained with a spatially uniform gain model, in which case we assume a z -independent normalized average intracavity pump intensity \bar{P}_T given by

$$\bar{P}_T = \frac{1}{L} \int_0^L |A_0^+(z)|^2 + |A_0^-(z)|^2 dz = \frac{g_0}{g_{th}} - 1, \quad (32)$$

and

$$g_{th} = \alpha_{in} + \frac{1}{2L} \ln \left(\frac{1}{R_1 R_2} \right) \quad (33)$$

is the threshold gain of the laser diode. Significant differences are observed between the propagation curves of the conjugate intensity computed with the two models, when the laser facet reflectivity is small. This is generally true for $R_1 = R_2 \leq 0.3$ and for lasers with highly asymmetric facet reflectivities. Similar differences are also observed in the values of the probe intensity, although the differences between the pump intensities from the two models are less pronounced. Fig. 2 also shows that the conjugate intensity along the z axis is highly nonuniform and thus the mean-field approximation can not be assumed in lasers with low facet reflectivities. The above results demonstrate that longitudinal variations of the internal gain should be taken into account in discussions of NDFWM when consideration is given to lasers with low or asymmetric facet reflectivities.

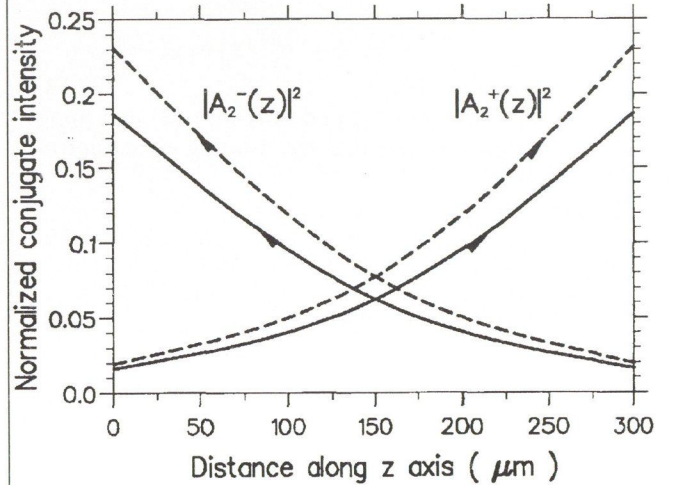


Fig. 2. Evolution of normalized conjugate intensity along the longitudinal direction of the laser cavity. Significant differences are observed between results obtained with the PCIP model (solid curves) and the uniform-gain model (dashed curves).

The probe and the conjugate output power at $z = L$ as a function of pump-probe frequency detuning are shown in Fig. 3(a) and 3(b), respectively. The facet reflectivities are $R_1 = R_2 = 0.3$. The solid and the dashed curves correspond to $\beta = 3$ and $\beta = 4$, respectively. Probe and conjugate output power peaks are observed at frequency detuning approximately equal to

$$\Omega_R = \left(\frac{g_{th} v_g \bar{P}_T}{\tau_s} \right)^{1/2}, \quad (34)$$

which corresponds to the relaxation oscillation frequency of the pumped laser. It is also observed that the conjugate output power curve is symmetric with respect to zero pump-probe frequency detuning, whereas the probe

output power curve exhibits strong asymmetry with higher probe output for negative frequency detuning. This agrees very well with experimental results of Simpson and Liu [19] and also observations in semiconductor optical amplifiers [4], [5]. Such probe gain asymmetry was theoretically predicted by Bogatov *et al.* [23]. The physical origin of the asymmetric nature of the probe gain is related to the fact that a change in carrier density affects both the gain and the refractive index of the active region in semiconductor lasers [17], [24]. Hence, population pulsations create both gain and index gratings simultaneously; the relative contributions of the two gratings are governed by the linewidth enhancement factor, β . Fig. 3 also shows that probe and conjugate output power increase for larger value of the linewidth enhancement factor, and confirms the significant contribution of refractive-index grating in the FWM process arising from the large β value in semiconductor lasers.

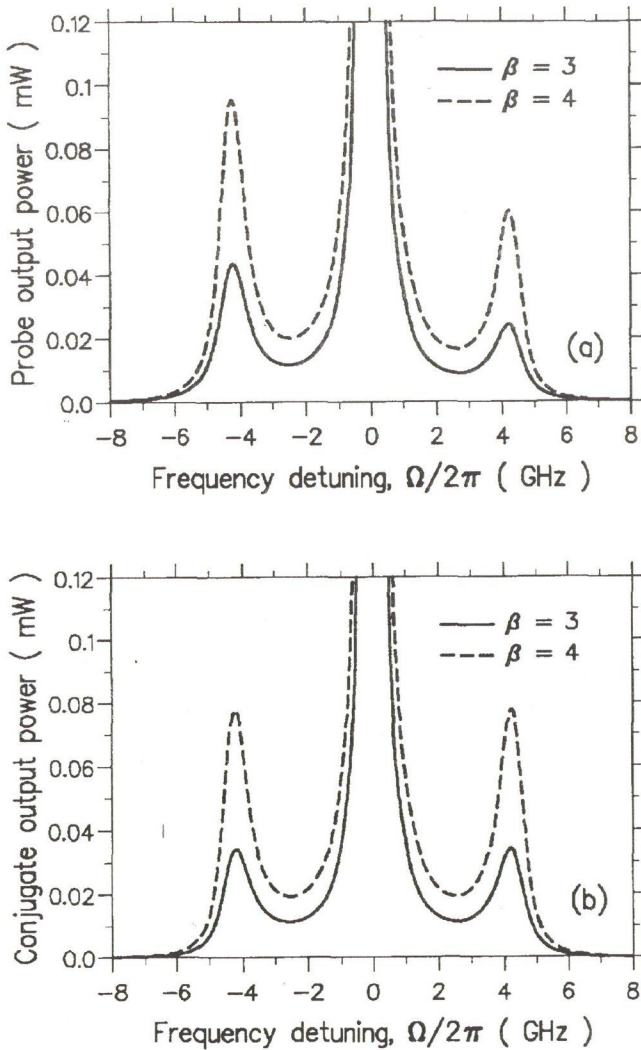


Fig. 3. (a) Probe and (b) conjugate output power versus frequency detuning for $\beta = 3$ (solid curves) and $\beta = 4$ (dashed curves). $R_1 = R_2 = 0.3$. $P_{out} = 7.73$ mW.

The transmittivity of the probe T_p and the conjugate T_c waves as a function of frequency detuning are plotted in Fig. 4(a) and 4(b), respectively, for different values of the spontaneous carrier lifetime, τ_s . T_p and T_c in the range of 30 – 40 dB can be obtained at frequency detunings near

the relaxation oscillation frequency, which agree well with experimental observations [14].

Because the relaxation oscillation frequency Ω_R is inversely related to τ_s as indicated in equation (34), we see that the bandwidth for positive conjugate transmittivity increases for smaller τ_s . For frequency detunings well above Ω_R , T_p and T_c decrease rapidly with roll-off rates of approximately –20 and –60 dB per-frequency decade, respectively, in accordance with experimental results reported in reference [14]. In this reference, Fabry-Perot cavity effects are indicated as being responsible for the observed roll-off rates. The cavity effect is indeed apparent in Fig. 4, in which, for very large frequency detunings, the transmittivities are seen to increase again because of the effect of the adjacent Fabry-Perot resonance.

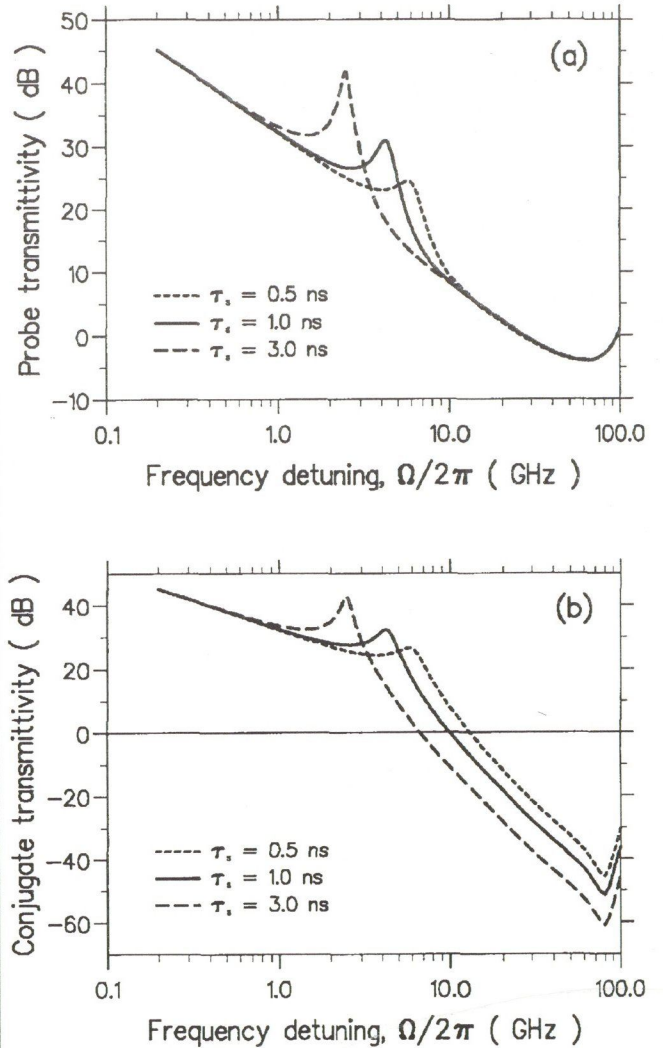


Fig. 4. (a) Probe and (b) conjugate transmittivity as a function of frequency detuning for different values of spontaneous carrier lifetime. $R_1 = R_2 = 0.3$.

3.2. Symmetric Low-Facet-Reflectivity Laser Diodes

The effects of varying the facet reflectivity $R = R_1 = R_2$ on conjugate transmittivity at a constant injection current density, chosen here to be $J/J_0 = 2.45$, are illustrated in Fig. 5. In symmetric facet reflectivity laser diodes, $R_c = T_c$. For low facet reflectivity, the average intracavity pump intensity is reduced because of high

mirror losses. The relaxation oscillation frequency of the laser is correspondingly reduced resulting in the shift of the side transmittivity peaks to smaller frequency detuning. Lower pump intensity also means that carrier depletion by the pump wave is decreased thus enhancing the effective gain experienced by the conjugate and the probe waves. Also, at low facet reflectivity, the coupling efficiency of the constant probe injection power into the laser cavity is increased. Both of these effects contribute to higher probe and conjugate transmittivities in laser diodes with low reflectivity facets. This nontrivial result can only be found using the present technique in which the coupled-wave equations incorporating the resonant-cavity effects and the z dependence of the nonlinear interaction are numerically integrated subject to the boundary conditions imposed at the laser facets.

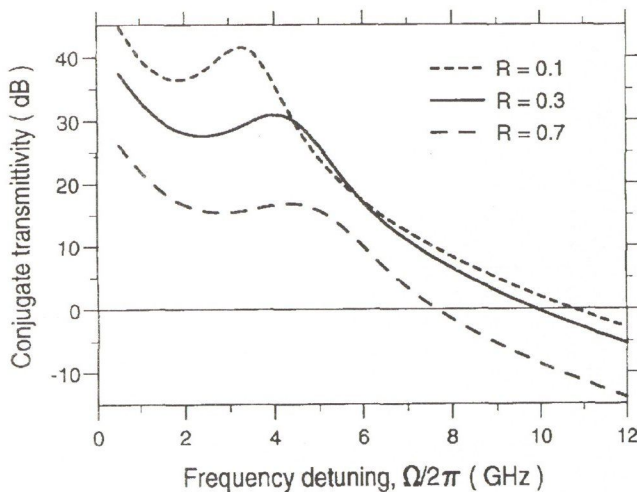


Fig. 5. Conjugate transmittivity versus frequency detuning for symmetric laser diodes with different facet reflectivities.

It is also observed from Fig. 5 that the bandwidth for positive conjugate transmittivity increases as the laser facet reflectivity is reduced. This is purely a cavity-effect resulting from the broadening of the Fabry-Perot resonant transmission bandwidth at low facet reflectivities. This explicit dependence of the conjugate transmission bandwidth on laser facet reflectivity can be computed, again, only by use of the present formalism.

The above results show that enhancement of both the conjugate transmittivity and the conjugate transmission bandwidth can be obtained in symmetric laser diodes with low facet reflectivity. We have thus shown that the bandwidth of NDFWM in laser diodes biased above threshold is dependent not only on the spontaneous carrier lifetime and the relaxation oscillation frequency as has previously been reported [18], but also on the facet reflectivities of the pumped laser. It is therefore suggested that experimental investigation could be profitably undertaken on NDFWM effects in low facet reflectivity laser diodes with a view to taking advantage of the enhancements of both the conjugate transmittivity and the FWM bandwidth revealed by the present analysis.

3.3. Asymmetric-Facet Laser Diodes

Fig. 6 shows the conjugate reflectivity versus frequency

detuning curves for three laser devices with different facet reflectivities. Here we consider devices with a constant product $R_1 R_2 = 0.09$, and thus with a constant threshold gain g_{th} , assuming the same cavity length and internal loss coefficient. As shown in Fig. 6, a 7–8 dB enhancement of the phase conjugate reflectivity can be obtained, compared to the case of a symmetric laser ($R_1 = R_2 = 0.3$), by applying anti-reflection (AR) coating to the front facet and applying high-reflection (HR) coating to the rear facet ($R_1 = 0.1, R_2 = 0.9$). The present work shows that there exist opportunities for enhanced phase-conjugate wave generation using highly asymmetric laser diodes. Experimental investigations of such devices would therefore be of some considerable interest.

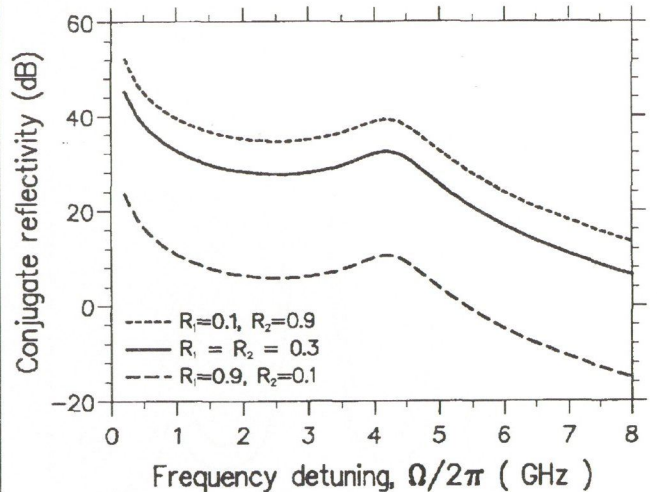


Fig. 6. Conjugate reflectivity versus frequency detuning for asymmetric laser diodes. $R_1 R_2 = 0.09$.

3.4. Twin-Section Laser Diodes

Having established the role of longitudinal gain variations in the NDFWM process, it is of interest to consider semiconductor laser structures where such variations can be controlled by current injection. The simplest structure which can be considered in this context is the twin-section laser diode illustrated in Fig. 7.

Consideration is given, first of all, to a symmetric laser diode where $R_1 = R_2 = 0.3$. Fig. 8 shows the conjugate reflectivity versus frequency detuning curves for three different current pumping conditions of a symmetric laser diode. Curve (a) corresponds to homogeneous pumping with $J_a = J_b = 2.20$. Curves (b) and (c) correspond to $J_a = 2.25, J_b = 2.19$ and $J_a = 2.15, J_b = 2.21$, respectively. In all the cases the pump output power per-facet is the same at $P_{out} = 7.73$ mW.

It is observed from Fig. 8 that the conjugate reflectivity versus frequency detuning curve is symmetrical with respect to zero frequency detuning. When the two sections are biased at different injection current levels (curves (b) and (c)), the conjugate reflectivity decreases. Because of the carrier-induced refractive index change, the nonuniform distribution of carrier density between the two sections resulting from inhomogeneous pumping induces different phase shifts when the intracavity fields propagate through the device. The phase mismatch inhibits injection-locking around zero frequency detuning for small probe

injection power (which, in accordance with reference [18], is assumed to be $0.02 \mu\text{W}$ in the present analysis) when the two sections are pumped differently.

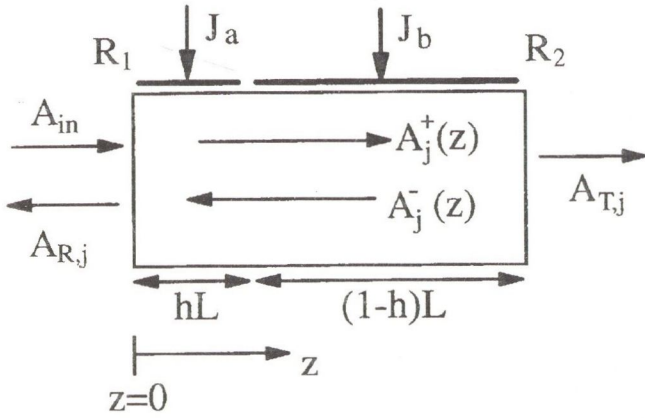


Fig. 7. Schematic diagram of nearly degenerate FWM in a two-section single-cavity laser diode with facet reflectivities R_1 and R_2 . J_a and J_b are the injection current density into the two-sections, respectively, which are normalized to the transparency value, J_0 . We consider devices with $h = 0.2$.

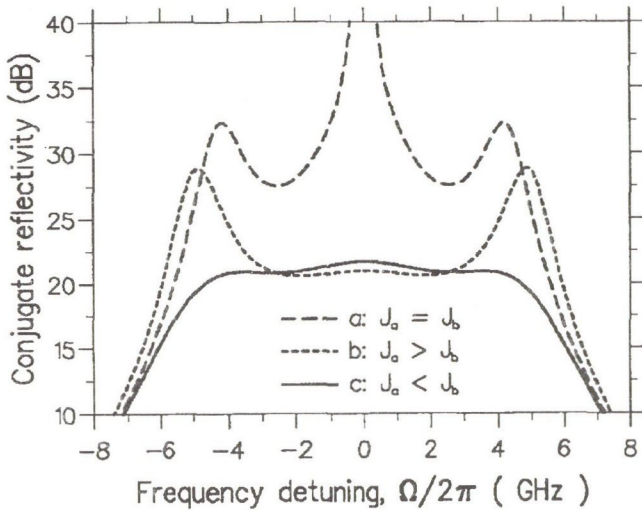


Fig. 8. Conjugate reflectivity versus frequency detuning for three different biasing conditions of a symmetric laser diode with $R_1 = R_2 = 0.3$.

It is also observed that the resonant peaks of the conjugate reflectivity near the relaxation oscillation frequency is enhanced when the probe injection is incident at the higher gain section (curve (b)) whereas the resonant peaks are highly damped when the probe injection is incident at the lower gain section (curve (c)). A uniform conjugate reflectivity response can thus be obtained using a two-section laser diode with the probe injection incident at the low-gain section. The uniform conjugate reflectivity over a frequency detuning range of more than 10 GHz as revealed by the present analysis is important for distortionless frequency conversion of wide-band signals. It should however be pointed out that only slightly inhomogeneous current pumping is considered in our analysis. When the two sections are pumped with highly different currents, the wavelength dependence of the gain in the two sections may need to be taken into account.

Fig. 9 shows the conjugate reflectivity versus frequency detuning curves with the same corresponding biasing conditions for curves (a), (b) and (c) as in Fig. 8. However, curve (a) is obtained for a symmetric laser with $R_1 = R_2 = 0.3$ (as in Fig. 8), but curves (b) and (c) are obtained for an asymmetric laser diode with $R_1 = 0.1$ and $R_2 = 0.9$. Note that the product $R_1 R_2$, and hence the threshold gain are the same in all three cases.

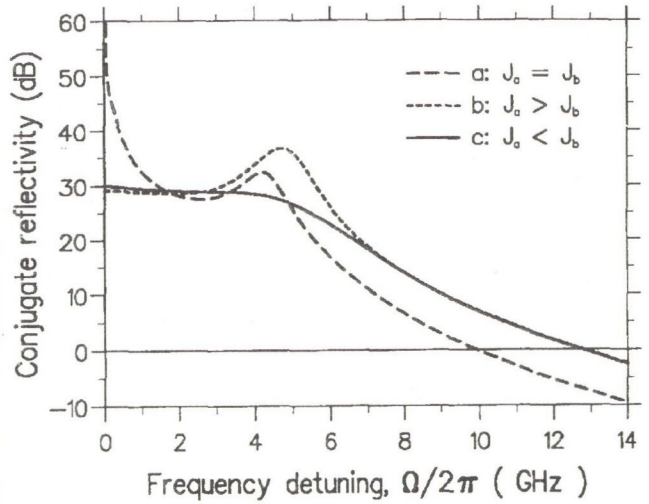


Fig. 9. Conjugate reflectivity versus frequency detuning curves. Curve (a) is for a symmetric laser diode, whereas curves (b) and (c) are obtained for an asymmetric laser diode with $R_1 = 0.1$ and $R_2 = 0.9$. Biasing condition for each curve is the same as the corresponding curve in Fig. 8.

By comparing curves (b) and (c) from Fig. 8 and Fig. 9, it is found that conjugate reflectivity enhancements of 7 – 8 dB can be obtained using asymmetric-facet laser diodes rather than symmetric laser diodes. In addition, FWM bandwidth (defined as frequency range for positive conjugate reflectivity) is also enhanced from 20 GHz in a symmetric laser to 26 GHz in an asymmetric laser diode. Higher FWM bandwidth is possible by biasing the laser diodes with higher injection currents above threshold.

The present analysis demonstrated that a uniform conjugate reflectivity response could be obtained in a two-section laser diode by injecting the probe signal at the low-gain section. Enhancement of conjugate reflectivity and FWM bandwidth can simultaneously be achieved by applying anti-reflection (AR) coating to the input facet at the low-gain section of an asymmetric two-section laser diode. Utilizing the flat conjugate reflectivity response in an inhomogeneously-pumped and asymmetric-facet laser diode, highly efficient optical frequency conversion (with approximately 30 dB amplification over the probe input power) of wide-band (few Gbit/s) signals could be achieved without pattern distortion which may otherwise arise because of the peak and trough in the conjugate reflectivity response typical of single-electrode laser diodes. The experimental verification of these predictions would appear to be a worthwhile tests.

4. CONCLUSION

We have theoretically investigated cavity-enhanced nearly

degenerate FWM in above threshold laser diodes with low and/or asymmetric facet reflectivities. It has been shown that enhancement of both the conjugate output and the FWM bandwidth can be obtained in symmetric laser diodes with low facet reflectivities. It has further been shown that a 7 – 8 dB enhancement of conjugate reflectivity can be achieved in an asymmetric laser diode by applying AR-coating to the input facet. The importance of incorporating the longitudinal variations of the nonlinear interaction and the internal gain distribution in the model has been established.

The model has also been applied to the study of FWM processes in multisection laser diodes. There it has been shown that enhanced uniform phase conjugation can be obtained using appropriately configured asymmetric two-section devices. It is noted additionally that the model can be utilized to analyse FWM in laser diodes used for all-optical frequency conversion. Finally, it is noted that a possibility exists of obtaining a further enhancement of the phase conjugate response of twin-section quantum well

laser devices by the exploitation of the so-called 'gain-lever' properties of such structures. The calibration of achievable enhancements by such means has yet to be undertaken.

The successful development of optimised laser diode phase conjugators will provide a key component for a range of ultra-high speed optical information processing functions including demultiplexing, spectral inversion and clock extraction. The flexibility of the proposed resonant cavity structures to act in both reflection and transmission modes serves to underline the wide applicability of the proposed structures. In addition to the use of the structures to effect four-wave mixing, it is pointed out that the use of optical phase conjugation for the cancellation of four-wave mixing in multichannel optical fibre communication systems — where the mixing process gives rise to cross-talk interference — has also been reported recently [25]. This additional role for laser diode phase conjugators adds further to the impetus for implementing the structures identified in the present work.

REFERENCES

- [1] S. Kawanishi, T. Morioka, O. Kamatani, H. Takara, J.M. Jacob, and M. Saruwatari: "100 Gbit/s all-optical demultiplexing using four-wave mixing in a travelling-wave laser diode amplifier", *Electron. Lett.*, 30, 981-982 (1994).
- [2] H. Nakajima and R. Frey: "Collinear nearly degenerate four-wave mixing in intracavity amplifying media", *IEEE J. Quantum Electron.*, QE-22, 1349-1354 (1986).
- [3] R. Nietzke, P. Panknin, W. Elsässer, and E.O. Göbel: "Four-wave mixing in GaAs/AlGaAs semiconductor lasers", *IEEE J. Quantum Electron.*, 25, 1399-1406 (1989).
- [4] F. Favre and D.L. Guen: "Four-wave mixing in traveling wave semiconductor laser amplifiers", *IEEE J. Quantum Electron.*, 26, 858-864 (1990).
- [5] T. Mukai and T. Saitoh: "Detuning characteristics and conversion efficiency of nearly degenerate four-wave mixing in a 1.5 μm traveling-wave semiconductor laser amplifier", *IEEE J. Quantum Electron.*, 26, 865-874 (1990).
- [6] S. Jiang and M. Dagenais: "Observation of nearly degenerate and cavity-enhanced highly nondegenerate four-wave mixing in semiconductor lasers" *Appl. Phys. Lett.*, 62, 2757-2759 (1993).
- [7] L.F. Tiemeijer, P.I. Kuindersma, P.J.A. Thijs, and G.L.J. Rikken, "Passive FM locking in InGaAsP semiconductor lasers", *IEEE J. Quantum Electron.*, 25, 1385-1391 (1989).
- [8] K.A. Shore and W.M. Yee: "Theory of self-locking FM operation in semiconductor lasers", *IEE Proc. Part J*, 138, 91-96 (1991).
- [9] W.M. Yee and K.A. Shore: "Multimode analysis of self-locked FM operation in laser diodes", *IEE Proc. Part J*, 140, 21-25 (1993).
- [10] L.F. Tiemeijer: "Effects of nonlinear gain on four-wave mixing and asymmetric gain saturation in a semiconductor laser amplifier", *Appl. Phys. Lett.*, 59, 499-501 (1991).
- [11] S.R. Chinn: "Measurement of nonlinear gain suppression and four-wave mixing in quantum well lasers", *Appl. Phys. Lett.*, 59, 1673-1675 (1991).
- [12] K. Kikuchi, M. Kakui, C.E. Zah, and T.P. Lee: "Observation of highly nondegenerate four-wave mixing in 1.5 μm traveling-wave semiconductor optical amplifiers and estimation of nonlinear gain coefficient", *IEEE J. Quantum Electron.*, 28, 151-156 (1992).
- [13] J. Zhou, N. Park, J.W. Dawson, and K.J. Vahala: "Highly nondegenerate four-wave mixing and gain nonlinearity in a strained multiple-quantum-well optical amplifier", *Appl. Phys. Lett.*, 62, 2301-2303 (1993).
- [14] S. Jiang and M. Dagenais: "Nearly degenerate four-wave mixing in Fabry-Perot semiconductor lasers", *Opt. Lett.*, 18, 1337-1339 (1993).
- [15] J.M. Liu, and T.B. Simpson: "Characterization of fundamental parameters of a semiconductor laser with an injected optical probe", *IEEE Photon. Technol. Lett.*, 4, 380-382 (1993).
- [16] G. Grosskopf, R. Ludwig, and H.G. Weber: "140 Mbit/s DPSK transmission using an all-optical frequency converter with a 4000 GHz conversion range", *Electron. Lett.*, 24, 1106-1107 (1988).
- [17] G.P. Agrawal: "Population pulsations and nondegenerate four-wave mixing in semiconductor lasers and amplifiers", *J. Opt. Soc. Am. B*, 5, 147-159 (1988).
- [18] A. Mecozzi, A. D'Ottavi, and R. Hui: "Nearly degenerate four-wave mixing in distributed feedback semiconductor lasers operating above threshold" *IEEE J. Quantum Electron.*, 29, 1477-1487 (1993).
- [19] T.B. Simpson and J.M. Liu: "Phase and amplitude characteristics of nearly degenerate four-wave mixing in Fabry-Perot semiconductor lasers" *J. Appl. Phys.*, 73, 2587-2589 (1993).
- [20] L. Li and K. Petermann: "Characteristics of the optical-frequency conversion in a semiconductor laser", *IEEE J. Quantum Electron.*, 29, 2793-2798 (1993).
- [21] W.M. Yee and K.A. Shore: "Nearly degenerate four-wave mixing in laser diodes with nonuniform longitudinal gain distribution", *J. Opt. Soc. Am. B*, 11, 1221-1228 (1994).
- [22] W.M. Yee and K.A. Shore: "Enhanced uniform phase conjugation in two-section asymmetric laser diodes", *Opt. Lett.*, (accepted for publication).
- [23] A.P. Bogatov, P.G. Eliseev, and B.N. Sverdlov: "Anomalous interaction of spectral modes in semiconductor laser", *IEEE J. Quantum Electron.*, QE-11, 510-515 (1975).
- [24] M. Yamada: "Theoretical analysis of nonlinear optical phenomena taking into account the beating vibration of the electron density in semiconductor lasers", *J. Appl. Phys.*, 66, 81-89 (1989).
- [25] S. Watanabe and T. Chikama: "Cancellation of four-wave mixing in multi-channel fibre transmission by midway optical phase conjugation", *Electron. Lett.*, 30, 1156-1157 (1994).

Authors photographs and biographies on page 11

HIGH OPTICAL POWER 1.22 MICROMETER InP/InGaAsP BURIED HETEROSTRUCTURE LASER DIODE

High power, 1.22 μm InP/InGaAsP buried heterostructure laser with optimized parameters can play important role as a pump source for upconversion fiber lasers. We report a single-step liquid phase epitaxial growth and characterization of double-channelled substrate InP/InGaAsP buried heterostructure laser diode for 1.22 μm wavelength. Optimum conditions for separate growth of InGaAsP buried active layer on double-channelled InP substrate have been obtained. Output power over 120 mW have been achieved by determining the appropriate reflectivity of the mirror facets.

1. INTRODUCTION

Recently, S. G. Grubb et al. reported an efficient blue upconversion fiber laser [1]. The pump source was a Nd:YAG laser. We believe that high power 1.1-1.2 μm InP/InGaAsP semiconductor laser diodes with optimized parameters can play important role as a pump source for upconversion fiber lasers. Using selective growth of InGaAsP on a structured InP substrate a number of buried heterostructure lasers for 1.3 and 1.55 μm have been developed so far [2]-[4]. The orientation dependent selective growth of different composition InGaAsP layers on double channelled InP at 630 $^{\circ}\text{C}$ has been described in our previous work [5]. We report here the single-step liquid phase epitaxial growth and characterization of double-channelled substrate InP/InGaAsP buried heterostructure laser diode for 1.22 μm wavelength. Optimum conditions for separate growth of InGaAsP buried active layer on double-channelled InP substrate have been obtained. Output power over 120 mW have been achieved by determining the appropriate reflectivity of the mirror facets.

2. LPE GROWTH OF THE LASER STRUCTURE

Fig. 1. shows the schematic cross-section of the double channelled substrate buried heterostructure InP/InGaAsP laser diode. After channel etching on the substrate, seven-layers were grown by one-step LPE technique. The soak temperature is 640 $^{\circ}\text{C}$ and growth temperature for the active layer is 590 $^{\circ}\text{C}$. Cooling rate is 0.5 $^{\circ}\text{C}/\text{min}$. The layers were grown successively, as follows:

- n-InP buffer layer (Sn doped, $1 \times 10^{18}/\text{cm}^3$, $d = 0.5 - 1 \mu\text{m}$, $\Delta T = 13^{\circ}\text{C}$);
- InGaAsP active layer (undoped, $\lambda_g = 1.15 \mu\text{m}$, $d = 0.1 - 0.2 \mu\text{m}$, $\Delta T = 5 - 10^{\circ}\text{C}$);
- p-InP clad layer (Zn doped, $0.5 - 1 \times 10^{18}/\text{cm}^3$, $d = 0.8 \mu\text{m}$, $\Delta T = 12^{\circ}\text{C}$);
- n-InP current-blocking layer (undoped, $d = 0.3 \mu\text{m}$, from two-phase solution);
- n-InP blocking layer (Sn, Te doped, $3 \times 10^{18}/\text{cm}^3$, $d = 0.5 - 0.8 \mu\text{m}$, from two-phase solution);
- p-InP embedding layer (Zn doped, $1 \times 10^{18}/\text{cm}^3$, $d = 3 - 4 \mu\text{m}$, $\Delta T = 3 - 8^{\circ}\text{C}$);

- p⁺-InGaAsP cap layer (Zn doped, $3 - 6 \times 10^{18}/\text{cm}^3$, $d = 0.5 - 1.5 \mu\text{m}$, $\Delta T = 5^{\circ}\text{C}$)

where

- d is the layer thickness;
- ΔT is the supersaturation of the melt.

Fig. 2 shows the SEM picture of the cleaved and etched cross-section of the laser structure.

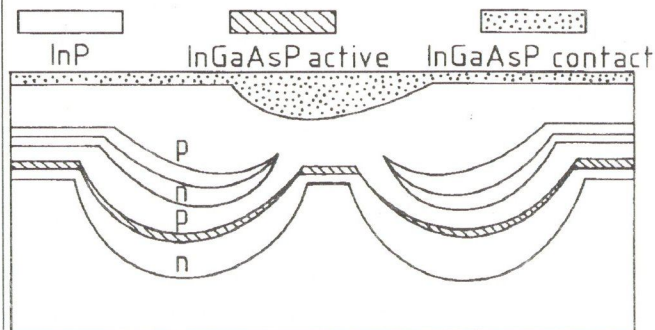


Fig. 1. Schematic cross-section of the 1.22 μm InP/InGaAsP DCS-BH laser diode

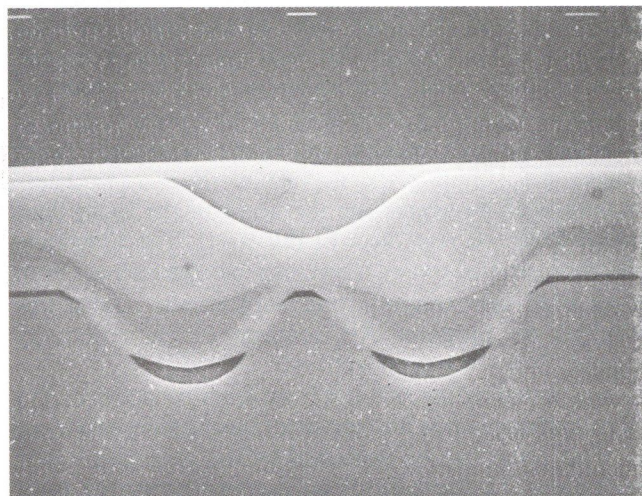


Fig. 2. SEM picture of the cleaved and etched cross-section of the 1.22 μm InP/InGaAsP DCS-BH laser diode

THRESHOLD CURRENT (mA)

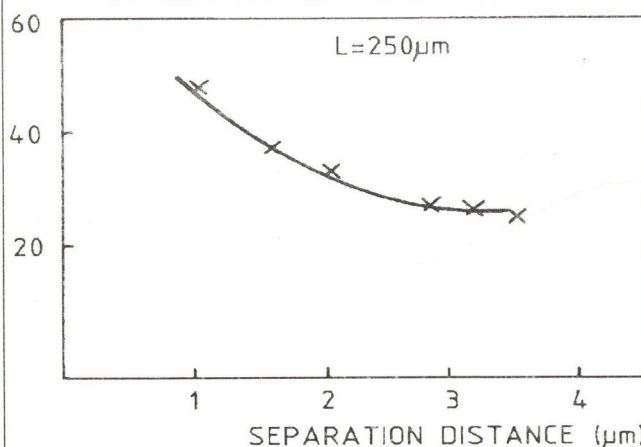


Fig. 3. Threshold current of 1.22 μm InP/InGaAsP DCS-BH lasers, as a function of the separation distances of quaternary active layer regions on the mesa stripe and at the bottom of the channels

In order to examine InGaAsP ($\lambda_g = 1.22 \mu\text{m}$) growth property, the active layer of the laser structure was grown from quaternary melts with various supersaturation degree. Increasing the supersaturation of the quaternary melt ($\Delta T = 10^\circ\text{C}$), the differences of the growth rates at the channel and mesa regions are reduced. Using short growth time (5 sec) a relatively long separation distances could be achieved. This is important because the threshold currents of the DCS-BH lasers are strongly effected by the separation distance between the buried active region on the mesa stripe and at the bottom of the channels (Fig. 3). To achieve fundamental transverse operation, the width and the thickness of the active region were designed to be 2.0 and 0.18 μm , respectively.

3. HIGH POWER LASER DIODE WITH ANTIREFLECTION COATING

To increase the laser performances a mirror coating technology was applied. The nearly quarter wavelength ($\lambda/4$) antireflection (AR) coating reduces the reflectivity of the facets of the laser chips. Therefore we get higher light power from the front facet of the laser. For the production of high quality AR coatings nonstoichiometric silicon nitride is used. The dielectric films are produced by reactive sputtering from high purity silicon targets in a commercial high vacuum sputtering equipment using nitrogen gas. During the deposition the film thickness was controlled by monitoring the decay of the lasing light emitted from the rear facet of the laser. The remaining reflectivity of the coated facet can be determined from the ratio of light outputs from both facets. Using this technique we prepared AR coatings in the reflectivity range of 20 %–0.1 % reflectivity.

It was found earlier that the front facet reflectivity (R_1) has an optimum value for high external quantum efficiency [6]. This result can be explained by the asymmetric field distribution. In the case of an asymmetric mirror facet structure the external quantum efficiency is:

$$\eta_d = \eta_i \frac{\frac{1}{2L} \ln \frac{1}{R_1 R_2}}{\alpha_i + \frac{1}{2L} \ln \frac{1}{R_1 R_2}} T_h(R_1, R_2), \quad (1)$$

where

L – cavity length,
 η_i – internal quantum efficiency,
 R_1, R_2 – facet reflectivities,
 α_i – internal loss.

The coefficient $T_h(R_1, R_2)$ was calculated in [6] considering the spatial hole burning (SHB) effect.

The optimum value of R_1 can be found where the increase of mirror loss is balanced by the decrease of the coefficient $T_h(R_1, R_2)$. The output optical power depends directly on the quantum efficiency of the front facet η_f and can be written as

$$\eta_f = \frac{\frac{1-R_1}{1-R_2} \left(\frac{R_2}{R_1}\right)^{\frac{1}{2}}}{1 + \frac{1-R_1}{1-R_2} \left(\frac{R_2}{R_1}\right)^{\frac{1}{2}}} \eta_d. \quad (2)$$

We calculated the dependence of the η_f efficiency on the front facet reflectivity using equations (1), (2) and the

plot of the $T_h(R_1, R_2)$ given in [6]. The parameters were $R_2 = 30\%$, $\eta_i = 1$, $\alpha = 27 \text{ cm}^{-1}$. Fig. 4. shows the calculated curves together with our experimental results.

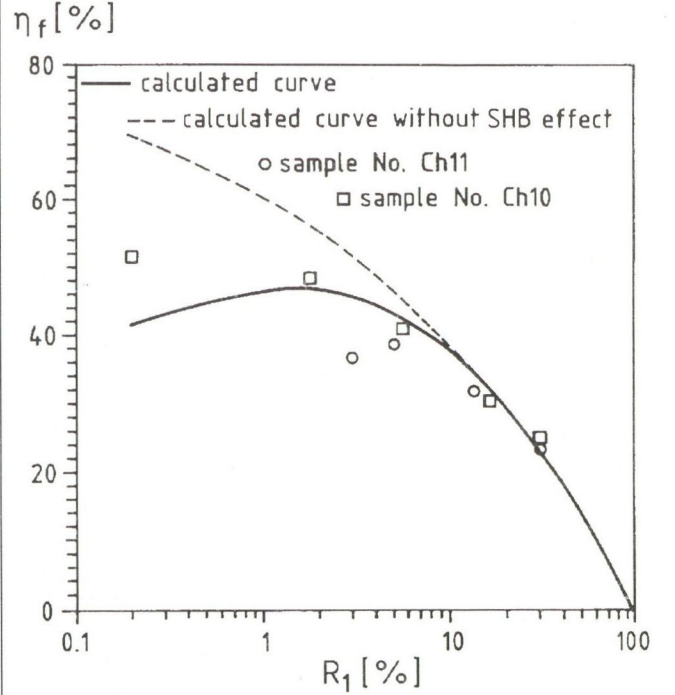


Fig. 4. Dependence of the front facet external quantum efficiency on the front facet reflectivity. Experimental results are compared with calculations

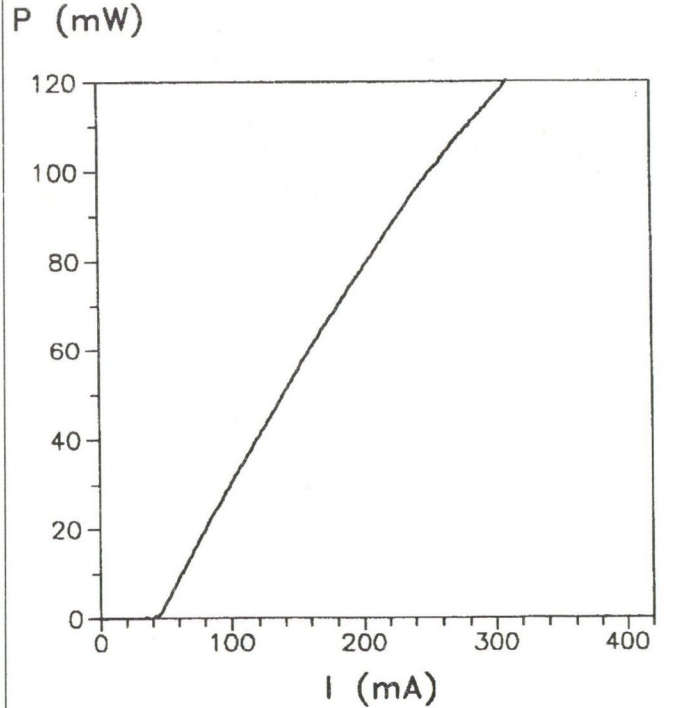


Fig. 5. Measured output light power versus current characteristics of an 1.22 μm DCS-BH laser. The front facet reflectivity was optimized to 2 % ($R_1 = 2\%$, $R_2 = 30\%$, $L = 500 \mu\text{m}$, $T = 25^\circ\text{C}$)

In Fig. 5. we show the output light power versus current characteristic of an 1.22 μm DCS-BH laser. Its front facet reflectivity was optimized to 2 % and the rear facet

was uncoated. Here we obtained 120 mW optical output power at $I = 310$ mA under CW operation at room temperature.

Finally it should be noted that reflecting coating on the rear facet of a laser diode is an important technique for obtaining a reduced threshold current and an increased external differential quantum efficiency from the front facet. To illustrate this two component materials were chosen — SiNx and a-Si — because of the large difference in their refractive indices. This large difference enables one to obtain a quarter wavelength reflector with a high reflectivity and a relatively wide wavelength range of reflection. The SiNx and a-Si films were both deposited using the sputtering technology in N_2 and Ar gas.

A two-layer or four-layer structure provides reflectivity of about 50 and 80 % respectively, significantly reducing the threshold current of the laser diode. The transmission electron microscope (TEM) picture of a four-layer reflector is depicted in Fig. 6.

4. CONCLUSIONS

We have experimentally defined the optimum conditions for separate growth of InGaAsP buried active layer on the double channelled InP substrate and have fabricated the proper laser structure by one-step LPE technique. Using an antireflection coating technology we have realized $1.22 \mu\text{m}$ InP/InGaAsP laser diodes with more than 120 mW

output light power.

5. ACKNOWLEDGEMENT

The authors wish to thank Dr. I. Habermajer for informative discussions. This work was supported by the Hungarian Research Fund (OTKA, Project number:1229 and 767).

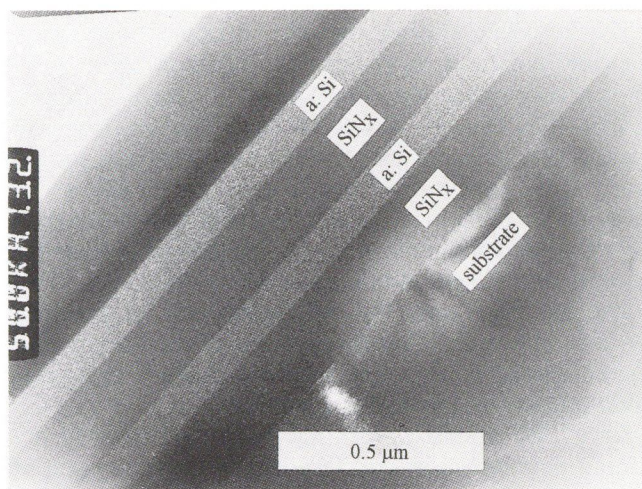


Fig. 6. TEM picture of a four-layer reflector structure

REFERENCES

- [1] S. G. Grubb, K. W. Benett, R. S. Cannon and W. F. Humer: C-W room-temperature blue up-conversion fibre laser, *Electron. Lett.*, 28, p. 1243 (1992).
- [2] K. Kishino, Y. Suematsu, Y. Takahashi, T. Tanbunek, and Z. Itaya: Fabrication and lasing properties of mesa substrate buried heterostructure GaInAsP/InP lasers at $1.3 \mu\text{m}$ wavelength, *IEEE J. Quantum Electron.*, QE-16, 160, (1980).
- [3] M. Oron, N. Tamari, H. Stickman, and C. Burrus: Lasing properties of InGaAsP buried heterojunction lasers grown on a mesa substrate, *Appl. Phys. Lett.* 41, 609, (1982).
- [4] H. Ishikawa, H. Imai, I. Umebu, K. Kori, and M. Takusagawa: V-grooved substrate buried heterostructure InGaAsP/InP laser by one step liquid phase epitaxy, *J. Appl. Physics*, 53, 2851, (1982).
- [5] V. Rakovics, F. Koltai, F. Beleznyay: Composition dependent selective growth of InGaAsP on double channelled InP substrate, Proc. of Fifth International Conference on InP and Related Compounds, Paris 1993, Post-deadline Papers p. 25.
- [6] T. Higashi, S. Ogita, H. Soda, H. Kobayashi, H. Kurakae, A. Aoki and N. Okazaki: Optimum Asymmetric Mirror Facet Structure for High-Efficiency Semiconductor Lasers, *IEEE J. of Quantum Electronics*, 29, No. 6., p. 1918 (1993).

FERENC KOLTAI, SÁNDOR PÜSKI
VILMOS RAKOVICS, MIKLÓS SERÉNYI
Research Institute for Technical Physics of the HAS
P.O.Box. 76, 1325 Budapest, Hungary

EDUCATION OF PHOTONICS AT THE TECHNICAL UNIVERSITY OF BUDAPEST

The academic staff of the T.U. Budapest has always put great emphasis on keeping the curricula up to date. The introduction in the education of the basic concepts, methods and devices, related to the branch of technical sciences that we summarize nowadays as photonics, started nearly at the time of their appearance. At the Faculty of Electrical Engineering a regular course of Optoelectronics was introduced about ten years ago for the eighth semester students on the special branch of Microelectronics. This course has been given by the Department of Electron Devices. However, other departments of the Faculty also offered special courses and involved students in several R&D projects on the field of photonics.

Since 1990 intensive work has been performed to develop a new curricular structure of the University and of the Faculty. The new structure allows a rather economical training in the basic subjects, assures more academic freedom for students and offers a grater choice in specialization.

The reformed curricula gave a good opportunity to unify the disperse educational enforcement on our special field of interest and for the organization of the Photonics module. The educational aim this group of technical subjects is to give a high level theoretical and practical background for the research, development and installation work for optoelectronic equipment and systems. The module starts at the seventh semester so that it can build on the basic technical subjects as follows: Material science, Network and Systems, Informatics, Electronics and Theory of Electromagnetic fields.

The subjects of the module (Table 1) are delivered by the following four departments: Dept. of Physics (DP), Dept. of Electron Devices (DED), Dept. of Electromagnetic Theory (DET), and by the Dept. of Microwave Telecommunications (DMT).

Table 1. Subjects and semester hours

Subject	Departments	7th sem.	8th sem.	9th sem.
Coherent Optics	DP	4		
Photonic Devices	ED, DET	4		
Optical Communication	DMT		4	
Non-linear and Integrated Optics	DET, ED			4
Laboratory I	DP, DET		2	
Laboratory II	DED, DMT			2

The main topics of subjects are the followings:

Coherent Optics

Wave Optics: The theory of interference and diffraction, Fourier representation of optical fields. Wave propagation in dispersive and anisotropic media. Crystal optics, Electro- and Acousto-optics. The physical background of

laser operation. Holographics: Image hologram, holographic optical elements, holographic interferometry. Optical Computers.

Photonic Devices

Semiconductor materials for optoelectronics. Optical processes in bulk solids and in fine structures. Optical waveguides in practice, directional couplers, isolators, circulators, and optical sensors. Devices for wavelength multiplexing and demultiplexing. Photo detectors: the problems of the high speed and phase sensitive detection. Image processing devices. Structures, optical and modulation properties of LED-s and Laser diodes. CD-ROM's and laser printers.

Optical Communications

Information theory of optical communications systems. Systems with non-coherent intensity modulation. Coherent transmission systems, modulation processes. Application of optical amplifiers. Long haul links, optical T.V. systems, computer links, LAN and MAN data networks. Design, computer simulation and measurement of optical telecommunications systems.

Non-linear and Integrated Optics

Wave propagation in non-linear media and in non-linear waveguide. Optical solitons, soliton lasers. Optical mixing, generation of harmonics, parametric amplification. Induced processes. Optical bistability. Technologies of Integrated Optics (IO). Waveguides, directional couplers, filters in IO. Wavelength multiplexing and demultiplexing in IO. Integrated modulators and switching arrays. Integration of LD-s detectors and it's electrical circuits. CAD of IO components and systems.

The first part of laboratory exercises consists of measurements on basic optical properties of optical materials, characterization of optoelectronic components. The second part is based on didactic prepared measurement of former R&D projects, while the third part of exercises gives an insight for the students in the currently running projects. These projects were significantly supported by the National Found for Scientific Research (OTKA), which is highly appreciated.

I think that the above listed topics do not need any further comments and cover the fields of photonics that may become in a practical use in Hungary. Similar programmes of teaching and research has been introduced in the last decade at numerous Electrical Faculties in the world.

This new module started at the first semester of the current academic year and it proved to be rather attractive for the students. We also hope that this course will give them a firm basis in this special field and will be of direct benefit in their engineering practice.

I. HABERMAJER

JOURNAL ON COMMUNICATIONS 1995

In 1995 we are continuing the practice of publishing alternately English and Hungarian issues. English issues will be devoted to topics in which activities and events in Hungary may be of international interest. Hungarian issues will be surveying important topics of telecommunications related to our domestic developments.

The topics of the planned issues are the followings:

English issues

- **PHOTONICS**
- **NOISE**
- **BROADCASTING**
- **INTELLIGENT NETWORKS**
- **MOBILE COMMUNICATIONS (double issue)**

Hungarian issues:

- **SECURE COMMUNICATIONS**
- **FREQUENCY MANAGEMENT**
- **CDMA SYSTEMS**
- **COMPUTER NETWORKS**
- **TELECOMMUNICATIONS IN GERMANY (double issue)**

1 year subscription rates:

6 English issues 72 USD

12 English and Hungarian issues 108 USD Single issues 20 USD

Subscription orders should be sent to the publisher:

Typotex Ltd.

Budapest, Retek u. 33-35. H-1024. Phone/Fax: (36-1)115-1759.

Information for authors

JOURNAL ON COMMUNICATIONS is published monthly, alternately in English and Hungarian. In each issue a significant topic is covered by selected comprehensive papers.

Other contributions may be included in the following sections:

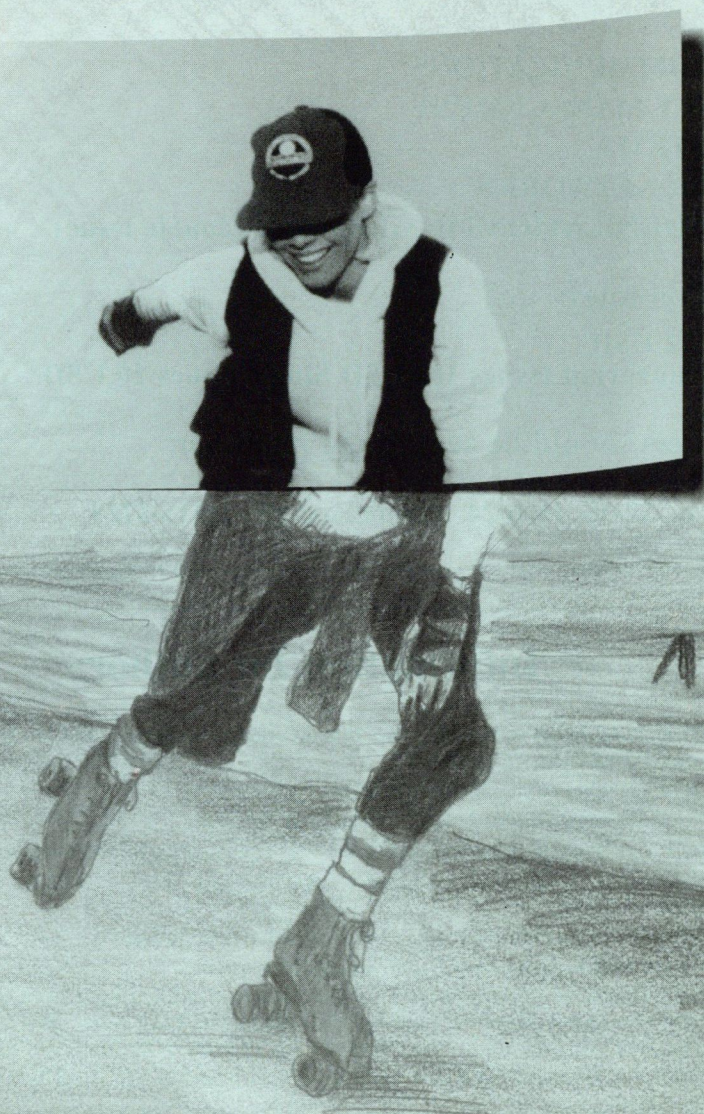
- **INDIVIDUAL PAPERS** for contributions outside the focus of the issue,
- **PRODUCTS-SERVICES** for papers on manufactured devices, equipments and software products,
- **BUSINESS-RESEARCH-EDUCATION** for contributions dealing with economic relations, research and development trends and engineering education,
- **NEWS-EVENTS** for reports on events related to electronics and communications,
- **VIEWS-OPINIONS** for comments expressed by readers of the journal.

Manuscripts should be submitted in two copies to the Editor in chief (see inside front cover). Papers should have a length of up to 30 double-spaced typewritten pages (counting each figure as one page). Each paper must include a 100–200 word abstract at the head of the manuscript. Papers should be accompanied by brief biographies and clear, glossy photographs of the authors. Contributions for the **PRODUCTS-SERVICES** and **BUSINESS-RESEARCH-EDUCATION** sections should be limited to 16 double-spaced typewritten pages.

Original illustrations should be submitted along the manuscript. All line drawings should be prepared on a white background in black ink. Lettering on drawings should be large enough to be readily legible when the drawing is reduced to one- or two-column width. On figures capital lettering should be used. Photographs should be used sparingly. All photographs must be glossy prints. Figure captions should be typed on a separate sheet.

EASY GOING

Digital exchanges ♦ Microwave and optical transmission ♦ Digital mobile telephony ♦ Land mobile radio-systems ♦ Various network elements ♦ Turn-key projects ♦ Software products for telecommunication ♦ Air-conditioning for telecommunication systems ♦ Power equipment for telecommunication systems



Ericsson Kft.

Budapest XIV., Hungária krt. 162.

Letters: H-1475 Budapest, P. O. Box 154

Tel.: +36 1 265 7100

FAX: +36 1 262 7861

ERICSSON 